# Characterising Intra-Cardiac Blood Flow Patterns in Cardiovascular Disease using Advanced Magnetic Resonance Techniques

Victoria Stoll

Green Templeton College

University of Oxford


Thesis Submitted for the Degree of Doctor of Philosophy

Trinity Term 2015

I dedicate this work to my family.

# *Acknowledgements*

I thank my supervisors Professor Stefan Neubauer and Associate Professor Saul Myerson for their input over the course of this thesis. Special thanks are extended to Dr Aaron Hess for coding my research sequence and his invaluable guidance. I am grateful to Mrs Jane Francis and Ms Anne Davis for teaching me how to conduct cardiovascular magnetic resonance examinations. Dr Malenka Bissell enthusiastically shared her knowledge and provided great encouragement throughout the course of this work. I would additionally like to thank Dr Eylem Levelt, Dr Oliver Rider, Dr Christopher Rodgers and Mr William Clarke, all of whom willingly gave me their time and expertise. I am indebted to Dr Andrew Lewis for his support over the three years and proof reading of numerous versions of my thesis.

My immense gratitude is extended to my collaborators at the University of Linköping, Sweden. Professor Tino Ebbers, Associate Professor Carl-Johan Carlhäll, Dr Jonathan Eriksson, Dr Petter Dyverfeldt and Dr Federica Viola have provided endless support, including use of their analysis tool, trouble shooting and research guidance.

Dr Margaret Loudon has provided an invaluable sounding board and I am grateful to her. I would like to thank Dr Rohan Wijesurendra, Dr Rina Ariga, Dr Alexander Liu, Dr Jenny Rayner and Dr Michael Pavlides for the useful discussions that have helped guide me. Mrs Hayley Harvey deserves special mention; she made me feel welcome from my first day and has supported me throughout my time at OCMR. Ms Joanne Sellwood and Mrs Judith Del

Santos provided additional valuable nurse support for the work presented in this thesis. Mrs Karen Whatley, Mrs Laura Bourne, Mrs Carla Cascone, Ms Pauline Collier, Mrs Sharon Dash, Mrs Kathryn Lacey, Mr Lukasz Owsiak, Ms Aggy Plachecka and Mrs Cate Wheatley deserve thanks for their administrative support.

I especially want to thank my family; my parents for their love, support and encouragement and my brother for his sense of perspective. Finally, to my ever patient husband, without whom I would not have completed this work.

I thank the British Heart Foundation for funding this research and a final special thanks to all my study participants.

# *Declarations*

The work in this thesis is my own and original. Dr Margaret Loudon provided the second operator for the blinded inter-observer analyses described in chapters 3 and 4. Dr Aaron Hess coded the retrospectively ECG gated 4D flow sequence and worked with me to optimise this for my study cohorts. Dr Christopher Rodgers and Mr William Clarke provided physics and scanning support leading to the results in chapter 6. Dr Alexander Liu provided the ethics to scan the 10 healthy volunteers at 7 tesla. Mrs Hayley Harvey assisted with recruitment of the participants in chapter 3 and in conducting the bubble contrast studies.

# *Abstract*

The end product of the numerous cellular, electrical and mechanical processes within the normal heart is the generation of blood flow. Blood flow within the cardiac chambers exerts forces upon the myocardium, which creates a continuous remodelling process. In heart failure pathological cardiac remodelling occurs; this is a complex process involving numerous transcriptional, molecular, cellular and architectural changes within both the cardiac myocytes and surrounding extracellular structures. Intra-cardiac blood flow can now be visualised *in vivo* using three-directional, three-dimensional time resolved velocity encoding cardiac magnetic resonance imaging (4D flow).

The interactions between intra-cardiac blood flow patterns and cardiovascular disease processes using 4D flow were determined. The relationship between atypical right atrial flow patterns and embolic stroke across a patent foramen ovale (PFO) were explored, as were the flow parameter changes in heart failure patients. It was found that in the presence of a PFO, participants with atypical flow patterns were more likely to have had an embolic event than those with classical vortical flow. Left ventricular 4D flow parameters were demonstrated to be highly repeatable and stable within a normal study population over time. In dilated (DCM) and ischaemic (IHD) cardiomyopathy patients, inefficient blood flow patterns and deranged kinetic energy profiles were found. The derangement in kinetic energy was demonstrated to correlate with worsening myocardial function, dilatation,

Brain-type natriuretic peptide (BNP) levels, six minute walk test (6MWT) and patient symptoms. These findings suggest that derangements in flow parameters are novel biomarkers of disease severity in heart failure patients, which may become useful in monitoring novel heart failure therapies and predicting prognosis. An association between impairment of cardiac energetics and derangement of intra-cardiac blood flow kinetic energy was demonstrated for the first time using phosphorus magnetic resonance spectroscopy ($^{31}$P MRS). The work on field strength effects on cardiac $^{31}$P-MRS has shown that 7T is feasible in a patient cohort with increased precision of metabolite quantification and increased signal to noise compared to 3T.

In summary, the work in this thesis demonstrates the powerful role of 4D flow in elucidating the detrimental effects of cardiovascular disease upon intra-cardiac blood flow parameters.

# *Abbreviations*

| | |
|---|---|
| 2D | Two dimensional |
| 2,3-DPG | 2.3 diphosphoglycerate |
| 3D cine PC-CMR | Three dimensional, three directional, time resolved phase contrast cardiovascular magnetic resonance sequence |
| $^{31}$P MRS | 31-Phosphorus magnetic resonance spectroscopy |
| 4D flow | Three dimensional, three directional, time resolved velocity encoded magnetic resonance imaging |
| 6MWT | Six minute walk test |
| ACE-I | Angiotensin-converting enzyme inhibitors |
| ADP | Adenosine diphosphate |
| AMARES | Advanced method of accurate, robust and efficient spectroscopic fitting |
| ANOVA | Analysis of variance |
| ATP | Adenosine triphosphate |
| ARB | Angiotensin receptor blockers |

| | |
|---|---|
| BMI | Body mass index |
| BNP | Brain type natriuretic peptide |
| BSA | Body surface area |
| bSSFP | Balanced steady state free precession |
| CMR | Cardiovascular magnetic resonance |
| CO | Cardiac output |
| COA | Acetyl coenzyme A |
| COV | Coefficient of variation |
| $CO_2$ | Carbon dioxide |
| CRLB | Cramer-Ráo lower bounds |
| CS | Cryptogenic stroke |
| DCM | Dilated cardiomyopathy |
| DICOM | Digital imaging and communications in medicine |
| ECG | Electrocardiogram |
| ED | End diastole |
| EDV | End diastolic volume |

| | |
|---|---|
| EF | Ejection fraction |
| ES | End systole |
| ESV | End systolic volume |
| EV | Eustachian valve |
| FOV | Field of view |
| FWHM | Full-width half maximum |
| HF | Heart failure |
| Hz | Hertz |
| HLA | Horizontal long axis |
| IAS | Interatrial septum |
| IHD | Ischaemic heart disease |
| IVC | Inferior vena cava |
| KE | Kinetic energy |
| LGE | Late gadolinium enhancement |
| LV | Left ventricle |
| MCA | Middle cerebral artery |

| | |
|---|---|
| MHFQ | Minnesota heart failure questionnaire |
| NADH | Reduced form of nicotinamide adenine dinucleotide |
| NS | Not significant |
| NYHA | New York heart association |
| PCr | Phosphocreatine |
| PFO | Patent foramen ovale |
| RF | Radio frequency |
| RA | Right atrium |
| RoPE | The Risk of Paradoxical Embolism study |
| SA | Short axis |
| SAR | Specific absorption rate |
| SERCA | Sarco/endoplasmic reticulum $Ca^{2+}$-ATPase |
| SPAMM | Spatial modulation of magnetisation |
| SNR | Signal to noise |
| SV | Stroke volume |
| SVC | Superior vena cava |

| | |
|---|---|
| T | Tesla |
| TCD | Transcranial Doppler |
| TE | Echo time |
| TIA | Transient ischaemic attack |
| TR | Repetition time |
| TTE | Transthoracic echocardiogram |
| UTE-CSI | Ultra-short echo time chemical shift imaging |

# Table of Contents

# List of Figures

## Chapter 1



## Chapter 2



## Chapter 3

## Chapter 4



## Chapter 5

## Chapter 6

# List of Tables

## Chapter 1



## Chapter 3



## Chapter 4



## Chapter 5



## Chapter 6

# Chapter 1

# Introduction

## 1.1 Importance of flow within the cardiovascular system

The importance of the heart as the pump of the cardiovascular system has long been recognised, since a seminal publication by William Harvey in 1628 [1]. Central to this role is the generation of pressure differences by contraction and relaxation of the four heart chambers, resulting in blood flow through both the heart and the wider cardiovascular system. However, instead of assessing blood flow itself most clinical assessments of cardiac function are based on anatomical imaging, even though the parameter of interest is flow [2]. Recent advances in phase contrast magnetic resonance imaging now afford the opportunity for visualisation of time resolved blood flow within the cardiac chambers [3].

In order for the heart to function efficiently as a pump it must have adequate blood inflow to both atria, the presence of electrically coordinated, functioning cardiac myocytes that produce a sufficient energy supply and unobstructed outflow tracts [4]. With an average heart rate of 72 beats per minute, the heart will pump approximately seven litres in total per minute. Hence, the cardiac output of the average human heart over a life time of 70 years would be about 300 million litres [5]. The forces that result from the interaction between the myocardium and the flowing blood stimulate a continuous remodelling process [2], interactively creating an optimal geometry for efficient flow. Myocardial disease can lead to alterations in these interactions, which although initially may only be minor, over time even small functional disturbances may have serious deleterious consequences when multiplied by the number of litres of blood pumped over a lifetime [6].

## 1.2 Development of the looped heart and physiological implications

During embryogenesis the heart develops from the straight heart tube and undergoes a morphogenetic process referred to as cardiac looping [7]. These structural changes result in chiral asymmetry of blood flow paths in the adult heart, with asymmetric redirection of the stream in the atria and ventricles [8]. The purpose of the development of a looped heart has been a source of debate as originally it was hypothesised that the asymmetry of the heart conserves energy by preserving the linear momentum of the blood flow [8]. However, evidence from computational modelling disputes this previous work and suggests that the looping serves to allow the ventricle to function in a 'first in, first out' mode of expulsion of blood [9]. In response to this work, Kilner [10] proposed that there are three important anatomical advantages of the looped heart:

1. Inflows in a looped heart tend to be aligned tangential to a cavity, which predisposes to more stable intra-cavity flow.
2. The recirculation of inflowing streams within the atrial and ventricular cavities of a lopped heart tend to turn predominantly towards, rather than away, from the next cavity, which may facilitate efficient onward passage of blood.
3. In a looped heart the appropriate direction of the inertial recoil of a vigorously ejecting ventricle may enhance rather than suppress the structural coupling of ventricular systole to atrial filling.

Kilner hypothesised that the importance of the presence of these three factors would increase during strenuous exertion, in order to allow the more than six fold increase in cardiac output [11] that can occur. During exercise, when the heart rate is elevated, the two peaks of early and late ventricular filling of the resting heart become one; when a single peak of rapid ventricular filling is followed by vigorous ejection with little or no intervening isovolumetric period [12]. Minimisation of the dissipation of kinetic energy of the inflowing blood during exercise would be functionally advantageous, allowing efficient transfers of energy between the inflowing and outflowing blood and other cardiac structures.

## 1.3 Heart failure and cardiac remodelling

Heart failure (HF) is a global health burden, which as more patients survive their initial myocardial insult, as well as the presence of an aging population, will continue to increase in incidence [13]. HF encompasses a wide range of pathologies that ultimately result in failure of the heart to pump efficiently. As part of the development of HF cardiac remodelling occurs. This is a complex process encompassing numerous transcriptional, molecular, cellular and architectural changes within both the cardiac myocytes and surrounding extracellular structures [14]. Cardiac plasticity allows the heart to remodel appropriately to physiological changes such as pregnancy. For example, a Burmese python in response to a large meal requires an increase in metabolic work by a factor of seven and a dramatic 40% increase in ventricular mass occurs within 48 hours of consumption to enable this [15]. Hence, although in HF the initial stages of cardiac remodelling may be beneficial and attempt to

compensate for the myocardial insult, over time the changes become maladaptive, resulting in a vicious downward spiral increasing the risk of development of heart failure [16].

Two important causes of heart failure are ischaemic heart disease and dilated cardiomyopathy [17]. Despite improvements in prognosis and survival [18], HF remains a substantial source of morbidity and mortality, as well as a financial burden for health care systems [17].

### 1.3.1 Ischaemic cardiomyopathy

Coronary artery disease is the most common cause of heart failure [17]. Ischaemic cardiomyopathy is characterised by myocyte loss, reactive cellular hypertrophy and ventricular scarring [19]. Myocyte loss occurs as a result of narrowing or occlusion of coronary arteries by atherosclerosis, spasm or paradoxical embolism, or alterations of the microcirculation, which, alone or in combination, produce varying degrees of ischaemia and tissue injury. The clinical spectrum ranges from acute myocardial infarction to chronic ischaemic cardiomyopathy [19]. Areas of myocardial infarction reduce the amount of functioning myocardium, resulting in a regional wall motion abnormality and causing an increased load on the surviving regions of the ventricle, which undergo compensatory reactive hypertrophy [20, 21]. This growth process may expand the length of the unaffected myocytes to a greater extent than the expansion in myocyte diameter, contributing to chamber dilation and relative thinning of the wall [22]. Ventricular dilatation has been identified as a marker for poor prognosis in both acute and chronic ischemic cardiomyopathy [23, 24].

### 1.3.2 Dilated cardiomyopathy

Dilated cardiomyopathy (DCM) is an intrinsic myocardial disease process characterised by enlargement of ventricular volumes with global impairment of systolic function. Familial disease accounts for one third to one half of cases [25]. Dilated cardiomyopathy is the end phenotype of non-ischaemic insults, such as alcohol, and despite advances in treatment, including medical therapies and cardiac resynchronisation therapy, the prognosis remains poor [26-29]. Left ventricular dilatation, systolic dysfunction, myocyte death and myocardial fibrosis are the main features of DCM [25].

## 1.4 Measuring intra-cardiac blood flow by cardiovascular magnetic resonance (CMR)

### 1.4.1 Basis of phase contrast CMR

MRI is based on a physical property called spin, which occurs because atoms with unpaired protons in their nucleus possess a net spin. When atoms possessing a net spin are exposed to a magnetic field, they will randomly align with the magnetic field in either a spin up (high energy state) or spin down (low energy state) orientation. When a radiofrequency (RF) pulse is applied to this field, the spins will shift their orientation, as the RF pulse is removed the spins will return to their original energy state during the so called relaxation time. The net sum of energy emitted as the spins return to their original state is the signal registered by the coil. Magnetic gradients in the three spatial directions (x, y and z) are used to choose an area of interest to image. By interleaving flow encoding bipolar gradients and RF pulses

time resolved, three directional velocity data in a three-dimensional volume i.e. 4D flow data can be acquired [30-32]. This is based on the principle that by adding bipolar gradients in different schemes a phase shift [31] is induced in the signal. If the spins are stationary, they will return to their original state when the entire bipolar gradient is applied; if the spins have moved, as is the case in flowing blood, the phase shift will remain in the signal. The phase shift will be proportional to the velocity [33, 34].

### 1.4.2 Visualisation of intra-cardiac blood flow

Visualisation of blood flow encompasses a collection of methods for the extraction and distinction of desired features in a multidimensional, complex volume of data [35]. Particle trace methods are a group of numerical tools that may be used to assess flow features. There are 3 main types of particle traces; streamlines [36], pathlines [35, 37] and streaklines. A streamline is at all points in space tangential to the velocity field; these are calculated from one time frame and do not take variations of flow into account. A pathline is integrated from the velocity data and represents the path an imaginary massless particle would travel along through the data volume. Streaklines are less frequently used and represent a virtual ink continuously emitted from a fixed point. These visualisation methods have been applied to various blood vessels including the aorta [38-40] and carotid arteries [41], cerebral vasculature [42] as well as the heart [3].

### 1.4.3 Vortical flow in the right atrium

In order for the heart to function as an efficient pump the supply of inflowing blood must be able to keep pace with demand. Hence, the pattern of blood flow within the atria is

likely to be of relevance to the overall efficiency of cardiac function. The inflow of blood into the right atrium consists of two streams; one from the inferior vena cava and one from the superior vena cava. Previous *in vivo* visualisations have demonstrated that these streams do not collide head on but turn forward, contributing to a forward clockwise rotation of blood [8].

The pattern of the blood flow within the right atrium may be important when there is the possibility of right to left shunting of blood, such as occurs in the presence of a patent foramen ovale (PFO) [43]. A PFO is an embryological remnant within the inter-atrial septum which occurs in approximately 25% of the population, when the foramen ovale fails to close completely after birth [44]. It acts as a flap like structure that can open when right atrial pressure exceeds that of left atrial pressure [45]. Case reports have identified it as a conduit for paradoxical embolism [46] and it has been implicated in cryptogenic stroke [47].

### 1.4.4 Quantification of left ventricular blood flow

The blood flow within the left ventricle (LV) is dynamically arranged with regions of straight and turning flow, flow-flow interactions, recirculating masses of blood and vortices that develop and extinguish with phases of the cardiac cycle [48]. The end diastolic volume of the left ventricle can be separated in to four separate function components, as described by Eriksson *et al* [3] and shown in **Figure 1.1** below:

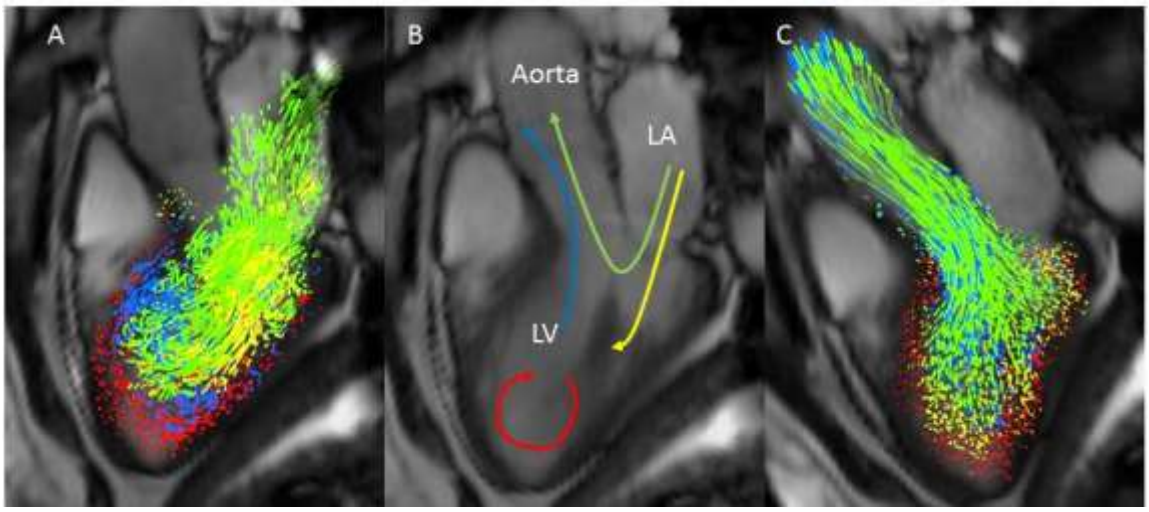


***Figure 1.1:*** *Left ventricular flow components. Direct flow, green; retained inflow, yellow; delayed ejection flow, blue and residual volume, red. Panel* ***(A)*** *shows diastolic flow,* ***(B)*** *shows the direction of movement of each flow component and* ***(C)*** *demonstrates systolic flow.*

This method is based upon emitting pathlines from the full end diastolic volume (EDV) both forwards (covering systole) and backwards (covering diastole) in time, resulting in full coverage of the cardiac cycle. The pathlines are then defined as one of the four flow

components according to their relative positions at end diastole and end systole. The definitions of the flow components are given in **Table 1.1** below.

**Table 1.1: Definition of left ventricular flow components.**

| Component name | Definition |
|---|---|
| **Direct flow** | Blood that enters the LV during diastole and leaves the LV during systole in the analysed heart beat |
| **Retained inflow** | Blood that enters the LV during diastole and resides in the LV throughout the cardiac cycle |
| **Delayed ejection flow** | Blood that starts and resides within the LV during the diastolic phase of the analysed cardiac cycle and is ejected during the systolic phase |
| **Residual volume** | Blood that resides in the LV for at least two cardiac cycles, not a component of inflow or ejected blood |

### 1.4.5 Kinetic energy of the left ventricular blood flow

Cardiac pumping delivers a pressurised blood volume to the systemic and pulmonary circulation. The amount of external work required to deliver the volume and pressure can be divided into kinetic energy (KE) and stroke work [49]. Additional information can be gained from the LV blood flow visualisations; the KE of each LV component can be calculated [50]. KE is defined as the mass of a moving object multiplied by its velocity squared, divided by 2 and has the unit Joule ($kgm/s^2$).

As each pathline emitted from the LV EDV is assumed to represent a volume of blood, the KE is calculated per pathline by utilising the equation:

$$KE = \tfrac{1}{2} \cdot \rho_{blood} \cdot V_{pathline} \cdot v^2_{pathline}$$

where $\rho_{blood}$ is blood density (1060 kg/m$^3$), $V_{pathline}$ the volume that one pathline represents and $v_{pathline}$ the velocity of the pathline at a given time point. The KE of each pathline within a flow component is then summed to calculate the total KE for that flow component. A typical kinetic energy profile is shown in **Figure 1.2** below.

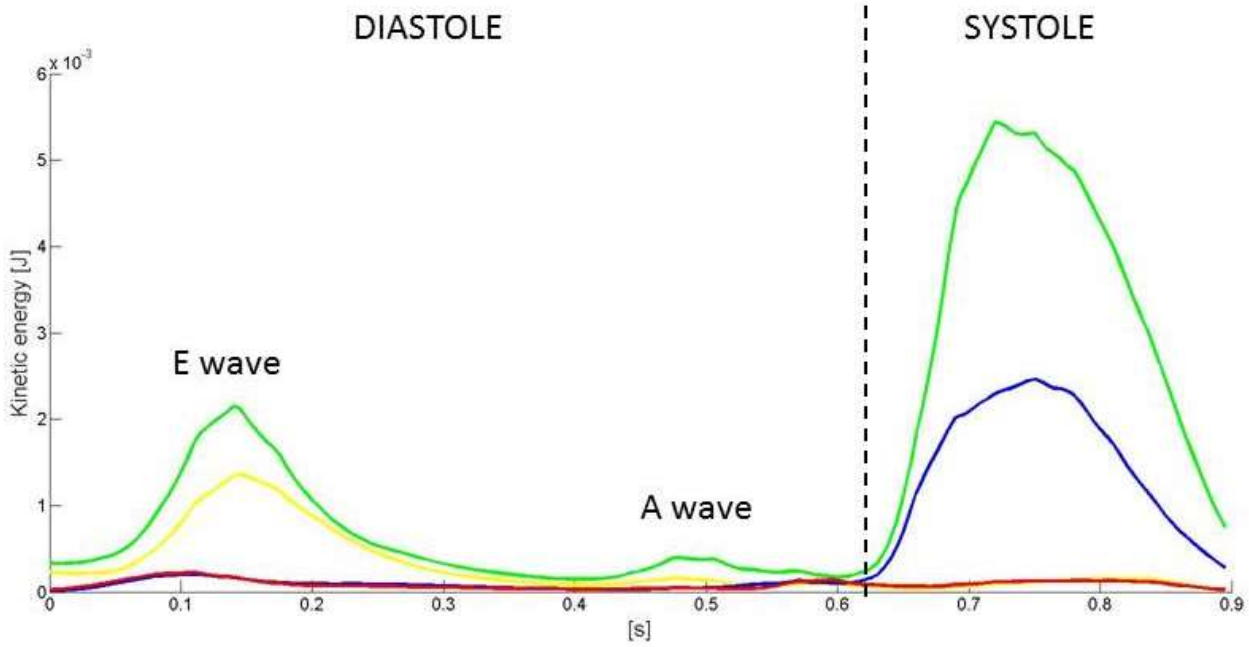


***Figure 1.2:*** *Typical kinetic energy profile for the four flow components. Direct flow, green; retained inflow, yellow; delayed ejection flow, blue and residual volume, red.*

## 1.5 Energy metabolism in health

The heart is an energy expensive organ, consuming approximately six kilograms of adenosine triphosphate (ATP) each day; more energy per gram of tissue than any other organ [13]. As the human heart contains less than one gram of ATP there must be adequate production of ATP by the cardiac myocytes. In order to produce the energy supply required for its function, the heart converts chemical energy stored in fatty acids and glucose into the mechanical energy of the actin-myosin interaction of myofibrils. If energy production does not keep pace with demand mechanical failure of the heart will occur [13]. Therefore, maintenance of adequate levels of cardiac high-energy phosphate metabolites, ATP, the energy source for contraction, and phosphocreatine (PCr), the major energy storage compound, are critical for normal heart function. Abnormal resting cardiac energetics have been demonstrated to be a common feature of numerous cardiac pathologies including non-ischaemic heart failure [51,52], ischaemic heart disease [53,54], hypertrophic cardiomyopathy [55, 56], hypertension [57, 58], diabetic cardiomyopathy [59, 60] and valvular disease [61,53]. However, a causal relationship between energy starvation and contractile dysfunction has not yet been established, but it is hypothesised that derangements in cardiac energetics can contribute significantly to disease aetiology and progression.

There are three main aspects of the cardiac metabolism pathway that are necessary for effective cardiac metabolism see **Figure 1.3** below.

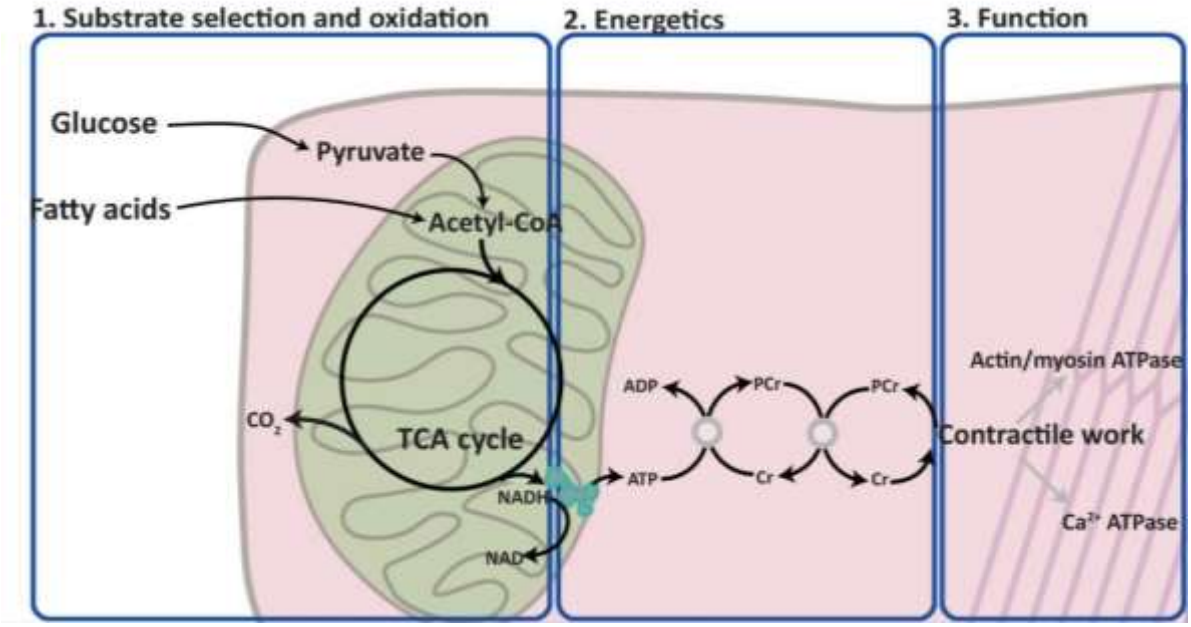


***Figure 1.3:*** *Cardiac energy metabolism. Energy metabolism in the heart has three components: 1. Substrate selection and oxidation; 2. Energetics and 3. Cardiac function as a result of energy utilisation.*

1. **Substrate selection and oxidation:** This is a multifactorial step requiring adequate myocardial blood supply with an appropriate hyperaemic response during exercise to deliver both substrate and oxygen under rest and exercise conditions. Cellular uptake of predominantly free fatty acids and glucose occurs. Subsequently these substrates are broken down via beta oxidation and glycolysis. This results in the formation of acetyl coenzyme A (CoA), which is fed into the Krebs cycle and produces the reduced form of nicotinamide adenine dinucleotide (NADH) and carbon dioxide ($CO_2$).

2. **Energetics:** High energy phosphate bonds are made in the form of ATP via a series of electron transfers in the mitochondria. Respiratory-chain complexes I through IV transfer electrons from NADH to oxygen, thereby creating a proton electrochemical gradient across the inner mitochondrial membrane as well as NAD and water. This gradient drives ATP synthase, which produces ATP by oxidative phosphorylation of ADP (adenosine diphosphate). Uncoupling proteins cause mitochondria to produce heat rather than ATP. The heart's energy transfer mechanism is the creatine kinase energy shuttle. Creatine, which is not produced in the heart, is taken up by the creatine transporter. Mitochondrial creatine kinase catalyses the transfer of the high energy phosphate bond in ATP to creatine to form PCr. This molecule is smaller and less polar and hence diffuses out of the mitochondria into the cytoplasm.
3. **Function:** At the site of energy usage, mainly at the sarcomere and for ion pump function, ATP is reformed in the reverse reaction. The free creatinine formed by the removal of phosphate from PCr, diffuses back to the mitochondria.

## 1.6 Energy metabolism in heart failure

Abnormalities of cardiac energy metabolism in heart failure are multifactorial and affect substrate utilisation, oxidative phosphorylation and high-energy phosphate metabolism:

1. **Substrate utilisation:** this may limit cardiac function in HF due to reduced substrate uptake, oxidation or both. The relative contributions of fatty acid and glucose substrate utilisation have been noted to change, with an initial increase in glucose metabolism. However, in advanced heart failure insulin resistance develops in the

myocardium with a subsequent decline in glucose metabolism. Fatty acid metabolism also declines in advanced heart failure.

2. **Oxidative phosphorylation:** Cardiac mitochondria have structural abnormalities and are probably increased in number [62]. The activity of the electron transport chain complexes and of ATP synthase is reduced.

3. **ATP transfer:** There are significant changes in the creatine kinase system in heart failure. Both mitochondrial and myofibrillar creatine kinase activities are reduced resulting in a decline in ATP transfer. This decrease in energy flux within the cell can result in a reduction in energy delivery to the myofibrils by up to 71% [63]. This may contribute to the contractile dysfunction that is typical of the myocardium in heart failure [13].

### 1.6.1 Measuring cardiac energy metabolism

ATP is used for most energy consuming reactions in the heart, including contraction of cardiac myofilaments (70%) and for active pump function and calcium uptake via sarco/endoplasmic reticulum $Ca^{2+}$-ATPase (SERCA). Myocardial levels of ATP are kept relatively constant over a wide range of cardiac loads in the normal heart, buffered by the transfer of energy from PCr. The equilibrium constant of this creatine kinase reaction favors the synthesis of ATP over PCr, by a factor of approximately 100. Therefore, in disease states with inefficient energy production or energy utilisation, the ATP levels would initially remain constant at the expense of PCr; hence, the ratio of PCr/ATP is a sensitive indicator

of the underlying energetic state of the heart. Even in the advanced stages of heart failure myocardial ATP levels decrease by no more than 30 to 40% [13].

Cardiac $^{31}$P MRS is the only technique that allows non-invasive measurement of cardiac high-energy phosphate metabolism *in vivo*. The first publication in 1980 on *in vivo* spectroscopy on rat heart [64] paved the way for this non-invasive technique to be applied to the human heart, some ten years later [65]. The technique is now an established research method for investigating cardiac energetics.

## 1.7 Aims of this research

This work aims to investigate the interactions between intra-cardiac blood flow patterns and cardiovascular disease processes. In particular the blood flow patterns within the right atrium and left ventricle shall be investigated. In order to accomplish this, the work in this thesis involves development and implementation of a retrospectively gated 4D flow sequence, which allows quantification of left ventricular flow.

The following were then explored:

1. The range of right atrial flow patterns within the normal population and associations between flow patterns and the risk of paradoxical embolism in participants assumed to have suffered an embolic event via their PFO.
2. The establishment of an understanding of the variability of left ventricular flow components and kinetic energy within the normal population over time.

3. Cardiac remodelling is a key process in the development of heart failure. This thesis explores the changes in left ventricular flow components and kinetic energy in dilated and ischaemic cardiomyopathy. The relationship between LV flow parameters and classical remodelling markers as well as prognostic markers in HF are explored for the first time.
4. $^{31}$P MRS has not been applied to broader use, partly as a consequence of the method's low intrinsic signal-to-noise ratio (SNR). Use of this technique at higher field strength may help to overcome this limitation and improve accuracy in myocardial metabolite quantification. This thesis compares $^{31}$P MRS at 7 tesla field strength to 3 tesla in DCM patients. The relationships between LV flow parameters and myocardial energetics were interrogated.

# Chapter 2

# General methods

## 2.1 Ethical approval and recruitment

The patent foramen ovale study described in chapter 3 was approved by Southampton Research Ethics Committee (REC Ref: 12/SC/0287). The study reported in chapters 4 and 5 was approved by South Central: Oxford A Ethics Committee (REC Ref: 12/SC/0546). The dilated cardiomyopathy study reported in chapter 6 was approved by the West Midlands: Solihull Ethics Committee (REC Ref: 13/WM/0155). The healthy volunteers scanned at 7 tesla were recruited to an additional study approved by South Central: Oxford A Ethics Committee (REC Ref 13/SC/0376). Each participant gave written informed consent to be involved. Patients were recruited from outpatient cardiology clinics, clinical magnetic resonance imaging lists and the community heart failure service. Healthy volunteers were recruited via word of mouth and study posters advertised on the John Radcliffe Hospital and University of Oxford information boards.

## 2.2 Eligibility criteria

### 2.2.1 Inclusion criteria

Due to the diverse nature of patient participants within each chapter the precise inclusion criteria will be given within the methods section of each results chapter. Generally participants were eligible for inclusion in the study if:

- Aged at least 18 years old or above.
- Willing and able to undergo all study procedures.

- Willing and able to give informed consent for participation in the study.

**Healthy volunteers:**

- Age-matched healthy volunteers with no known history of cardiac disease.
- Able to perform exercise testing.

### 2.2.2 Exclusion criteria

Participants were excluded if any of the following were present:

- Contra-indications to magnetic resonance imaging (pacemaker, cranial aneurysm clips, metallic ocular foreign bodies, severe claustrophobia).
- Pregnancy, or breastfeeding female.
- Atrial fibrillation.
- Known hypersensitivity to gadolinium.
- Terminally ill patients.
- Participants with a diagnosis of significant (> mild, diagnosed by their GP or a Cardiologist) valve disease.
- Any other significant disease or disorder which, in the opinion of the investigator, may compromise the safety of participants or staff, or the scientific value of results from the study.

## 2.3 Clinical assessments

In the methods section of chapter 3 the assessments that were undertaken for the PFO study participants are described. All participants enrolled in the studies reported in chapters 4, 5 and 6 on the day of the magnetic resonance scan, underwent a clinical assessment. This included history for:

- The presence of exclusion criteria as documented above.
- Drug history, including allergies.
- Cardiac history, including duration since diagnosis, symptoms and presence of complications.
- Patients completed the Minnesota heart failure questionnaire (MHFQ) [66] (see **Appendix 1**). This is a quality of life score consisting of 21 questions assessing symptoms from heart failure over the preceding 4 week period, with scores ranging from 0 (no effect) to 5 (great effect).

Cardiovascular examination was also performed to assess for the presence of ventricular hypertrophy and valvular heart disease. The following measurements were carried out:

- Blood pressure was recorded as an average of 3 supine measures taken over 10 minutes using an automated sphygmomanometer (DINAMAP-1846-SX, Critikon Corp).
- Height (cm) and weight (kg) using calibrated scales. Body mass index (BMI) was calculated.
- 12 lead electrocardiogram (ECG).

Blood tests for Brain-type natriuretic peptide (BNP) and creatinine (if required, as per standard operating policy) prior to administration of gadolinium based contrast were taken. Participants undertook a 6 minute walk test to determine exercise capacity. The maximum distance walked within 6 minutes along a 30m walkway was recorded, standardised encouragement was provided during the 6 minutes [67].

## 2.4 Scan protocols and data analysis

The precise image sequences undertaken for each study will be highlighted in the appropriate methods section of the relevant results chapter. CMR sequences used included the following:

(i) 4D flow data acquisition- either prospectively or retrospectively ECG gated

(ii) Cine imaging for left ventricular function and mass.

(iii) Myocardial strain imaging

(iv) Late gadolinium enhancement, (LGE) to assess myocardial infarction.

(v) $^{31}$P MRS at rest at 3 and 7 tesla

Scanning was conducted on a Siemens 3T Trio MR system (Erlangen, Germany).

### 2.4.1 Prospective 4D flow data acquisition

A flow-sensitive gradient-echo pulse sequence was used to visualise flow within the RA. Data were acquired with prospective ECG-gating during free breathing, using a respiratory navigator. The image acquisition volume was placed in a transverse plane encompassing the right atrium, inflow of the inferior vena cava (IVC) and superior vena cava (SVC).

Sequence parameters were echo time 2.5ms, repetition time 5.1ms, flip angle 7°, voxel size reconstructed to 1.7x1.7x2.2 $mm^3$ with 82% and 66% phase and slice oversampling, and temporal resolution 40ms. Scout measurements within the IVC were used to determine the velocity encoding range in order to avoid aliasing (1-1.5m/s). Data was processed with customised Matlab software version R2012a (The Mathworks Inc, Natick, MA) and EnSight version 10.0.3(b) (CEI Inc, Apex, NC), as previously described [68-71].

### 2.4.2 Prospective 4D flow data post processing and analysis

As this sequence was only utilised for the PFO study, the analysis technique of the 4D flow data acquired is described in detail in the methods section of chapter 3.

### 2.4.3 Retrospective 4D flow data acquisition

4D flow data acquisitions were acquired during free breathing, using a retrospectively ECG triggered, respiratory navigator gated three dimensional, three directional, time resolved phase contrast CMR sequence (3D cine PC-CMR). The echo time was 2.75 ms with a repetition time of 4.3 ms and temporal resolution of 52 ms. The flip angle was 7°, read field of view 390 mm and voxel size 3x3x3 $mm^3$. The velocity encoding was 1.0m/s. The field-of-view (FOV) was sagittal and adjusted for each participant to fully encompass the whole heart. The average data acquisition times were between 15-20 minutes.

### 2.4.4 Retrospective 4D flow post processing and data analysis

The background phase was corrected with a third order polynomial fit to remove phase errors arising from concomitant fields and data quality control steps were applied as

previously described [3] using automated customised Matlab software (The Mathworks Inc., Natick, Massachusetts, USA). Velocity data was converted into a file format compatible with commercially available visualisation software (EnSight, CEI Inc., Research Triangle Park, NC, USA).

All data sets were analysed using a method previously described by Eriksson *et al* [3, 72], with freely available software (Segment, version 1.9 R2842)[73] which consists of manual segmentation of the LV endocardium from short-axis (SA) images at end diastole (ED) and end systole (ES). The segmentation at ED is resampled to give a volume with isotropic voxels equal to the size of the flow data voxels. A pathline is emitted from the centre of each voxel included in the LV segmentation. Pathlines are created forwards and backwards in time until the preceding or subsequent ES, respectively. Combined these forward and backward pathlines represent the entire LV end diastolic volume tracked over one complete cardiac cycle. The positions of all pathlines at the time of ES relative to the LV cavity as defined by the segmentation at ES are then used to divide them into four functional flow components; direct flow, retained inflow, delayed ejection flow and residual volume as described previously [3, 72, 74]. Direct flow is defined as blood that enters and exits the LV in the analysed cardiac cycle, retained inflow enters the LV but does not exit during the analysed cardiac cycle, whilst delayed ejection flow starts within the LV but exits during the analysed cardiac cycle, residual volume is the component that neither enters nor exits the LV for at least 2 cardiac cycles. Accuracy of this quantification was evaluated by comparing the LV inflow components (direct flow and retained inflow) to the

LV outflow components (direct flow and delayed ejection flow), any data sets with >10% difference were excluded from further analysis.

The KE of these flow components can be calculated throughout the cardiac cycle by utilising

$KE = ½ \cdot \rho_{blood} \cdot V_{pathline} \cdot v^2_{pathline,}$ where $\rho_{blood}$ is blood density, $V_{pathline}$ the volume that one pathline represents and $v_{pathline}$ the velocity of the pathline at a given time point. The KE for each component is the sum over all pathlines in the group. The KE values were calculated over the cardiac cycle.

### 2.4.5 Left ventricular function and mass

CMR is accurate, reproducible and well validated for measuring left ventricular volumes and mass [75]. Cardiac volumes were acquired using balanced steady state free precession (bSSFP) imaging. Pilot, horizontal long axis, vertical long axis and short axis stack images were acquired with the patient in the supine position. Each slice was 8mm thick with no gap and was retrospectively gated with echo time, 1.5 ms; repetition time, 3 ms and flip angle, 50°. The slices were obtained during a breath-hold at the end of normal expiration to minimise the effects of respiratory motion.

LV short axis epicardial and endocardial borders were manually contoured at end diastole and end systole (**Figure 2.1**), for determining end diastolic volume (EDV); end systolic volumes (ESV) and stroke volume (SV) using cmr42© (Circle Cardiovascular Imaging Inc., Calgary, Canada). Ejection fraction (EF) and cardiac output (CO) were calculated (EF = SV/EDV, CO = SV x heart rate). Myocardial mass was also calculated by subtracting the

endocardial volume from the epicardial volume. Left ventricular mass was calculated based on prior knowledge of myocardial specific gravity (1.05 g/cm$^3$) [75].

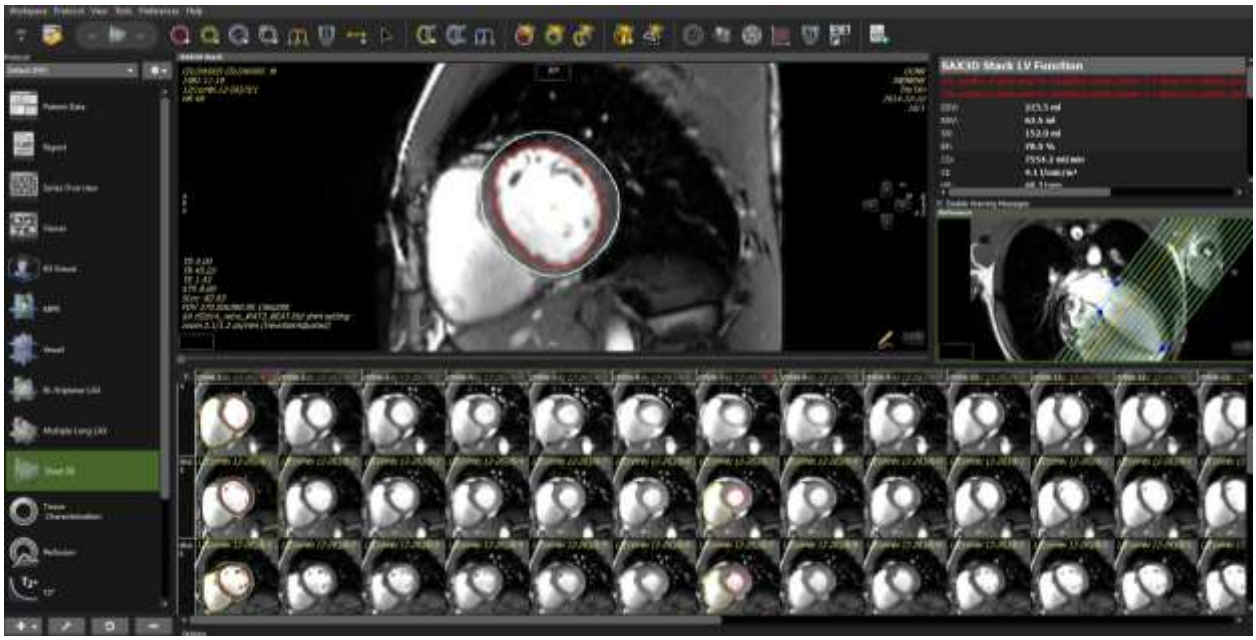

***Figure 2.1**: Analysis of left ventricular function using CMR42 (Circle Cardiovascular Imaging Inc., Calgary, Canada).*

### 2.4.6 Myocardial strain imaging

Myocardial strain is defined as the relative deformation of the myocardium during contraction and relaxation [76]. Strain is reported as a percentage change of myocardial deformation, referring to the change of the myocardial fibre length at end-systole compared to its original length at end-diastole. Strain rate is the change in strain per unit time [77]. With contraction, the myocardium is shortened (negative strain), while during relaxation, the myocardium lengthens (positive strain). Strain can be measured in longitudinal, circumferential and radial directions and is thought to partially reflect sub-endocardial, mid-wall and sub-epicardial myocardial function respectively.

CMR is a well validated tool for measurement of multidirectional strain using a sequence known as "*tagging*" [76]. Non-invasive markers that appear as dark lines (tags) in the acquired images follow myocardial motion during the cardiac cycle, thus representing myocardial deformation. Persistent tags throughout the cardiac cycle allow accurate assessment of both systolic and diastolic function. However, due to T1 relaxation, the tag lines fade towards the end of diastole.

A gradient echo-based tagging pulse sequence was performed in the long-axis and in the short-axis slice, with a segmented k-space, multi-shot sequence (repetition time 4.47ms, echo time 7.4ms, and flip angle 25˚). Spatial modulation of magnetisation (SPAMM)[78] produced images with a grid-based pattern of horizontally and vertically modulated 'stripes' 7mm apart, acquired during a single breath-hold, using a prospectively gated sequence. The temporal resolution (TR x no. of segments, 9) was 40.2 ms in all data sets, and 15-25 frames per cardiac cycle were recorded, depending on heart rate.

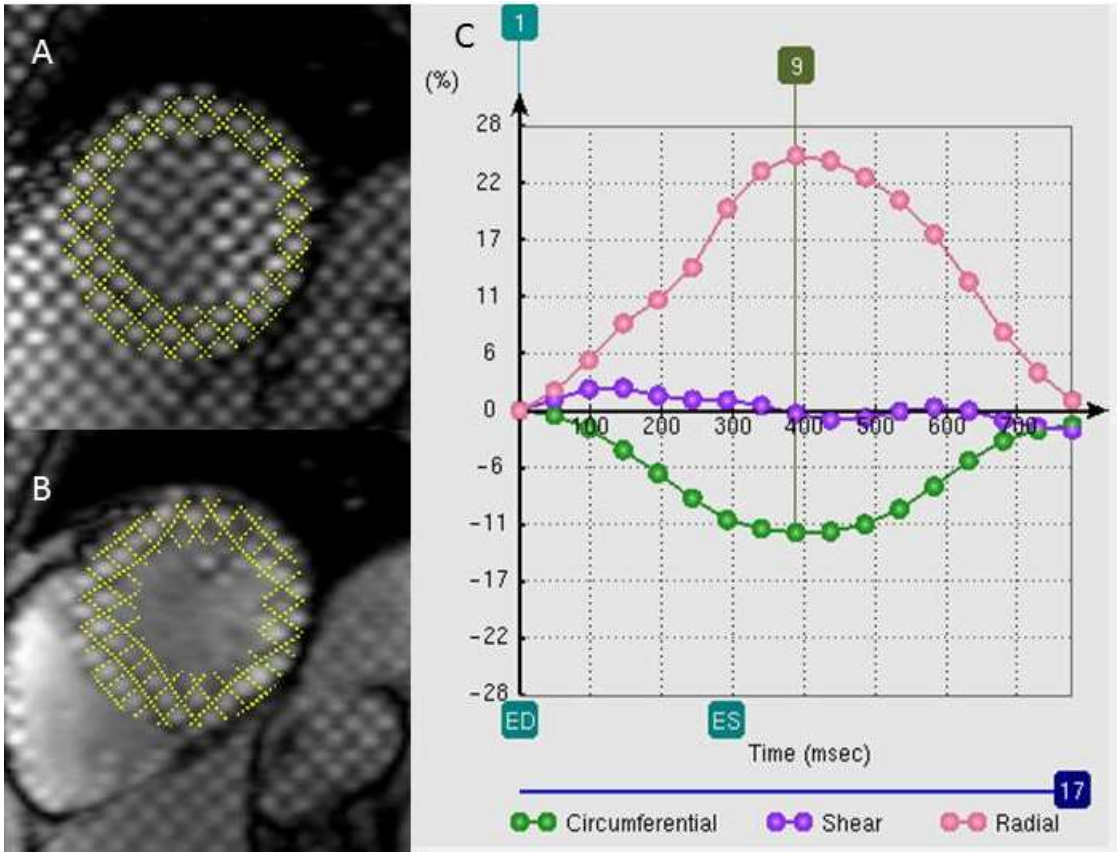


***Figure 2.2:*** *An example of CMR myocardial tagging in a mid-left ventricular short axis slice from a dilated cardiomyopathy patient. The deformation of the tag lines are tracked throughout the cardiac cycle and shown in* ***(A)*** *diastole and* ***(B)*** *systole. The peak systolic strain rates are shown in the graph in figure* ***(C)****. The peak systolic circumferential strain, as demonstrated by the green curve is -11.8% in this patient.*

Tagged images were analysed using Cim Tag2D version 7 (Auckland Medical Research, Auckland, New Zealand), see **Figure 2.2**. Outcome parameters measured in this study were: mid ventricular peak systolic circumferential strain, circumferential diastolic strain rate and peak systolic longitudinal strain. Circumferential strain is mainly focused upon in this thesis, as up to 70% of myocardial contraction is circumferential.

### 2.4.7 Late gadolinium enhancement

For late gadolinium enhancement (LGE) images, 0.1mmol per kilogram of Gadovist (Bayer PLC, Newbury, United Kingdom) followed by a 10mL saline flush was administered through an intravenous cannula inserted into the antecubital fossa. Electrocardiographically gated images were acquired after a 10 minute delay in long- and short-axis planes using a breath-hold T1-weighted segmented inversion-recovery turbo fast low-angle shot sequence previously described [79]. The scan parameters used were: slice thickness 8 mm, flip angle 20°, Repetition time/ Echo time = 3 ms/7.5 ms.

In the ischaemic cardiomyopathy (IHD) patients and healthy controls areas of LGE were visually scored as absent or present. No healthy volunteers had areas of LGE, therefore quantitative analysis was only undertaken on the IHD patients using the full-width half maximum (FWHM) technique which uses half of the maximal signal within the area of enhancement as the threshold. It was performed by contouring of the endo and epicardial borders, avoiding papillary muscle, blood pool and trabeculations. FWHM has been found to be the most reproducible method of quantification for LGE irrespective of aetiology [80]. LGE was expressed as a percentage of total left ventricular mass.

### 2.4.8 $^{31}$Phosphorus magnetic resonance spectroscopy

The methods for $^{31}$P magnetic resonance spectroscopy at 3 and 7 tesla are explained in the methods section of chapter 6.

### 2.4.9 Statistical analysis

All statistical analysis was performed with commercially available software packages (IBM SPSS Statistics, version 22, Chicago, USA). Data were tested for normality using the D'Agostino and Pearson omnibus normality test and presented as mean ± standard deviations, unless otherwise specified. For 2 group comparisons the Student's t test or Mann Whitney U test was used. One-way ANOVA with post hoc Bonferroni's multiple comparisons test or Kruskal-Wallis H with post hoc Dunn's multiple comparison tests were performed as appropriate for multiple groups. Correlation was assessed using the Pearson or Spearman method as appropriate.

Additional statistical methods that are specific to a results chapter are described within the appropriate methods section.

# *Chapter 3*

# *In the presence of a patent foramen ovale paradoxical embolism risk increases with atypical right atrial blood flow*

## 3.1 Abstract

**Background**

Despite the fact that stroke is a leading cause of disability, in up to 40% of cases no cause is found on routine clinical investigation. Although a patent foramen ovale (PFO) is an attractive mechanism to explain cryptogenic stroke, using current imaging techniques, distinguishing between a causative rather than an incidental PFO remains elusive.

I hypothesised that, in the presence of a PFO, atypical right atrial (RA) flow patterns would be linked to embolism risk by increasing the shunting of blood, and as such thrombus through the PFO. In order to investigate this I assessed RA flow patterns and interatrial shunt size in participants with a PFO and determined whether these metrics predicted the incidence of paradoxical embolism.

**Methods**

3 groups of participants were recruited to the study; 1) patients with presumed paradoxical embolism via their PFO (n = 20) 2) participants with a PFO but no embolism (n = 12) and 3) participants without an embolism or a PFO (n = 28). All underwent RA 4D flow assessment, bubble transthoracic echocardiography and transcranial Doppler to determine interatrial shunt size. Atypical RA flow was defined as any pattern that did not demonstrate classical vortical flow.

**Results**

RA flow patterns were significantly different in the embolism + PFO group compared to all controls, (P = 0.0002). In addition, whilst flow patterns were similar between the no embolism, no PFO and no embolism + PFO groups, they were both different from that seen in the embolism + PFO group, which had a higher incidence of atypical RA flow patterns (P = 0.0067).

When considering all the participants with a PFO (n = 32), the presence of an atypical flow pattern was 11.5 times more common in those who had an embolic event (P = 0.002, Fisher's exact test). To explore whether this effect was mediated by changing the degree of shunting, moderated multiple regression was performed. This showed that flow patterns were related to shunt grade (a pathway, β 34.0, P <0.01), and that shunt grade was related to embolism incidence (b pathway, β 0.08, P <0.01). As the a and b pathways were significant, mediation analysis was tested using 2,000 bootstrap resamples to generate a 95% confidence interval (bias corrected) of the indirect effect. This showed that the effect of an atypical flow pattern upon an embolic event is indeed mediated by increasing the shunt across the PFO (CI 0.45-18.42). As the direct effect of flow patterns on embolic risk becomes insignificant (c1 pathway, P = 0.06) this suggests full mediation.

**Conclusions**

Participants with a PFO and an atypical RA flow pattern were 11.5 times more likely to have had an embolic event. This increased embolic risk seems to be mediated via increasing the

shunt size across the PFO. As a result, not only will identification of the presence or absence of RA classical vortical flow in individuals presenting with a cryptogenic stroke help distinguish a causative PFO, it may also identify patients with a PFO who are at elevated risk of future embolism.

## 3.2 Introduction

Stroke remains the most common cause of serious long term disability in the developed world [81] . The majority of strokes are ischaemic, but up to 40% of strokes are cryptogenic and no cause can be identified [82, 83]. There has been much interest in attempting to identify potential risk factors for 'cryptogenic' strokes, with the aim of reducing the likelihood of recurrent events. The presence of a patent foramen ovale (PFO), which theoretically allows paradoxical embolism from the right to left atrium [47] has been a major focus of this research. Cryptogenic stroke (CS) and PFO in younger patients (<55 years old) [47, 84-88] are strongly associated, with PFO prevalence rates of up to 56% and in the elderly a PFO is more frequent in patients with CS than in patients with a known cause of stroke [89].

However, given that a PFO is a natural variant found in approximately 25% of the population [44], distinguishing this as a causative factor in stroke remains a challenge, and notwithstanding the small number of cases where clot has been visualised within the PFO of embolic stroke [46, 90], in the majority of cases the casual link is assumed rather than proved [45].

As the link between PFO and embolic events remains unclear, the management of these patients remains controversial. Three randomised control trials comparing PFO closure to standard medical therapy failed to show superiority of PFO device closure [91-93]. However there has been much criticism of these trials in terms of selection bias, crossover, power and device choice [94] and a better way of identifying those at risk of embolus with a PFO is needed.

The Risk of Paradoxical Embolism (RoPE) Study has attempted this through creation of an index score based on clinical and imaging parameters [95]. Other studies focused upon identifying single measures of right atrial (RA) or PFO anatomy as evidence of the PFO being causative in the 'cryptogenic' event. In some, but not all studies, a mobile interatrial septum (IAS) with or without an atrial septal aneurysm [89], a larger PFO with a substantial shunt especially at rest [96] and a more prominent Eustachian valve (EV) [97] were identified [98]. However no one factor was conclusive for involvement of the PFO in the cryptogenic stroke. However, given that it is RA blood flow, rather than anatomical variation itself that is likely to be responsible for paradoxical embolism I propose that this is a better way of characterising those at risk of paradoxical embolism. I hypothesise that the behaviour of the blood within the right atrium and the subsequent flow pattern would influence whether blood shunts across a PFO and may provide additional value in identifying whether a PFO is a 'culprit' rather than incidental finding.

Recent developments in cardiovascular magnetic resonance (CMR) have facilitated the measurement of time resolved 3-dimensional flow patterns (4D flow) [99] within the right atrium. As a result, I aimed to use CMR to characterise the types of RA flow patterns and determine the prevalence of these flow patterns within 1) patients with a PFO who had experienced an embolic event, 2) the normal population with no embolic event and a PFO and 3) the normal population with no embolic event and no PFO.

## 3.3 Methods

This study was approved by Hampshire B ethics committee (REC Ref 12/SC/0287) and all participants gave written informed consent.

### Study population

20 patients (embolism + PFO group) were prospectively recruited upon acceptance for PFO closure following an embolic event. Patient inclusion criteria required a history of stroke, transient ischemic attack (TIA), coronary or peripheral embolism, thought to be secondary to paradoxical embolism via their PFO. Imaging evidence of end organ infarction/ischaemia was required for inclusion in the study. Patients over 60 years of age were excluded, as were patients with contra-indications to CMR scanning. The decision to close patients PFO's was made by their treating physicians and a multi-disciplinary panel including neurologists, non-interventional cardiologists and interventional cardiologists. This panel also decided upon the need for additional investigations for other causes of the ischaemic event prior to PFO closure. Patients were only included if paradoxical embolism across their PFO was thought to be the cause of the ischaemic event. 40 matched controls with no history of cardiac disease or stroke were recruited. The increased number of volunteer to patient participants was in order to identify approximately 10 controls with a PFO (no embolism + PFO group) and approximately 30 controls without a PFO (no embolism, no PFO group).

## Study protocol

All participants underwent prospectively gated 4D flow CMR scanning and anatomical right atrial data acquisition at 3T.

## Anatomical CMR acquisition and image analysis

Balanced steady-state free precession (bSSFP) cine or gradient echo sequences acquired during a single breath hold were used for anatomical measurements. Real time free breathing cine images were acquired in the horizontal long axis (HLA) view to assess for IAS mobility. The peak velocity in the inferior vena cava (IVC) was measured using in-plane phase contrast velocity mapping. Data was analysed using cmr42©(Circle Cardiovascular Imaging Inc, Canada). All data were analysed in a blinded fashion. The data from the 40 controls (no embolism ± PFO) were analysed first in order to establish the range of normal anatomical findings and flow patterns seen within the right atrium, this was then compared to the embolism PFO group data.

### Anatomical measurements

A modified short axis view was acquired to visualise the IVC inflow in to the RA. In atrial diastole the EV length was measured and the distance across the RA from inside edge to inside edge of the RA wall measured at the same position. The percentage of the RA inflow diameter occupied by the EV was calculated. The angle between the EV and the wall of the IVC was also measured, as was the angle between the IVC and IAS at the junction of these two structures.

The maximal displacement of the IAS from its midpoint in atrial diastole was measured on the HLA view. A reference line was placed along the IAS at atrial diastole and the maximal displacement of the IAS either side of this reference line was measured. The same procedure was repeated, in 47 of the participants, for real time images to assess whether the intra-thoracic pressure changes seen during respiration altered this mobility.

## Four dimensional flow data post processing and analysis

All 4D flow CMR data were corrected for eddy currents, Maxwell terms and velocity aliasing. Corrected velocity data was imported into 3D visualisation software where cross sectional measurement planes were placed in the IVC, after the entry point of the hepatic veins and the SVC. Particle traces were then emitted from these planes. These particle traces took the form of pathlines which follow the path of virtual mass-less particles [100] aligned with the local velocity field and tracked over time [101]. The interaction of the pathlines from the IVC and SVC were visually assessed and graded as classical vortical (typical) flow or non-classical (atypical) flow.

Further measurements were undertaken using the 4D flow data. The IVC flow was extracted from the IVC plane and in Matlab the component of the IVC flow angled towards the IAS was extracted. The maximum velocity of the jet in space and time was recorded. An additional cross-sectional measurement plane was placed at the junction of the IVC/right atrium. The angle between the particle traces from this IVC entry plane and the IAS was calculated. A measurement plane was placed on the IAS using cine images acquired in the same table position for placement reference. The percentage of particle traces from the

IVC measurement plane that were incident on the IAS plane was calculated using customised Matlab software [102]. The relative orientation (antero-posterior, right-left and head-foot) of the IVC and SVC were calculated using the offset between the centres of the IVC and SVC planes. The directions were either positive or negative with a positive value in 1) the antero-posterior direction meaning the IVC is posterior to the SVC; 2) the right-left position meaning the IVC is orientated more to the left (i.e. medially) to the SVC. All head-foot values were negative meaning the IVC is below the SVC.

## Assessment for a patent foramen ovale

All participants underwent both transthoracic echocardiogram (TTE) and transcranial Doppler (TCD) with bubble contrast injection. 3 injections were undertaken, 1 without a Valsalva manoeuvre and 2 with a Valsalva. Contrast injections consisting of 9mls of normal saline, 0.5ml of blood and 0.5ml of air vigorously mixed using a three way tap were used. Participants were instructed how to perform a Valsalva manoeuvre and adequate performance of this was confirmed by bowing of the atrial septum into the left atrium after release of the Valsalva on TTE and a reduction in TCD peak velocity of 25-30%.

### Transthoracic bubble echocardiogram

Transthoracic echocardiography was performed using a standard ultrasound transducer (Philips iE33 Medical Systems, The Netherlands). Apical 4 chamber views focused on the interatrial septum were acquired with contrast injections, with and without Valsalva manoeuvers as described above. The number of bubbles transiting to the left atrium, within 3 cardiac cycles of right sided chamber opacification, were graded as follows: Grade 0: 0

bubbles, Grade 1: 1-5 bubbles, Grade 2: 5-25 bubbles, Grade 3>25 bubbles and Grade 4: chamber opacification [103].

### Transcranial Doppler

Transcranial Doppler ultrasound was performed with bilateral 2-MHz probes fastened to the temporal window by means of a commercial probe holder (Compumedics DWL, Singen, Germany). The middle cerebral artery (MCA) was insonated between 50 to 60mm; optimised to obtain the best signal. Recordings were undertaken, using DWL QL 2.8 software, for 2 minutes following contrast injections. The number of embolic tracks seen on the power M-mode and Doppler spectrogram in real time were counted and graded from I-V according to the Spencer grading [104]; Grade 0: 0, Grade I: 1-10, Grade II: 11-30, Grade III: 31-100, Grade IV: 101-300, Grade V >300 or shower effect.

### Transcranial Doppler during PFO closure

18 of the 20 patients underwent TCD monitoring during their PFO closure procedure. Data was collected for the number of embolic tracks after contrast injections with a catheter via the femoral vein from the IVC.

## 3.3 Statistics

Likelihood ratio's with Fisher's exact test were used to assess categorical data. To assess the associations between flow patterns (categorised as typical: classical vortical, atypical: other flow patterns) and morphological features binary logistic regression was performed using parameters with significant correlations to flow pattern. Kappa statistics were derived

to assess intra and inter-observer agreement for the assessment of RA flow patterns. A multiple mediator model developed by Preacher and Hayes was used to assess the mechanism of the interaction of RA flow patterns, grade of embolic shunt and presence of an embolic event, with 2,000 sample bootstrapping of indirect effects. P values <0.05 were considered significant.

### Reproducibility

Each RA flow pattern was blinded and graded twice by the same operator; the intra-observer Kappa value was excellent at 0.90 (95% CI 0.78-0.98). A second operator blinded to the grading scores of the first operator graded 20% of the data with **Figure 3.1** as reference for the defined flow patterns. The data sets were selected across the 4 categories to ensure proportional representation of the different flow patterns, but with cases selected at random within each category. Inter-observer variability was very good with a Kappa value of 0.88 (95% CI 0.60-1.0).

## 3.4 Results

### Participant characteristics

3 groups of participants were recruited to the study. Group 1-'embolism + PFO' consisted of 20 patients (10 male (50%), mean age 45 ± 10 years), scheduled for closure of their PFO following a suspected paradoxical embolism; of these 14 (70%) had a history of stroke, 4 (20%) TIA and 2 (10%) an embolic myocardial infarction, see **Table 1.1.** 40 age, gender and blood pressure matched (27 male (68%), mean age 43 ± 13 years) controls were also

studied comprising of 12 participants with no embolism but with a PFO (group 2) and 28 controls without embolism or a PFO (group 3).

**Table 3.1: Demographics and clinical characteristics.**

| | **All Controls N=40** | **Embolism + PFO N=20** | **P value** |
|---|---|---|---|
| **Age, years** | 43 ± 13 | 45 ± 10 | 0.544 |
| **Male, %** | 68 | 50 | 0.195 |
| **Systolic blood pressure, mmHg** | 127 ± 14 | 129 ± 16 | 0.747 |
| **Diastolic blood pressure, mmHg** | 75 ± 11 | 78 ± 11 | 0.278 |
| **BMI, kg/m$^2$** | 24.6 ± 4.4 | 27.1 ± 3.5 | 0.034 |
| **Heart rate, beats per minute** | 65 ± 10 | 65 ± 7 | 0.616 |
| | **Medications, n (%)** | | |
| **Antiplatelet** | - | 13 (65) | <0.0001 |
| **Anticoagulant** | - | 7 (35) | <0.0001 |
| **Antihypertensive** | 1 (3) | 5 (25) | 0.013 |
| **Statin** | 2 (5) | 13 (65) | <0.0001 |

Values are mean ± standard deviations or percentages. BMI indicates body mass index; PFO, patent foramen ovale.

## Right atrial anatomical variation

In agreement with previous studies [89] the IAS was more mobile in the embolism + PFO group compared to all controls (8.3 ± 2.9mm vs 6.8 ± 2.2mm, P = 0.030), see **Table 3.2**. 35% of the embolism + PFO group had IAS mobility ≥10mm consistent with an interatrial septal aneurysm[105], compared to 8% of controls (P = 0.006). The trend towards this mobility difference was also seen on real time imaging for the 47 participants who underwent this (embolism + PFO group 10.3 ± 4.2mm compared to 9.1 ± 3.4mm, P = 0.297) and there was a reasonable correlation between these two measures of IAS mobility (r = 0.642, P = 0.0001). The significant difference in mobility was due to the movement of the IAS from the midpoint towards the left (embolism + PFO group 6.5 ± 3.1mm vs all controls 4.4 ± 3.3mm, P = 0.028 on breath-hold measurements), rather than the movement towards the right which was not significantly different (P = 0.527). The IAS movement was not related to the type of flow pattern seen suggesting that the movement is not simply a consequence of the right atrial blood flow (r = 0.99, P = 0.454).

The right-left and antero-posterior position of the IVC relative to the SVC was different between the embolism + PFO group and controls. In the embolism + PFO group the IVC and SVC were further apart in the RL orientation but closer together in the AP direction. Otherwise other anatomical parameters measured were found to be similar between groups.

**Table 3.2: Anatomical findings.**

| | All Controls N=40 | Embolism PFO N=20 | P value |
|---|---|---|---|
| **Interatrial septal mobility (movement towards left), mm** | 6.8 ± 2.2 (4.4 ± 3.3) | 8.3 ± 2.9 (6.5 ± 3.1) | 0.030 (0.028) |
| **Presence of interatrial septal aneurysm ≥10mm, no (%)** | 3 (8) | 7 (35) | 0.006 |
| **Real-time interatrial septal mobility (movement towards left), mm** | 9.1 ± 3.4 (5.6 ± 4.3) | 10.3 ± 4.2 (7.7 ± 3.4) | 0.297 (0.092) |
| **Angle of IVC to interatrial septum, °** | 122 ± 25 | 119 ± 22 | 0.606 |
| **Eustachian valve length, mm** | 8.9 ± 4.5 | 8.1 ± 4.1 | 0.566 |
| **Inflow diameter at Eustachian valve, mm** | 34.4 ± 5.7 | 32.3 ± 5.3 | 0.176 |
| **Percentage of Eustachian inflow diameter occupied by Eustachian valve, %** | 25.3 ± 11.4 | 25.1 ± 12.2 | 0.945 |
| **Angle of Eustachian valve to IVC, °** | 126 ± 18 | 124 ± 22 | 0.755 |
| **Antero-posterior position of IVC to SVC, mm** | 15.2 ± 7.0 | 10.4 ± 9.3 | 0.034 |
| **Right-left position of IVC to SVC, mm** | 5.6 ± 7.6 | 12.0 ± 9.2 | 0.007 |
| **Head-foot position of IVC to SVC** | -86.2 ± 25.4 | -88.6 ± 14.4 | 0.701 |

Values are mean ± standard deviation. PFO indicates patent foramen ovale; IVC, inferior vena cava; SVC, superior vena cava.

## Right atrial flow pattern variation

Four differing patterns of IVC and SVC blood flow interaction were identified (**Figure 3.1**); 1) classical vortical ('typical') flow where the IVC and SVC flow turn in a clockwise vortex[8]; 2)spiral-vortical flow, where the IVC forms a vortex whilst the SVC passes laterally and is then enveloped in a spiral fashion by the IVC; 3)spiral flow where the IVC and SVC combine in a spiral; 4)complex flow, involving multiple vortices arising from the IVC and SVC flow. Flow patterns 2-4 when combined were classified as non-classical (atypical) flow.

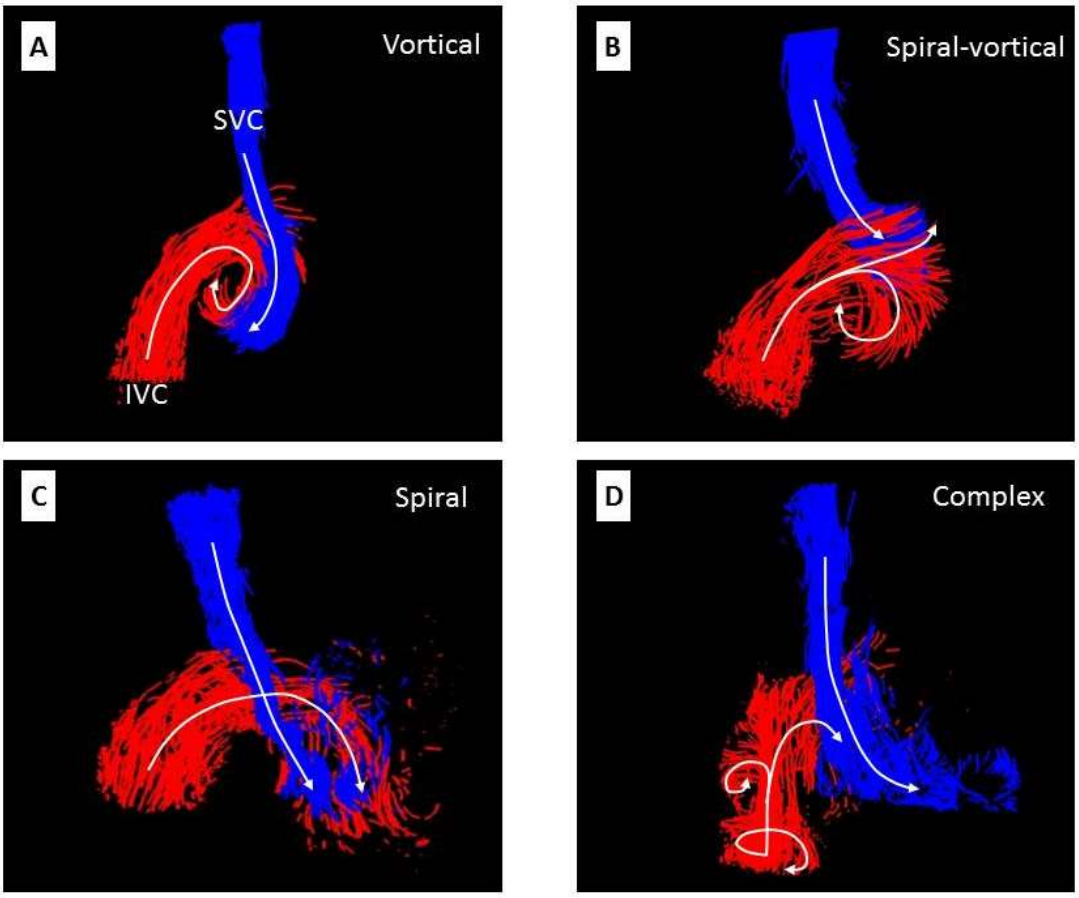


***Figure 3.1:*** *Right atrial flow patterns. The four flow patterns are* ***(A)*** *vortical,* ***(B)*** *spiral-vortical,* ***(C)*** *spiral and* ***(D)*** *complex. Inferior vena cava (IVC) blood is red, superior vena cava (SVC) blood is blue.*

In all controls (no embolism ± PFO) the most frequent flow pattern seen was vortical (56%), followed by spiral-vortical (26%) and spiral (18%). In the embolism + PFO group the most common flow pattern observed was spiral-vortical (55%), followed by spiral (30%), vortical (10%) and complex (5%). Apart from the 1 patient with complex flow, the other 3 flow pattern classifications were seen across groups, however the frequency of the flow patterns between the embolism + PFO group and all controls was significantly different (P = 0.0002, **Figure 3.2A**).

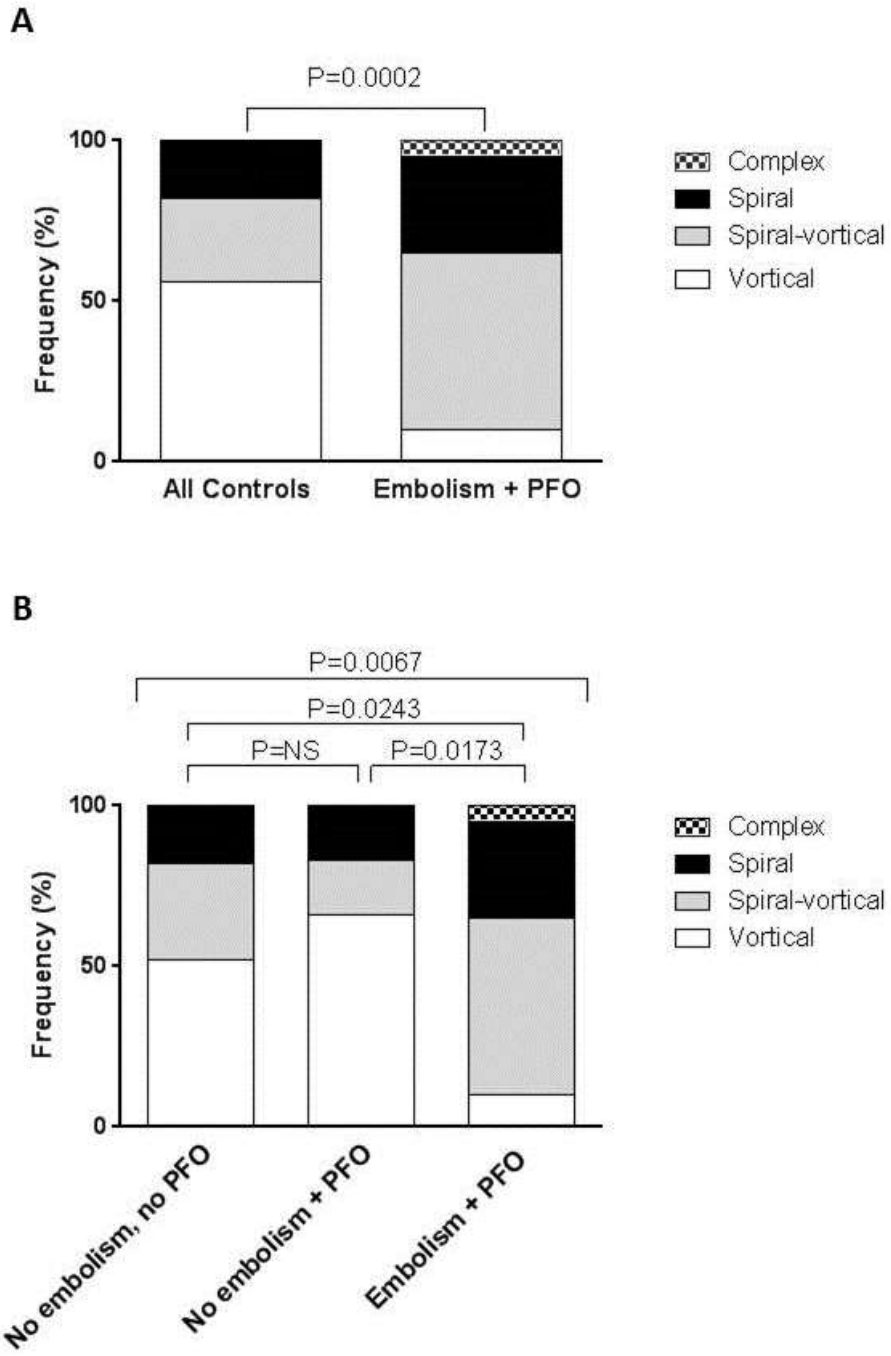


***Figure 3.2:*** *Prevalence of right atrial flow patterns in* ***(A)*** *all controls compared to the embolism + PFO group and* ***(B)*** *no embolism, no PFO group; no embolism + PFO group compared to embolism + PFO group. NS=non-significant.*

The 2D peak IVC velocity and the derived 4D flow peak velocity of the blood directed towards the IAS were significantly different between the embolism + PFO group and all controls, with the embolism + PFO group having a 14-20% higher peak velocity than controls. The percentage of the IVC blood flow upon the IAS was also higher for the embolism + PFO group compared to all controls (P = 0.018), see **Table 3.3**.

**Table 3.3: Flow parameters.**

| | **All Controls N=40** | **Embolism PFO N=20** | **P value** |
|---|---|---|---|
| **IVC peak velocity (2D), m/s** | 0.55 ± 0.18 | 0.68± 0.24 | 0.036 |
| **Peak velocity of IVC flow directed towards IAS, m/s** | 0.57 ± 0.13 | 0.80 ± 0.24 | <0.0001 |
| **% of IVC flow incident upon the interatrial septum** | 2.2 ± 2.8 | 4.1 ± 2.8 | 0.018 |
| **Calculated angle of IVC blood flow, °** | 125 ± 19 | 124 ± 18 | 0.766 |

Values are mean ± standard deviations or percentages. IVC indicates inferior vena cava; 2D, two-dimensional; IAS, interatrial septum.

## Factors determining the right atrial flow pattern

To test our hypothesis that the RA blood flow pattern would be influenced by the morphology of the RA, I assessed for any associations between the flow pattern and the anatomical features of the RA. In order to improve the power of our statistical analysis and

to simplify the flow pattern classification, I adopted the classification of 'typical' (type 1) and 'atypical' flow (types 2-4).

The anatomical/flow related features that had significant correlations were EV size (r = -0.336, P = 0.010), diameter at the EV (r = -0.440, P = 0.001), right-left orientation of the IVC to SVC (r = 0.510, P <0.0001), peak 2D IVC velocity (r = 0.352, P = 0.008) and peak 4D flow IVC velocity directed towards the IAS (r = 0.519, p <0.0001).

A binary logistic regression was performed to ascertain the effects of the five factors identified above, on the likelihood that participants have an atypical flow pattern. The logistic regression model was statistically significant, $\chi^2$ (5) = 32.50, P <0.0001. The model explained 62% (Nagelkerke $R^2$) of the variance in flow patterns and correctly classified 87% of cases. Increasing right-left distance with the IVC orientated more to the left of the SVC was 1.17 times more likely to exhibit atypical flow patterns (P = 0.018). No other variables came out as independently statistically significant.

## Association of flow patterns and occurrence of an embolic event

To assess whether the RA flow patterns influence the likelihood of an embolic event, the control group was subdivided into those with a PFO (no embolism + PFO) and those without (no embolism, no PFO); the no embolism + PFO group were then compared to the embolism + PFO group. Of the 12 participants in the no embolism + PFO group 9 of these had shunts on bubble TTE and TCD, whilst 1 had only a positive TTE and 2 (including 1 with non-diagnostic echo windows) only a positive TCD. All 20 participants in the embolism + PFO group had a positive TTE and 19 had a positive TCD.

The embolism + PFO group had more severe grades of right to left shunting at rest on both bubble TTE (≥ grade 3 70% embolism + PFO vs no embolism + PFO 18%) and bubble TCD (≥ grade III 40% embolism + PFO vs no embolism + PFO 0%). This was also true when a Valsalva manoeuvre was performed (**Figure 3.3**). Although the embolism + PFO group had more severe right to left shunts this only correlated modestly with the presence of an embolic event ($r = 0.444$, $P = 0.011$ for rest TCD and $r = 0.518$, $P = 0.002$ for TCD with Valsalva), suggesting that the occurrence of an embolic event involves additional factors as well as the degree of right to left shunting.

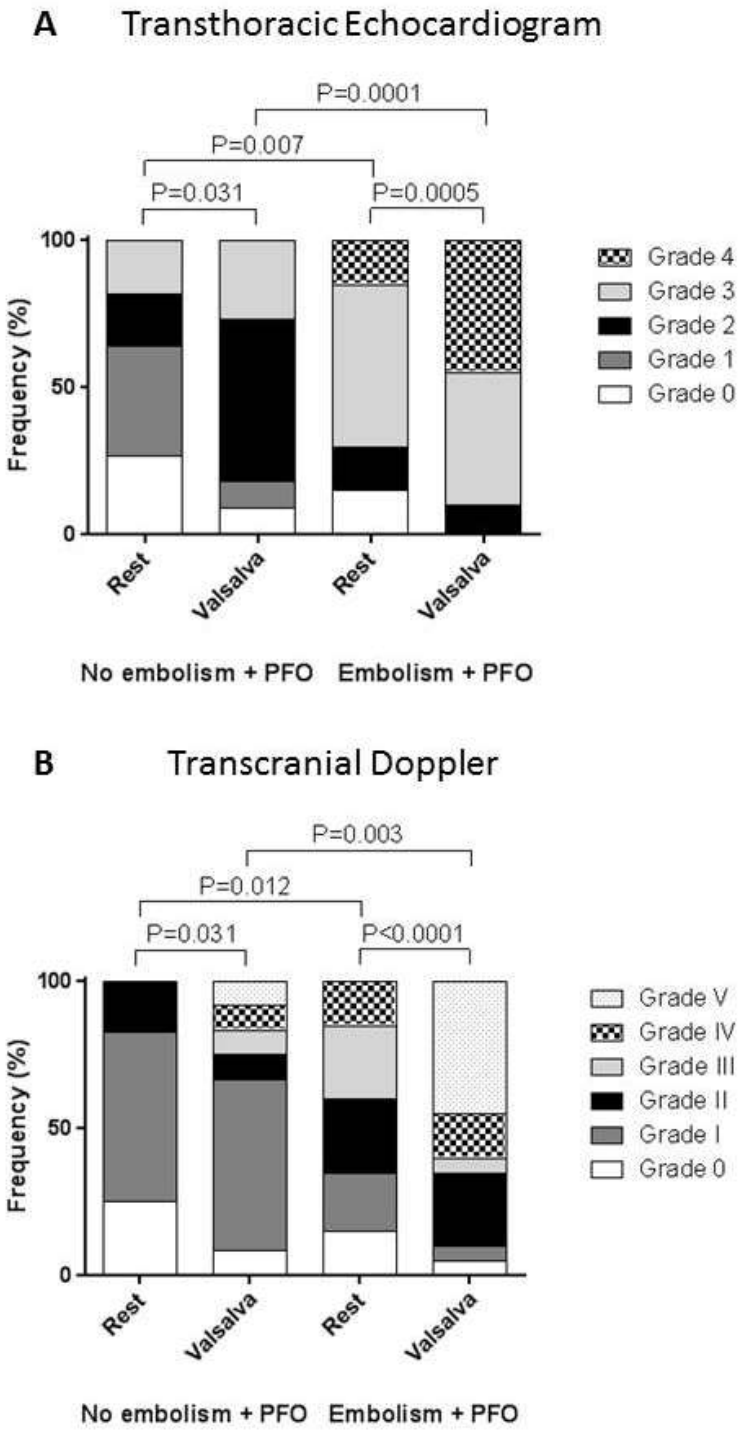


***Figure 3.3:*** *Quantification of the degree of right to left shunting in no embolism + PFO group compared to embolism + PFO group using* ***(A)*** *transthoracic bubble echocardiography and* ***(B)*** *bubble transcranial Doppler.*

When considering all the participants with a PFO (n = 32, embolism + PFO group and no embolism + PFO group), the presence of an atypical flow pattern was 11.5 times more common in those who have had an embolic event (P = 0.002, Fisher's exact test). To explore whether this effect was mediated by changing the degree of shunting, moderated multiple regression was performed. This showed that flow patterns were related to shunt grade (a pathway, β 34.0, P <0.01), and that shunt grade was related to embolism incidence (b pathway, β 0.08, P <0.01). As the a and b pathways were significant, mediation analysis was tested using 2,000 bootstrap resamples to generate a 95% confidence interval (bias corrected) of the indirect effect. This showed that the effect of an atypical flow pattern upon an embolic event is indeed mediated by increasing the shunt across the PFO (CI 0.45-18.42, **Figure 3.4**). As the direct effect of flow patterns on embolic risk becomes insignificant (c1 pathway, P = 0.06) this suggests full mediation.

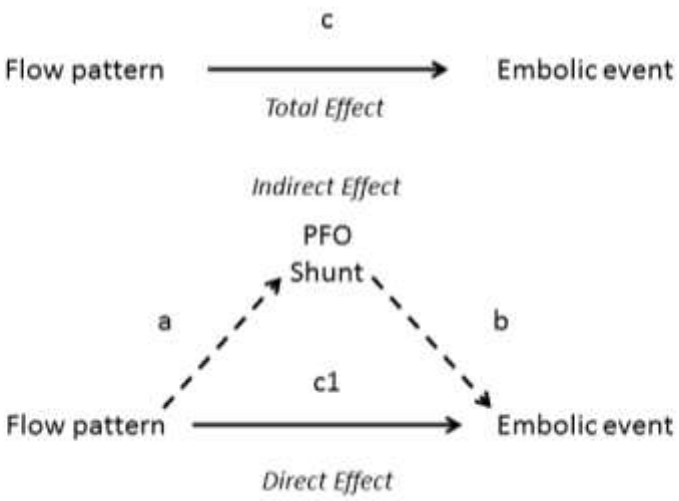


| | Coefficient (β) | SE | P |
|---|---|---|---|
| Flow Pattern to PFO Shunt Effect (a pathway) | 34.06 | 11.49 | 0.0059 |
| Direct Effect of PFO Shunt on Embolism (b pathway) | 0.08 | 0.03 | 0.0090 |
| Total Effect of Flow Pattern on Embolism (c pathway) | 2.89 | 0.96 | 0.0027 |
| Direct Effect of Flow Pattern on Embolism (c1 pathway) | 2.26 | 1.24 | 0.0681 |

***Figure 3.4:*** *Multiple mediator model assessing the mediation of the increased risk of embolism seen with an atypical right atrial flow pattern.*

## Transcranial Doppler during PFO closure

TCD data during the PFO closure were available for 18 of the 20 embolism + PFO group. Comparing injections from the IVC to a peripheral cannula in the antecubital fossa the most severe shunting occurred with bubble injections from the IVC, but this was not significantly different to the injections from the antecubital fossa cannula, suggesting that peripheral injections are a good surrogate for IVC shunt grade quantification (**Figure 3.5**). The PFO was sized during the closure procedure; the mean PFO size was 7.9 ± 3.0 mm. As expected

this correlated with the degree of right to left shunting seen during IVC injection (r = 0.469, P = 0.05), as well as rest bubble TCD (r = 0.566, P = 0.014) and TTE (r = 0.707, P = 0.001) via an antecubital fossa injection.

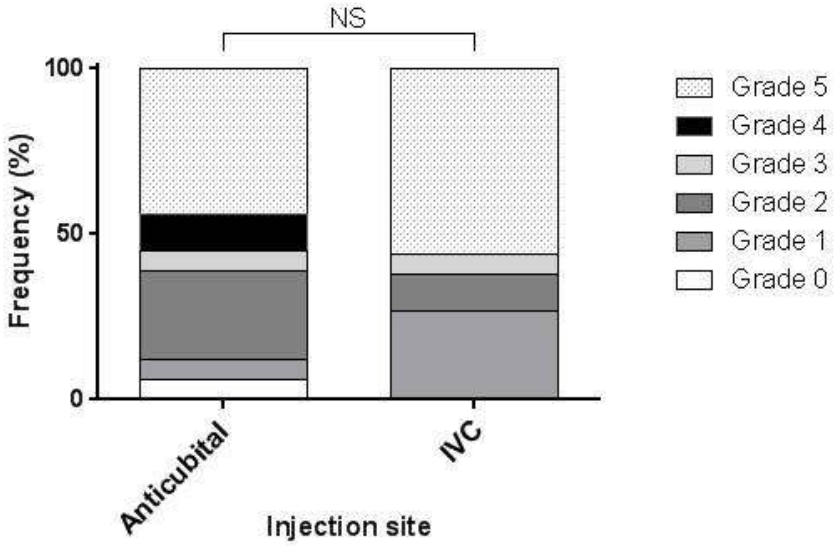


***Figure 3.5:*** *Shunt grade quantification using transcranial Doppler, with a Valsalva manoeuvre, for embolism + PFO patients undergoing closure of their PFO comparing two different routes of bubble contrast injection (the anticubital fossa versus the inferior vena cava (IVC)). NS = non-significant.*

## 3.3 Discussion

Distinguishing between a causative rather than an incidental PFO in cryptogenic events has remained an elusive goal [106]. In this study, novel 4D flow CMR techniques were used to investigate the differing blood flow patterns in the RA and to assess for relationships between RA flow patterns, the degree of right to left shunting and an embolic event in

participants with a PFO. I confirmed the findings of previous studies [107] that the IAS was more mobile in patients with a PFO compared to controls, with a higher percentage meeting diagnostic criteria for an interatrial septal aneurysm. It was also demonstrated that classical RA vortical flow, as previously described [8], was present in only around half of all my normal controls. In the embolism + PFO group, the pattern of RA flow patterns was significantly different to that of my control groups without embolism and there was a greater prevalence of atypical flow patterns. The generation of these atypical flow patterns was related to morphological and flow related parameters, with the relative right-left position of the IVC to SVC independently predictive of the generation of an atypical blood flow pattern. These structural changes may therefore represent a surrogate quantitative measure for the presence of atypical flow patterns.

The degree of right to left shunting on bubble echocardiography and TCD was greater in the embolism + PFO group compared to the no embolism + PFO group. Importantly, I show that in the presence of a PFO, participants with atypical flow patterns were more likely to have had an embolic event than those with classical vortical flow.

### Anatomical variation and association with embolic events

Much previous work has focused upon single anatomical measurements to distinguish between an incidental versus culprit PFO in embolic events [45, 89, 107]. Assessing these previously identified anatomical variants, I found the mean IAS mobility in the PFO + embolism group to be higher than in all the controls; interestingly the mobility difference was due to the movement of the IAS from the midline towards the left atrium. This

direction of movement may mechanistically explain the association of this finding in the embolism + PFO group, as this movement indicates right atrial pressure is exceeding that of left atrial pressure; this is a necessary physiological condition for the passage of a paradoxical embolism from the right to left atrium.

I did not find the Eustachian valve to be more prominent in our embolism + PFO group compared to controls, however the role of the EV as a co-factor in stroke risk is controversial and results have varied between studies [97, 108]. Data from post mortem studies have found the mean size of a PFO to be 4.9mm [109], the data from the closure procedures of our embolism + PFO group found the mean PFO size to be larger, which according to some studies suggests a greater likelihood for a causative role of the PFO [96]. However, as in many previous studies no single anatomical variable was able to provide sufficient discrimination on an individual basis between a participant with a paradoxical embolic event and a PFO and a control participant with no embolism but a PFO.

### Atypical right atrial blood flow patterns and mechanism of embolic stroke

The four identified patterns of RA flow were found at significantly different frequencies between the embolism + PFO group and all controls (no embolism ± PFO). The PFO + embolism group had a higher proportion of atypical flow patterns compared to the combined control group where classical vortical flow was the predominant flow pattern. The orientation of the IVC more to the left of the SVC was found to be an independent predictor for the presence of an atypical blood flow pattern within our study. This offset

between the inflowing blood streams of the IVC and SVC resulted in a different flow interaction which appears to not favour the formation of the typical vortical flow.

The presence of vortical flow is thought to be advantageous in the cardiovascular system as it allows movement of fluid with minimal dispersion of energy [110]. Previous phase-velocity mapping studies [8] have identified that RA flow forms a clockwise vortex, associated with movement of the anterior part of the RA blood volume towards the inlet of the tricuspid valve. In the right atrium, the vortical blood flow may prevent shunting of blood across a PFO as the particles, including any thrombus, within the blood would be drawn towards the centre of the vortex. The precise mechanism by which the non-vortical blood flow patterns increase right to left shunting across a PFO is unclear. It may be that the non-vortical flow exerts a greater pressure upon the IAS and causes the PFO to open for longer or more fully. An alternative explanation is that, it may be due to more efficient transit of blood across the PFO, as the particles in the blood are less constrained than when a vortical flow pattern is present.

The degree of right to left shunting across a PFO has been mechanistically implicated in previous case-control studies [96]; with a greater degree of shunting associated with embolic events. The embolism + PFO group had more severe grades of right to left shunting across their PFO than the participants in the no embolism + PFO group. I found the relationship between the presence of an atypical RA blood flow pattern and an embolic event was fully mediated by the degree of shunting across the PFO. Hence, the blood flow pattern per se is

not the cause of embolism, but rather it is the effect of the flow pattern upon the severity of shunt across the PFO that increases the risk of embolism.

## Risk scoring strategies for identifying an implicated rather than incidental PFO in cryptogenic stroke

The RoPE study [95] created an index based upon the age, lack of conventional risk factors and infarction pattern seen on imaging of patients with cryptogenic stroke in order to stratify the likelihood that stroke was related to their PFO. The higher the score (maximum 10), the greater the likelihood that the PFO was implicated. The mean RoPE score in this study was 7, which equates to an attributable risk of the stroke being due to the PFO of 72% according to the RoPE model. Currently the RoPE index does not include any features of the PFO, however it may be that the inclusion of flow related or anatomical features, such as the presence of atypical RA flow and PFO shunt size may further refine this model and aid identification of which PFO's are more appropriate for closure, once an individual with a PFO has a cryptogenic event.

It is unlikely that any studies will be able to identify one single factor that can distinguish on an individual basis between a causative PFO in an embolic event and an incidental PFO. Even in patients who experience a PFO related embolic event the incidence is very low; population studies have estimated the yearly incidence of cryptogenic stroke in the healthy population with a PFO, to be as little as 0.1% [98]. This is because the occurrence of a paradoxical embolism via a PFO is a complex, dynamic event in which numerous factors have to concurrently exist; arterial embolism, venous thrombosis, interatrial connection,

orientation of the thrombus with the connection and a favourable pressure gradient for right to left shunting [98].

This study has shown that identification of right atrial flow patterns may provide additive diagnostic value, especially if used in combination with other clinical parameters and imaging features of the PFO, to help identify PFO's implicated in embolic events.

## 3.4 Limitations

This observational study is limited by a relatively small sample size in keeping with its proof-of-principle nature and hence, I cannot prove whether the observed relationship between atypical flow patterns and the occurrence of an embolic event are a causal finding. This would require a large population based longitudinal study. However given the low incidence of cryptogenic embolic events in those with a PFO it is unlikely that the necessary power would be reached.

As with other case-control studies within this area, patients were assumed to have had an embolic event due to their PFO based on the absence of other causes, rather than firm evidence. Equally although controls with a PFO had not suffered an embolic event it is impossible to know if this will occur in the future, patients and controls were well age matched to control for this confounder.

## 3.5 Conclusion

When compared to age matched controls with a PFO, patients with a previous embolic event and PFO exhibit more atypical blood flow patterns within their right atrium. The presence of an atypical flow pattern is related to an increased risk of an embolic event. Identification of atypical right atrial flow patterns may help better identify which patients are at risk of recurrent paradoxical embolism via their PFO and allow appropriate targeting of management strategies, including PFO closure.

# *Chapter 4*

# *Left ventricular 4D flow components are a repeatable and stable imaging parameter in health*

## 4.1 Abstract

**Background**

The function of the cardiovascular system is to maintain blood flow through the heart and vessels. Quantification and visualisation of left ventricular (LV) blood flow components are afforded by three dimensional, time resolved phase contrast magnetic resonance imaging (4D flow). However, few data exist upon the repeatability of these flow components and the variability of these parameters over time in a healthy population. I aimed to assess the repeatability of quantification of the LV flow components, including the volume and kinetic energy value for each component, and the variability of these parameters over time.

**Methods**

45 healthy controls underwent cardiovascular MR for 4D velocity and anatomical data acquisition. Of these 45 controls, 10 underwent a second scan within the same study visit (scan-rescan), whilst 26 returned for a second study visit (interval scan) with a median time interval of 52 days (IQR 28-57 days). A previously validated method was used to separate the LV-end diastolic volume (EDV) into four functional flow components based upon the location of the blood at the start and finish of the cardiac cycle. For each flow component the volume was related to the EDV (volume-ratio) and the kinetic energy was calculated over the cardiac cycle and measured at end-diastole (ED).

**Results**

The dominant LV flow component in healthy controls was the direct flow component (volume ratio 38 ± 4%); which is the LV inflow that passes directly to ensuing ejection. The direct flow component also possessed the highest kinetic energy at ED (7.8 ± 3.0 microJ/ml). The coefficients of variation for the scan-rescan results varied between 2.5 to 9.2% for the volume ratio of the flow components and between 13.5 to 17.7% for the kinetic energy of the flow components. The interval scan results showed higher coefficients of variation with values ranging from 6.1 to 16.1% for the volume ratio of the flow components to 16.9 to 29.0% for the kinetic energy of the flow components. There were no significant differences in mean flow components volume ratio or kinetic energy between the interval scan 1 and 2 for the study population as a whole.

**Conclusions**

LV flow components relative volume and their associated kinetic energy values are highly repeatable and are stable within a population over time. However, the variability of these measures in individuals over time is greater than can be attributed to inherent sources of error in the data acquisition, post processing and analysis, suggesting that additional physiological factors may influence LV flow components volume and kinetic energy profiles.

## 4.2 Introduction

The main purpose of the cardiovascular system is to drive, control and maintain blood flow through the heart and vessels [2]. Insights into intra-cardiac blood flow are now afforded by the use of retrospectively ECG gated, three-dimensional, time resolved flow encoded MRI (3D+time = 4D flow) [3, 37, 72, 74, 111]. The 4D flow within the left ventricle (LV) can be separated into four functional flow components and the kinetic energy (KE) of the blood throughout the cardiac cycle can be quantified [3, 50, 74]. In healthy hearts these functional flow components have specific routes and energetics that may represent important aspects of normal ventricular function [48]. Typically a third of the inflow to the LV passes directly to the outflow in healthy hearts allowing a preservation of LV inflow KE, which may assist with an efficient systolic ejection phase. Alterations in left ventricular blood flow components have been found in patients with early clinically compensated dilated cardiomyopathy, where a substantial proportion of the inflow is retained within the LV and there is an associated decrease in preservation of the LV inflow KE [74]. These findings suggest that the volume and KE of the 4D flow components may contribute to early detection of cardiac pathology. 4D flow also provides a potential future tool for the evaluation of therapeutic interventions [112]. However the use of 4D flow components for early diagnosis and monitoring of changes in individual patients requires an understanding of the intra-subject repeatability of the measures and the variability of these parameters over time.

To date, studies reporting healthy control data have enrolled small numbers, typically 6-17 participants with data acquired at a single time point [3, 37, 72, 74]. To our knowledge no study

has assessed the stability of LV 4D flow components over time. Thus, this study aims to understand the stability of the LV flow components volume and kinetic energy profiles in health. In order to achieve this I first assessed the repeatability of the 4D flow data acquisition, post-processing and analysis, in order to understand the error associated with the technique. Subsequently I determined how these components change over time by repeating a data acquisition after a period of a few weeks.

## 4.3 Methods

### Study population

45 healthy volunteers were recruited. All participants had no contraindication to CMR scanning, no history of cardiac disease, nor symptoms of cardiac disease. This study was approved by the local research ethics committee and informed written consent was obtained from each participant.

10 of the participants underwent two 4D flow data acquisitions within the same study visit to assess 'scan-rescan' repeatability. Between each data acquisition the participant was removed completely from the scanner so each data set was acquired with the same potential real-life sources of variance, including subtle changes in subject positioning in the CMR system. 25 of the participants returned for a second 'interval' 4D flow data acquisition at least 10 days later.

### Study protocol

Prior to recruitment of this healthy volunteer cohort for the retrospectively ECG gated 4D flow sequence, optimisation of the data acquisition, post processing and analysis steps occurred, details of this are shown in the results section. All study participants underwent CMR scanning at 3T for retrospectively ECG gated 4D flow data acquisition and LV anatomical imaging. Kinetic energy for each blood component was recorded at end-diastole. KE values at this time point reflect the preservation of the inflowing kinetic energy prior to the rapid ejection of blood during systole. The KE at ED for each component was then divided by its volume to remove any variation due to LV cavity size.

### Intra- and Inter-observer variability

Intra-observer variability was determined by blinded assessment of 10 randomly selected data sets with each analysis separated by more than one month. Inter-observer variability was conducted independently by a second experienced observer with the same 10 datasets.

## 4.4 Statistics

Normally distributed data were analysed using the Student's t test for 2 group comparisons and one way ANOVA with post hoc Tukeys's multiple comparisons test for multiple groups. Assessment of repeatability was assessed by consideration of the absolute difference between the results obtained from scan 1 and 2 for each subject. The coefficient of

variation [113] was calculated for scan-rescan and interval scan repeatability and the data plotted in the form of a Bland-Altman plot.

## 4.5 Results

### Sequence optimisation

When developing the retrospectively gated 4D flow sequence, a major challenge was balancing the inevitable imaging trade-offs between the length of scan for data acquisition and the temporal and spatial resolution of the images acquired. I initially tested the sequence on healthy controls and the scan time with whole heart coverage was acceptable at ~15-20minutes. However when the sequence protocol was applied to a patient with a dilated left ventricle, I realised that the number of slices in the left-right direction provided inadequate coverage of the whole heart and that both ventricles were unable to fit in the acquisition volume. In order to allow an increased imaging volume whilst maintaining an acceptable data acquisition time I trialed the sequence parameter changes described in **Table 4.1**.

The compromises that were made to achieve an acceptable scan time were to increase segments from 2 to 3, increase the bandwidth from 700 to 1000 Hz/Pix, which together increased the temporal resolution from 40 ms to 52 ms. Total scan time was further reduced with phase partial Fourier in both phase encode directions, and 80 % slice resolutions. Average scan time for patients with these parameters was in the order of 20 minutes.

| | Parameter changed | Advantage | Disadvantage | Direct flow, %EDV | Retained inflow, %EDV | Delayed ejection flow, %EDV | Residual volume, %EDV | Parameter chosen and reason |
|---|---|---|---|---|---|---|---|---|
| **iPAT reference lines** | Integrated | Accurate respiratory and cardiac specific reference lines | Slower scan | 39 | 12 | 29 | 21 | Integrated, as scans already completed with this parameter. |
| | Separated and acquired in inspiration | Quicker scan as only one set of reference lines | Assessing for respiratory sensitivity to reference lines | 41 | 13 | 23 | 23 | |
| | Separated and acquired in expiration | Quicker scan as only one set of reference lines | | 40 | 15 | 23 | 22 | |
| **Contrast (tested in patient)** | No contrast | Use conventional gadolinium | Lower signal to noise ratio | 2 | 16 | 16 | 66 | No contrast as no significant quantification improvement and would be unable to perform LGE |
| | With MultiHance | Increase signal to noise ratio | Risk of allergy and unable to perform conventional LGE | 2 | 18 | 18 | 62 | |
| **Number of segments** | 2 segments | Higher temporal resolution | Longer scan | 35 | 24 | 18 | 22 | 3 segments as decreases scan time, whilst still achieving an acceptable temporal resolution |
| | 3 segments | Shorter scan | Lower temporal resolution | 38 | 20 | 17 | 25 | |
| **iPAT** | GRAPPA 2 | Increased SNR and fewer artefact | Longer scan acquisition | 44 | 17 | 10 | 27 | GRAPPA 2 for reduced artefacts |
| | GRAPPA 3 | Shorter scan acquisition | Decreased SNR and greater artefact | 44 | 10 | 18 | 27 | |
| **Slice resolution** | Full slice resolution without phase oversampling | Better spatial resolution | Longer data acquisition | 34 | 14 | 20 | 32 | No significant difference in data acquired therefore reduced slice resolution with phase oversampling utilised to reduce scan duration |
| | Reduced slice resolution with phase oversampling | Shorter data acquisition | Reduced spatial resolution | 36 | 14 | 20 | 30 | |

**Table 4.1: Sequence parameters changed; advantages and disadvantages of changes; results for each change of the four left ventricular flow components; parameter chosen and reason why.**

## Data analysis optimisation

The post-processing pathway for left ventricular 4D flow data is a multi-step workflow with both automated and user-dependent elements. Data is loaded into the analysis 'CMR tool' which creates a folder of cine images. The SA stack from these cine images are contoured at end diastole and end systole utilising a tool called Segment [73] to create a segmentation file, as described in the methods section. The segmentation file is used to create two binary masks which are then matched to the 3D cine PC-CMR data for analysis; hence any differences in the way the contours are drawn at ED and ES can influence the final results of the 4D flow. In particular I noted that the basal end diastolic and end systolic slice contoured particularly influenced the percentage of direct flow, as shown in **Table 4.2**.

**Table 4.2: Effects of differing left ventricular contours upon the volume ratio of each of the four flow components.**

| | Direct flow, %EDV | Retained inflow, %EDV | Delayed ejection flow, %EDV | Residual volume, %EDV | Comments |
|---|---|---|---|---|---|
| **Contours with partial ED frame, partial ES frame** | 25 | 15 | 16 | 44 | Low direct flow, high residual volume |
| **Contours with full ED frame, partial ES frame** | 46 | 16 | 14 | 24 | High direct flow, low residual volume |
| **Contours with partial ED frame, full ES frame** | 35 | 15 | 17 | 33 | Good data quality and in keeping with contours used in clinical practice |
| **Contours with full ED and full ES frame** | 28 | 15 | 16 | 41 | High residual volume |

Utilising the information gained from the different contour combinations above I devised a consistent method for contouring the basal slices of the SA cines. At end-diastole I ensured that the whole of the LV outflow track was included, using a partial slice if necessary to achieve this and at end systole I drew a full basal systolic slice ensuring no left atrial volume was included. This method of contouring is in keeping with those used when reporting our clinical CMR studies.

The flow data and the segmentation file are then reloaded into the CMR tool. Prior to any further analysis of the flow data the DICOM data exported from the MRI scanner requires background correction to remove any signal from static tissue such as the chest wall. To ascertain the order of background correction required I visualised a data set as shown in **Figure 4.1** below.

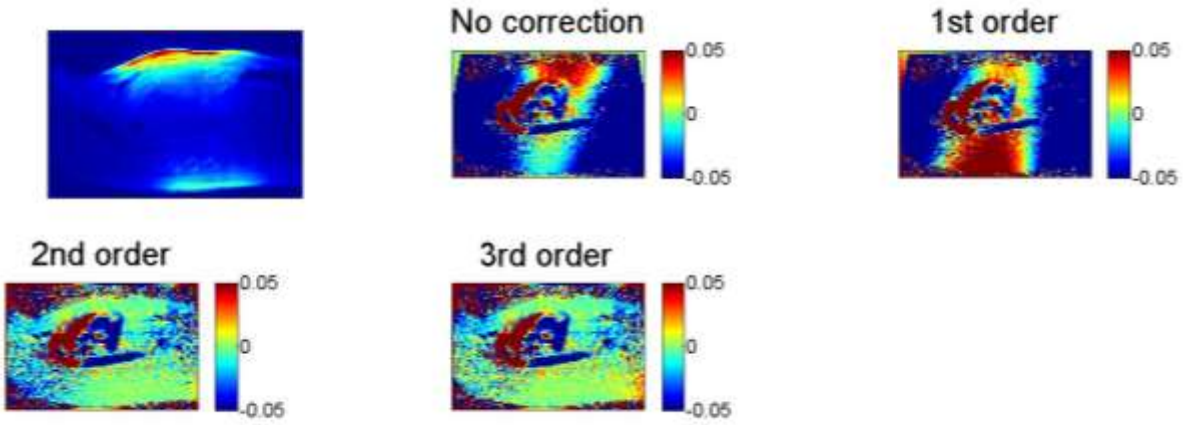


***Figure 4.1:*** *Background order correction. Uncorrected data showing heterogeneous signal in the chest wall, which becomes more homogenous as the order of the background correction increases.*

The 3rd order weighted least-squares fit to the static tissue of the measured velocity data, where the weighting function was obtained from a combination of the signal magnitude and the standard deviation of the velocity over time [3], gave the best background static tissue correction as demonstrated by the homogenous signal then present in the chest wall.

Datasets with >10% difference between the LV inflow and outflow volumes were excluded from the analysis in order to maintain data quality. However when some of these datasets were visualised in EnSight the anatomical 3 chamber view was offset to the 4D flow data volume suggesting that the participant had moved during the data analysis. In order to correct for this a Matlab tool was written that allowed overlay of the segmentation file generated from the SA cines onto the 4D flow magnitude data as demonstrated in **Figure 4.2** below.

This then allowed movement of the segmentation contours onto the overlying LV magnitude data. If the inflow/outflow mismatch then improved to <10% the dataset was included in the final analysis.

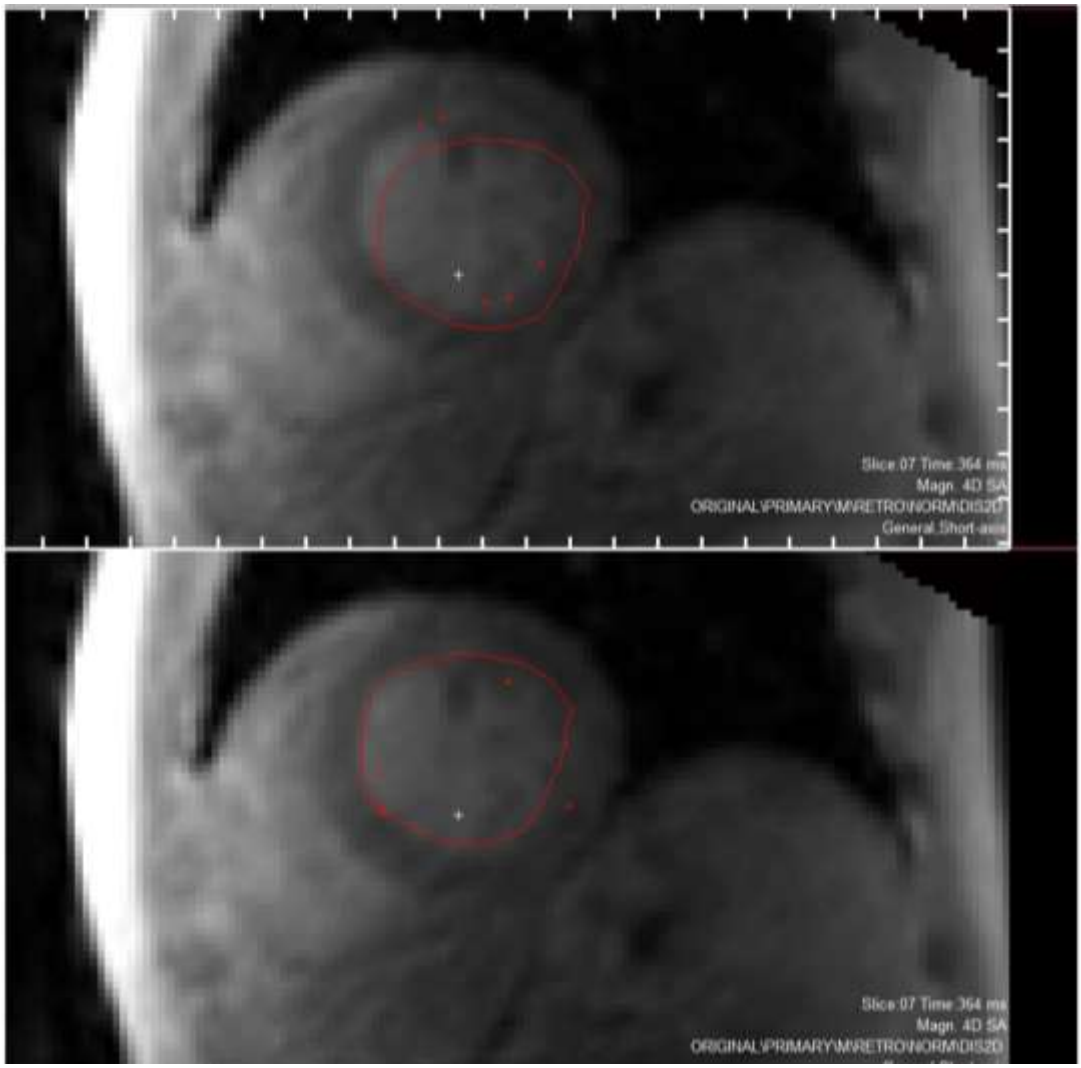


***Figure 4.2:*** *Magnitude data from the 3D cine PC-CMR sequence with the LV segmentation (red contour) overlaid. Note the misalignment in the top panel between the endocardial border of the LV and the contour due to participant movement. The bottom panel demonstrates the corrected alignment.*

## Participant characteristics

45 participants were recruited; mean age 54 ± 14 years (range 24-75 years) and 27 (59%) male. Demographic, anthropometric and routine CMR measurements are shown in **Table**

**4.3.** All LV volumes were within the normal range and the mean ejection fraction was 66 ± 4%.

**Table 4.3: Demographic, anthropometric and routine CMR measurements.**

| | **Controls N=45** |
|---|---|
| **Age, years** | 54 ± 14 (range 24-75) |
| **Male, %** | 59 |
| **Systolic blood pressure, mmHg** | 133 ± 20 |
| **Diastolic blood pressure, mmHg** | 78 ± 10 |
| **BMI, kg/m$^2$** | 24.7 ± 3.8 |
| **Heart rate, beats per minute** | 65 ± 13 |
| **CMR data** | |
| **LV ejection fraction, %** | 66 ± 4 |
| **LV end diastolic volume, ml** | 155 ± 31 |
| **LV EDV indexed BSA, ml/m$^2$** | 82 ± 14 |
| **LV end systolic volume, ml** | 52 ± 13 |
| **LV stroke volume, ml** | 103 ± 21 |
| **Cardiac output, L/min** | 6.5 ± 1.4 |
| **Left atrial ejection fraction, %** | 57 ± 6 |

Values are mean ± standard deviations. BMI indicates Body mass index; LV, Left ventricle; EDV, End diastolic volume; BSA, Body surface area

## 4D flow components volume and kinetic energy

All 45 data acquisitions passed data quality checks, with no significant difference in inflow versus ejected volume (inflow 82 ± 21ml, outflow 81 ± 22ml, P = 0.57). As found previously [3, 50, 74] the direct flow component as a percentage of the EDV was the largest of the four functional flow components (38 ± 4%), with the residual volume the second largest component (30 ± 4%). The retained inflow (16 ± 4%) and delayed ejection flow (16 ± 3%) were essentially equal (see **Figure 4.3A** and **4.3B**).

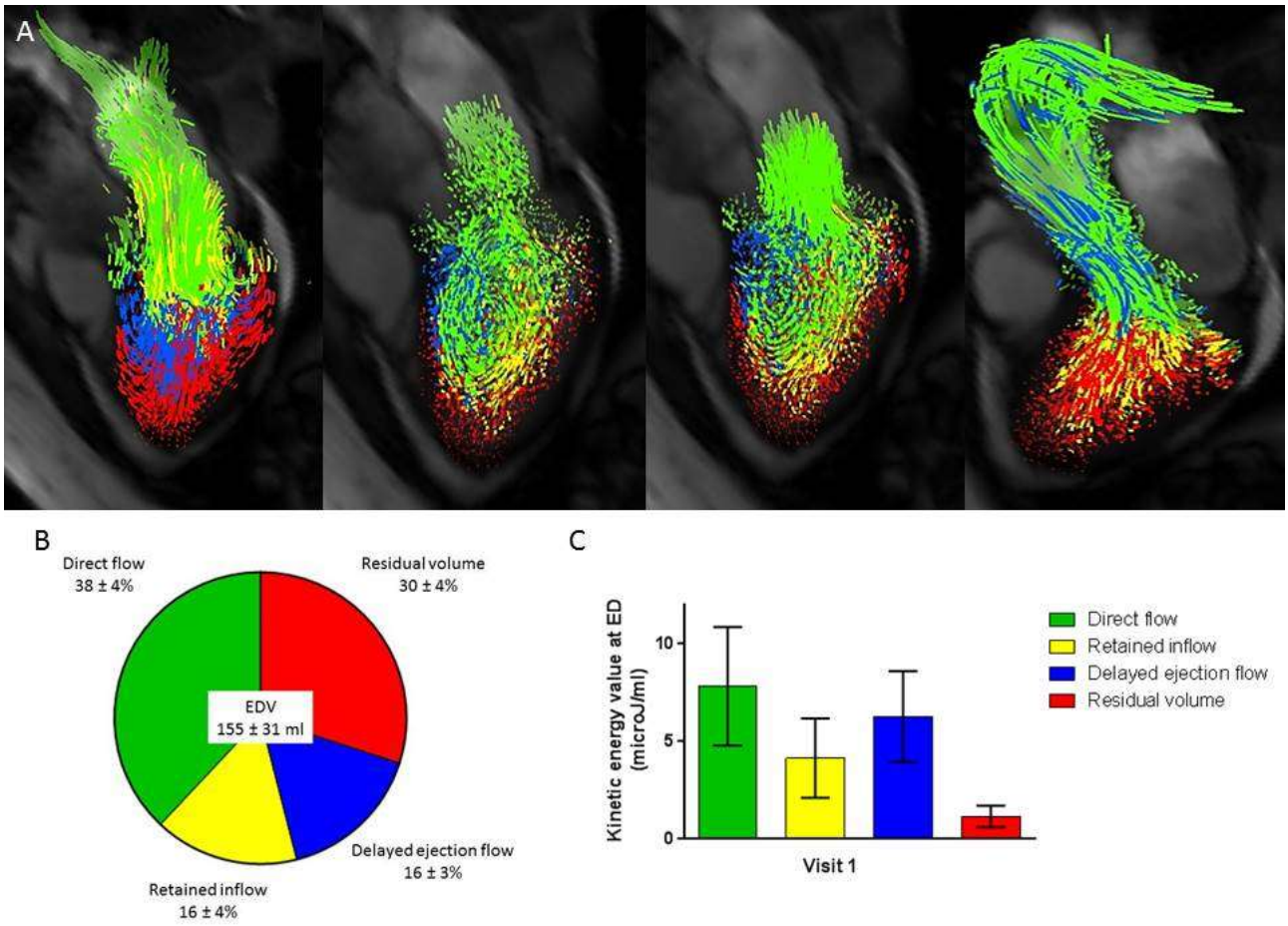


***Figure 4.3:*** *Visualisation and quantification of LV blood flow components volume and kinetic energy values at end-diastole.* ***(A)*** *Flow visualisation throughout the cardiac cycle from left to right panel; early diastole, diastasis, atrial contraction and systolic ejection.* ***(B)*** *flow components by percentage of EDV.* ***(C)*** *Kinetic energy at end-diastole related to blood volume of the four flow components.*

The results for multiple ANOVA comparisons with Tukey post-hoc testing for flow components as a percentage of EDV and Kruskal-Wallis test for KE at ED for the four flow components are shown in **Table 4.4**.

**Table 4.4: Multiple comparisons following ANOVA for flow components as a percentage of EDV and Kruskal-Wallis test for KE at ED.**

| | **Mean ± SD** | **Retained inflow (P value)** | **Delayed ejection flow (P value)** | **Residual volume (P value)** |
|---|---|---|---|---|
| **Multiple comparisons for volume, % EDV** | | | | |
| **Direct flow, %** | 38 ± 4 | <0.0001 | <0.0001 | <0.0001 |
| **Retained inflow, %** | 16 ± 4 | – | 0.88 | <0.0001 |
| **Delayed ejection flow, %** | 16 ± 3 | 0.88 | – | <0.0001 |
| **Residual volume, %** | 30 ± 4 | <0.0001 | <0.0001 | – |
| **Multiple comparisons for KE at ED, µJ/ml** | | | | |
| **Direct flow, µJ/ml** | 7.8 ± 3.0 | <0.0001 | 0.4502 | <0.0001 |
| **Retained inflow, µJ/ml** | 4.1 ± 2.0 | – | 0.0085 | <0.0001 |
| **Delayed ejection flow, µJ/ml** | 6.3 ± 2.3 | <0.0001 | – | <0.0001 |
| **Residual volume, µJ/ml** | 1.2 ± 0.5 | <0.0001 | <0.0001 | – |

SD indicates Standard deviation; EDV, End-diastolic volume; KE, kinetic energy.

The kinetic energy at end diastole in proportion to blood volume for each flow component is shown in **Figure 4.3C**. The direct flow component possessed the highest energy (7.8 ± 3.0 microJ/ml), whilst the residual volume possessed the lowest (1.2 ± 0.5microJ/ml). The mean kinetic energy per millilitre at ED was statistically significantly different between all flow components, except for the direct flow compared to the delayed ejection flow, see **Table 4.4**.

## Scan-rescan repeatability

10 individuals underwent 2 data acquisitions within the same study visit; Bland-Altman plots are shown in **Figure 4.4A** for the relative volume and kinetic energy value at ED of each flow component.

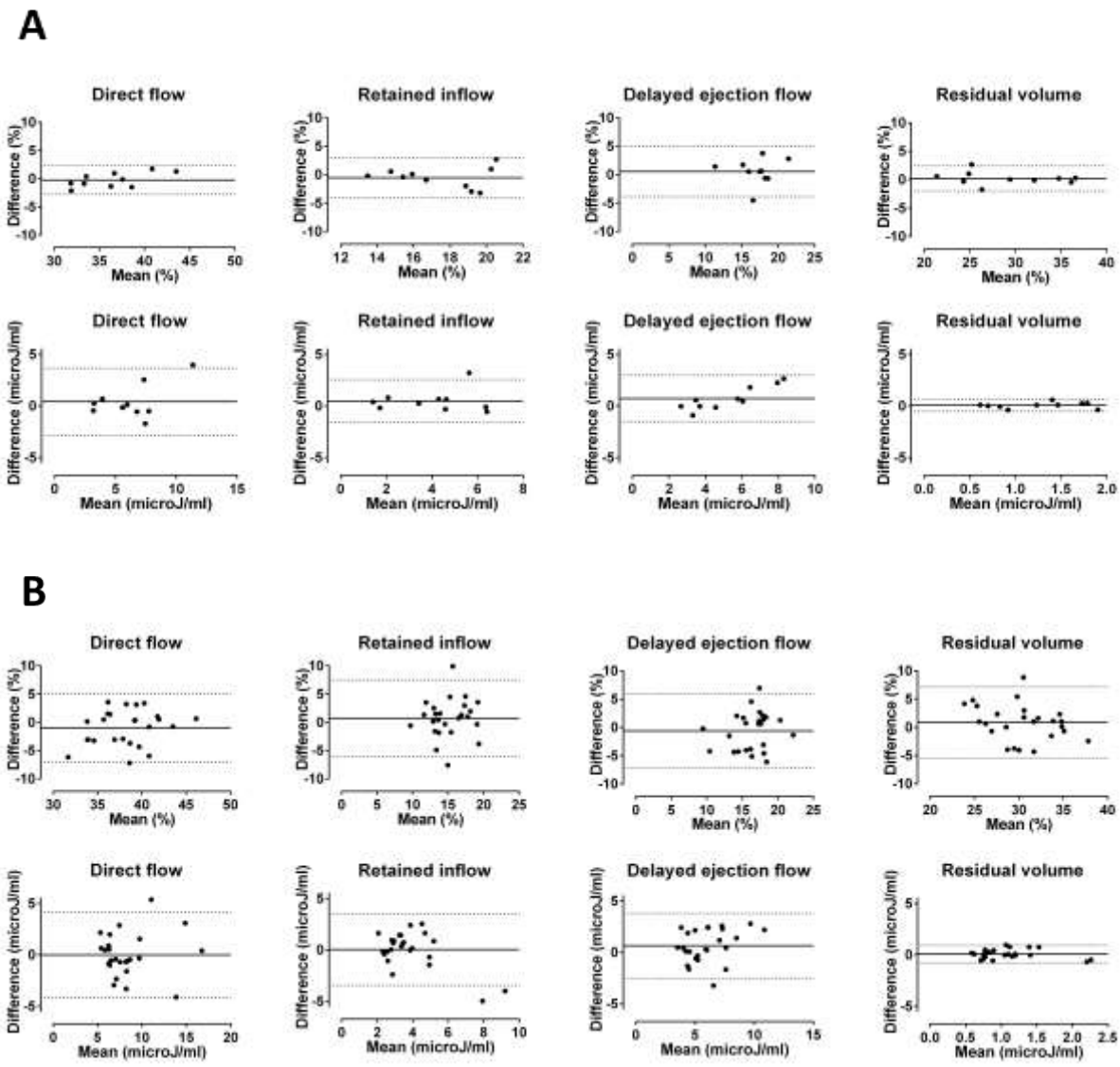


***Figure 4.4**: (**A**) Bland-Altman plots for scan-rescan data; flow components as percentage EDV (top row) and kinetic energy at end diastole (bottom row). Dotted lines represent 95% confidence intervals, unbroken line represents bias. **(B)** Bland-Altman plots for interval scan data; flow components as percentage EDV (top row) and kinetic energy at end diastole (bottom row). Dotted lines represent 95% confidence intervals, unbroken line represents bias.*

The bias and coefficient of variation for these results are summarised in **Table 4.5**. The flow component with the lowest coefficient of variation was the direct flow (2.5%), whilst the most variable flow component as a percentage of the EDV was the delayed ejection flow (coefficient of variation 9.2%). The kinetic energy values had higher coefficients of variation than those for the percentage of each flow component; varying from 13.5% for direct flow to 17.7% for delayed ejection flow.

**Table 4.5: Repeatability of measurements comparing scan-rescan and interval scans.**

| | **Scan-rescan** | | **Interval scans** | |
|---|---|---|---|---|
| | **Bias (95% limits of agreement)** | **CoV** | **Bias (95% limits of agreement)** | **CoV** |
| **Direct flow, % EDV** | -0.2 (-2.8 to 2.3) | 2.5 | -1.0 (-7.1 to 5.1) | 6.1 |
| **Retained inflow, % EDV** | -0.5 (-4.1 to 3.0) | 6.6 | 0.7 (-6.0 to 7.5) | 16.1 |
| **Delayed ejection flow, % EDV** | 0.6 (-3.9 to 5.0) | 9.2 | -0.6 (-7.2 to 6.0) | 15.0 |
| **Residual volume, % EDV** | 0.2 (-2.0 to 2.4) | 3.0 | 0.9 (-5.4 to 7.2) | 8.0 |
| **Direct flow KE at ED, µJ/ml** | 0.4 (-2.8 to 3.7) | 13.5 | -0.01 (-4.2 to 4.2) | 16.9 |
| **Retained inflow KE at ED, µJ/ml** | 0.5 (-1.6 to 2.6) | 13.8 | 0.03 (-3.5 to 3.5) | 20.4 |
| **Delayed ejection flow KE at ED, µJ/ml** | 0.7 (-1.5 to 3.0) | 17.7 | 0.6 (-2.5 to 3.8) | 27.5 |
| **Residual volume KE at ED, µJ/ml** | 0.06 (-0.5 to 0.6) | 15.4 | 0.1 (-0.8 to 0.9) | 29.0 |

CoV indicates Coefficient of variation; KE, kinetic energy; ED, end diastole

## Influence of physiological variance upon LV flow components

25 participants returned for a second scan after a median scan interval period of 52 days (IQR 28-57 days). The mean for each flow component as a percentage of the EDV did not differ significantly between visit 1 and 2, nor did the mean kinetic energy per millilitre at ED (**Figure 4.5**).

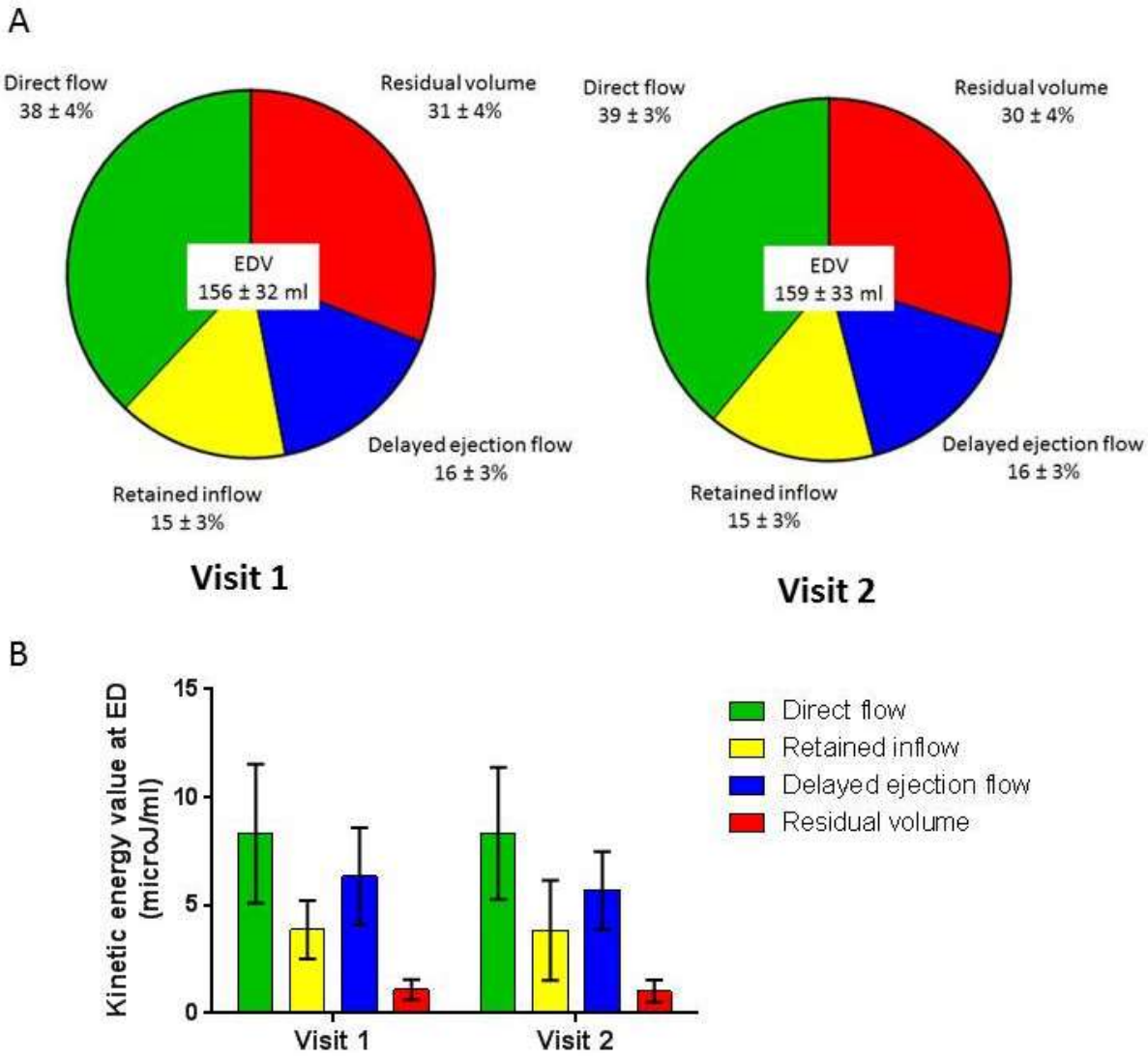


***Figure 4.5:*** *Quantification of the four LV flow components for interval scans :* ***(A)*** *As percentage of EDV at visit 1 and 2.* ***(B)*** *Kinetic energy at end-diastole related to blood volume at visit 1 and 2.*

**Figure 4.4B** shows the Bland-Altman plots for the interval scans flow components volume and kinetic energy values; bias values and coefficients of variation are provided in **Table 4.5**. The 95% limits of agreement and coefficient of variation for each parameter measured are increased compared to those for the 10 scan-rescan datasets.

As before the most stable flow parameter by percentage of EDV was the direct flow (coefficient of variation 6.1%), the most variable changed from the delayed ejection flow for the scan-rescan data to the retained inflow (coefficient of variation 16.1%). The coefficients of variation for the kinetic energy values were again higher than those for the flow components as a percentage of EDV. The least variable component for KE was the direct flow (coefficient of variation 16.9%), whilst the residual volume KE was the most variable with a coefficient of variation of 29.0%.

In order to understand whether the variability seen in each flow component and the associated kinetic energy value, between the interval scans, was related to physiological parameters the changes in these results were correlated against each other. The mean difference between scan 1 and 2 was calculated for heart rate (2 ± 7 beats/minute), LV EDV (3 ± 11ml), stroke volume (1 ± 9ml), LV EF (1 ± 3%) and cardiac output (10 ± 90 ml). There were no correlations seen between any of the flow component percentages or kinetic energy changes with the change in stroke volume, LV EDV or cardiac output. The change in the kinetic energy of the delayed ejection flow correlated weakly to the change in ejection fraction ($r = 0.435$, $P = 0.03$). Additional correlations were seen between the change in heart rate and each flow component as a percentage of the EDV (direct flow $r = 0.509$,

P = 0.009, retained inflow r = 0.424, P = 0.035, delayed ejection flow r = 0.500, P = 0.009 and residual volume r = 0.414, P = 0.04).

## Intra and inter-observer variability

The results from the intra and inter-observer variability for the flow components as a percentage of the EDV are shown in **Table 4.6**. The coefficients of variation for the different flow components were low and similar for both intra and inter-observer results (range intra-observer 3.6-6.1%, vs inter-observer 2.6-5.7%), suggesting good intra and inter-observer variability.

**Table 4.6: Intra and Inter-observer variability.**

| | Intra-observer (Investigator 1) | | | Inter-observer (Investigator 2) | |
|---|---|---|---|---|---|
| | **Analysis 1.1** | **Analysis 1.2** | **CoV** | **Analysis 2** | **CoV** |
| **Direct flow, %** | 38 ± 4 | 37 ± 5 | 3.9 | 36 ± 5 | 5.7 |
| **Retained inflow, % EDV** | 14 ± 3 | 15 ± 3 | 3.6 | 15 ± 3 | 2.6 |
| **Delayed ejection flow, % EDV** | 17 ± 3 | 17 ± 3 | 6.1 | 18 ± 3 | 4.8 |
| **Residual volume, % EDV** | 31 ± 3 | 30 ± 3 | 3.5 | 31 ± 4 | 5.0 |
| **Ejection fraction, % EDV** | 70 ± 3 | 69 ± 3 | 4.0 | 67 ± 4 | 4.1 |
| **EDV, ml** | 162 ± 46 | 166 ± 44 | 4.3 | 154 ± 40 | 5.8 |
| **ESV, ml** | 50 ± 16 | 51 ± 17 | 5.7 | 51 ± 16 | 5.6 |

CoV Coefficient of variation; EDV End diastolic volume; ESV, End systolic volume.

## 4.6 Discussion

This study presents results from the largest cohort of healthy controls for the quantification of left ventricular flow components volume and kinetic energy values to date. These results confirm those from previous studies [3, 50, 72] showing that the largest flow component as a percentage of the EDV is the direct flow, which is also the component that possesses the highest kinetic energy value at ED. I found the retained inflow and delayed ejection flow components to be very similar as a proportion of the EDV, which provides a reassuring data quality control as they are inter-related components. I successfully conducted scan-rescan data acquisitions to assess for repeatability and interval scans to assess for the additional effect of subject variability.

### Repeatability of data acquisition and post-processing

To our knowledge this is the first study to report 4D flow data from scan-rescan data acquisitions, where the aim was to attempt to quantify the magnitude of variation that is due to inherent sources of error in the data acquisition, post-processing and analysis. The scan-rescan repeatability was very good for the flow components as a proportion of the EDV and slightly more variable for the kinetic energy values but still within reasonable limits. The coefficients of variation I found for our flow component volumes were of a similar magnitude to those from a previous scan-rescan study assessing quantification of LV parameters including LV EDV, LV ESV and LV EF that found coefficients of variation of between 4.1-10.3% [114].

Analysis of the influence of the post-processing steps including LV segmentation and selection of the appropriate time frame for ED and ES was assessed via the intra and inter-observer variability. The coefficients of variation for the flow component proportions were very similar between the intra and inter-observer results and in agreement with previous studies assessing volumetric intra and inter-observer variability [114, 115]. This finding is expected; the main influence the operator has upon the post processing of the data is the contouring of the short axis cines at ED and ES which are then used to create the mask for analysis of the flow data. Both investigators undertaking analysis in this study are experienced at placing LV contours and were trained in the same CMR unit so will have very similar contouring styles. The intra-observer coefficient of variation for the flow components as a proportion of the EDV was similar to that obtained for the scan-rescan data analysis suggesting that much of the variability in the results will be from the post-processing steps and not the data acquisition itself.

## Influence of physiological variability upon interval scans

The flow components as a percentage of the EDV and the kinetic energy of each component at ED were not significantly different between visit 1 and 2 when mean values for the group were assessed, however comparison of study visits for individuals demonstrated greater variability. Thus, as expected the coefficients of variation were higher for all measured parameters for the 2 scans performed at an interval compared to the 2 scans performed in the same study visit. The results from the scan-rescan data acquisitions provide an estimation of the inherent error in the 4D flow data acquisition and

post-processing. The additional variability seen with the interval scans suggests that as well as the inherent errors in the data acquisition and post processing there are additional influencing factors. I hypothesised that the increased variability seen was most likely due to a degree of normal physiological variability. I found that the change in heart rate recorded between the 2 interval scans correlated modestly to the changes seen in the flow components as a proportion of the EDV. This is an interesting finding and may be explained by the longstanding physiological observation that changes in heart rate predominantly affect the diastolic phase of the cardiac cycle, as the systolic phase is of a relatively fixed duration [116]. Hence, it may be that as the heart rate changes the proportions of the flow components alter to adapt to the shorter diastolic period, whilst still maintaining an efficient systolic ejection phase. This may be an important physiological adaptation for exercise, which would be interesting to assess in future studies. However, the correlations with heart rate alone were only modest suggesting further additional physiological factors such as fluid status, vascular tone and hormonal influences may be implicated in the variability seen for interval data acquisitions.

The direct flow was consistently the largest component with the highest possession of energy at ED; it was also the least variable of the four flow components in both composition and kinetic energy values. The direct flow represents the blood that transits directly from the left atrium via the LV cavity to be ejected into the aorta within the same cardiac cycle. Previous studies have demonstrated that the direct flow follows an efficient pathway to the LV outflow track with the shortest distance, more favourable angle and

increased linear momentum in comparison to the other flow components [50]. This suggests that in a healthy heart the percentage of blood pumped via the efficient shorter pathway taken by the direct flow component is relatively consistent; this may allow conservation of the kinetic energy of this component which may be important in reducing the additional energy that is required for its ejection during systole. The residual volume was the second most stable component over time in terms of composition, but possessed the most variable amount of kinetic energy. The residual volume is located at the periphery of the LV cavity, outlining the functional border of the chamber, providing a fluid-fluid interface that interacts with the exchanging blood flow [48]. The location and stability in terms of the percentage of the residual volume would imply it is a static component of the LV blood flow volume; however the variability of the kinetic energy it possesses suggests it remains part of the dynamic interactions that occur with the incoming and outgoing cardiac blood flow within the LV cavity during each cardiac cycle. The variability in the kinetic energy of the residual volume over time may be an important factor in preventing blood stasis and thrombus formation within the healthy heart.

The kinetic energy for the retained inflow component at end diastole was significantly lower than that of the delayed ejection flow. This finding is in keeping with the notion proposed by *Bolger et al* [72] that the retained inflow blood has to decelerate at the end of diastole and then prior to ejection during a subsequent systole (as part of the delayed ejection flow) acquire additional kinetic energy to achieve this. Previous studies have demonstrated a late diastolic boost in the kinetic energy of the delayed ejection flow

which was presumed to result from transfer of energy from the inflow components, so it may be that the kinetic energy is interchanged predominantly from the retained inflow to the delayed ejection flow. The amount of energy present within the delayed ejection flow at ED was not significantly different to the energy possessed by the direct flow; suggesting that a threshold level of kinetic energy is required for ejection of blood from the LV during systole.

## 4.7 Limitations

The 4D flow data acquisitions undertaken in this study were conducted at rest, without exercise or pharmacological stress; given the relationship between the change in heart rate and the flow components as a percentage of the EDV it would be interesting to assess whether these proportions vary to a greater degree in an exercising heart. Blood flow within the heart is a dynamic process, 4D flow data acquisitions are acquired over many heart beats with the end data representing the blood flow over an averaged cardiac cycle. In order to understand further if any haemodynamic changes during the data acquisition had influenced the final results continuous monitoring of heart rate and blood pressure would have needed to have been undertaken. For these measurements to be reliable they would need to be invasive which I felt would be too high a burden for our participants. The findings presented here are from a single study, although they are in keeping with previous studies direct site to site comparisons with the same study participants would provide additional validation of the 4D flow LV flow components volume and kinetic energy profiles.

## 4.8 Conclusion

This study provides an increased understanding of the variability of blood flow within the healthy heart. LV flow components relative volume and kinetic energy values are highly repeatable and are stable within a population over time. However, the variability of these measures in individuals over time is greater than can be attributed to inherent sources of error in the data acquisition, post processing and analysis, suggesting that additional physiological factors may influence LV flow components volume and kinetic energy profiles. These findings have relevance to the design of future longitudinal studies using 4D flow.

# *Chapter 5*

# *Left ventricular 4D flow components and kinetic energies correlate with established markers of prognosis and represent novel imaging biomarkers in heart failure*

## 5.1 Abstract

**Purpose**

In dilated cardiomyopathy (DCM) and ischaemic cardiomyopathy (IHD) left ventricular (LV) remodelling leads to heart failure (HF). 4D (3D+time) flow cardiac magnetic resonance (CMR) affords insights into flow patterns and kinetic energy (KE) of the LV blood.

**Hypothesis:** Increasing derangement in 4D flow measures would relate to: 1) decreased mechanical function and increased dilatation, 2) increased levels of biochemical remodelling markers and 3) worsening patient symptoms and functional capacity.

**Methods**

34 DCM, 30 IHD and 36 controls underwent CMR for 4D velocity and anatomical data acquisition. A 6 minute walk test (6MWT), BNP analysis and Minnesota Heart Failure Questionnaire (MHFQ) were additionally completed. The LV blood flow was separated into four functional components based on the movement of the blood during the cardiac cycle. For each flow component the volume was related to the EDV (volume-ratio) and the kinetic energy was recorded over the entire cardiac cycle and at end-diastole (ED).

**Results**

DCM and IHD patients demonstrated adverse cardiac remodelling with ventricular dilatation, and impaired systolic function (DCM LVEF 36 ± 11 %, IHD LVEF 39 ± 12% vs controls 67 ± 4%, $P<0.0001$). The volume ratio and KE at ED of the total LV inflow that

passed directly to ejection (direct flow) was significantly decreased in both patient groups compared to controls (volume ratio: DCM 11 ± 6%, IHD 14 ± 9% vs 38 ± 4% P <0.0001; KE: DCM 0.19 ± 0.17mJ, IHD 0.25 ± 0.22mJ vs 0.47 ± 0.19mJ, P <0.0001). The LV component residing for >2 cardiac cycles (residual volume) was significantly increased in proportion and KE at ED (volume ratio: DCM 51 ± 11%, IHD 49 ± 10% vs 30 ± 4% P <0.0001; KE: DCM 0.47 ± 0.43mJ, IHD 0.32 ± 0.30mJ vs 0.05 ± 0.03mJ, P <0.0001).

Direct flow KE at ED correlated positively to LVEF (r = 0.66), 6MWT (r = 0.46) and negatively to LVEDV (r = -0.35), LVESV (r = -0.55), BNP (r = -0.45) and MHFQ (r = -0.56). Residual volume KE at ED correlated negatively to LVEF (r = -0.88), 6MWT (r = -0.51), and positively to LVEDV (r = 0.79), LVESV (r = 0.89), MHFQ (r = 0.60) and BNP (r = 0.53). Correlation P values <0.0001.

**Conclusions**

DCM and IHD patients demonstrated inefficient blood flow patterns and deranged kinetic energy. Greater derangement of flow parameters was associated with worsening myocardial function, dilatation, BNP, 6MWT and patient symptoms. Derangements in flow parameters are novel biomarkers of disease severity in HF patients and correlate with established markers of cardiac remodelling and prognosis, which may become useful in monitoring novel heart failure therapies and predicting prognosis.

## 5.2 Introduction

Heart failure (HF) is a global health problem; with significant morbidity and mortality, as well as representing a substantial health care burden [117]. HF is a complex multifactorial syndrome that is initiated by a myocardial insult which activates cardiac remodelling; a process encompassing numerous transcriptional, molecular, cellular and architectural changes within both the cardiac myocytes and surrounding extracellular structures [14]. The ability of the heart to remodel in response to stimuli is an important part of physiological adaptations required in response to situations including pregnancy [6], however in pathological remodelling this initially beneficial plasticity response become maladaptive with a propensity toward decompensation, ventricular dilatation, systolic dysfunction and electrophysiological changes resulting in malignant ventricular arrhythmias [6] .

The fundamental role of heart is as the pump of the cardiovascular system, hence blood flow within the heart chambers is intrinsic to this function. Fluid dynamic studies indicate that the morphological structure of a compliant vessel is inextricably linked to the flow that occurs within it [118]. Hence, as ventricular flow is altered in the early stages of remodelling [74], it is probable that the flow itself can influence disease progression [118]. New insights into and quantification of left ventricular (LV) blood flow and kinetic energy (KE) are now afforded by three dimensional, time resolved cardiac magnetic resonance imaging (4D flow). Previous studies have demonstrated altered patterns of left ventricular flow in seemingly clinically compensated dilated cardiomyopathy patients [74].

Brain type natriuretic peptide (BNP) produced by cardiac myocytes in response to volume expansion and pressure overload [119] is a powerful marker for prognosis and risk stratification in the context of heart failure [120, 121]. Functional capacity in heart failure, as represented by the distance covered during a 6 minute walk test, is also a predictor of mortality and morbidity [122] as is the presence of symptoms as assessed with a standardised questionnaire (Minnesota heart failure questionnaire) [123].

Much is still not fully understood about cardiac remodelling [14]; the aim of this study was to investigate the relationship between ventricular morphology and blood flow during cardiac remodelling. Patients with two of the commonest causes of heart failure- ischaemic heart disease (IHD) and dilated cardiomyopathy (DCM) were included in this study [29]. I hypothesised that increasing derangement in 4D flow measures would relate to: 1) conventional markers of cardiac remodelling, including decreased mechanical cardiac function and dilatation 2) increased levels of biochemical remodelling markers and 3) worsening patient symptoms and functional capacity. I hypothesised these changes to be independent of the initial aetiology of the myocardial damage, instead reflecting the self-propagating nature of cardiac remodelling.

## 5.3 Methods

### Study population

This study complied with the Declaration of Helsinki and was approved by the National Research Ethics Committee. Each participant gave written informed consent.

103 participants were recruited; 35 patients with a history of dilated cardiomyopathy, 32 patients with a history of ischaemic cardiomyopathy and 36 healthy controls. DCM and IHD patients were recruited from outpatient cardiology clinics, MRI lists and the community heart failure service.

DCM patients were included if they had a clinical diagnosis of dilated cardiomyopathy and imaging evidence of a dilated (>55mm), impaired left ventricle with an ejection fraction of <50%. IHD patients were eligible for inclusion if they had a previous myocardial infarction- either ST elevation MI or non-ST elevation MI with significant coronary artery disease at coronary angiography and imaging evidence of an impaired left ventricle; LV EF <50%. IHD patients were excluded if they had a history of coronary artery bypass grafting. Other exclusion criteria as reported in chapter 2 were adhered to.

## Study protocol

Participants underwent CMR scanning protocol at 3 T as follows:

1. Retrospectively gated 4D flow data acquisition.
2. Cine imaging to measure LV volumes, mass and function.
3. Myocardial strain imaging with tagging.
4. Healthy volunteers and IHD patients underwent LGE imaging. DCM patients did not undertake LGE imaging as 25 of them underwent $^{31}$P-MRS, the results of which would have been compromised by the presence of gadolinium. These results are presented in chapter 6.

Study participants also undertook a 6 minute walk test, had venous blood drawn for BNP analysis and patient participants completed a Minnesota heart failure questionnaire.

The KE values were calculated over the cardiac cycle. As in previous studies KE values for each component were recorded at end-diastole, as these reflect the preservation of the inflowing kinetic energy prior to the rapid ejection of blood during systole [50, 74]. Additionally I calculated the average kinetic power for each flow component throughout the cardiac cycle, to assess whether the inclusion of all time frames within the cardiac cycle provided additional information.

## 5.3 Statistics

A multiple linear regression model was performed, using stepwise entry and the dependent variable as the patient 6MWT result. Variables with $P < 0.05$ that had the strongest relationship with 6MWT were included in the model. Standardised ($\beta$) values are reported.

A *priori* sample size calculation was performed to detect a 40% reduction in the kinetic energy of the direct flow component at end diastole in DCM patients compared to controls. Based on pilot data (direct flow KE DCM patients 0.22 ± 0.02mJ, direct flow KE controls 0.37 ± 0.18mJ) assuming a two-tailed independent *t*-test analysis ($\alpha = 0.05$, $\beta = 0.8$), calculations suggested that 13 controls and 13 patients would need to be recruited. A second a *priori* sample size calculation was also performed to detect a 32% reduction in the kinetic energy at ED of the direct flow component in IHD patients compared to controls. Based on pilot data (direct flow KE IHD patients 0.25 ± 0.1mJ, direct flow KE controls 0.37 ± 0.18mJ), with

the same test assumptions 25 IHD patients and 25 controls would need to be recruited. These targets were achieved in this study.

## 5.4 Results

### Study population

Of the 103 participants recruited to the study, 3 were unable to complete the CMR study, 2 IHD patients due to claustrophobia and 1 DCM patient who was unable to fit, due to body habitus. Consequently 100 participants (34 DCM, 30 IHD and 36 controls) were studied.

Demographic and clinical data are shown in **Table 5.1**. There were no significant differences in age or heart rate between the 3 groups. The IHD group was predominantly male (93%), whereas the DCM group was 65% male. Both the DCM and IHD groups had higher BMI's than the control group. Blood pressure tended to be lower in the patient groups, likely reflecting heart failure and pharmacotherapy.

**Table 5.1: Baseline characteristics of the study cohort.**

| | Controls (n=36) | DCM patients (n=34) | IHD patients (n=30) | P value |
|---|---|---|---|---|
| **Demographics** | | | | |
| **Age, yrs** | 57 ± 12 | 57 ± 14 | 63 ± 12 | 0.087 |
| **Male, n (%)** | 25 (70) | 22 (65) | 28 (93)* | 0.020 |
| **Body mass index, kg/m$^2$** | 25 ± 4 | 28 ± 4 § | 28 ± 4 ł | 0.005 |
| **Systolic BP, mmHg** | 134 ± 20 | 128 ± 18 | 120 ± 15 ł | 0.010 |
| **Diastolic BP, mmHg** | 78 ± 10 | 72 ± 12 § | 69 ± 9 ł | 0.003 |
| **Heart rate, bpm** | 64 ± 14 | 65 ± 14 | 65 ± 14 | 0.970 |
| **LBBB on ECG, no (%)** | - | 9 (26) | 8 (27) | >0.999 |
| **Prognostic markers** | | | | |
| **BNP, pmol/L** | 7 ± 5 | 51 ± 105 § | 77 ± 108 ‖ | <0.0001 |
| **6 minute walk test, m** | 624 ± 77 | 500 ± 84 ¶ | 470 ± 101 ‖ | <0.0001 |
| **MHFQ** | - | 18 ± 19 ¶ | 22 ± 22 ‖ | 0.401 |
| **Medications, n (%)** | | | | |
| **ACE-I/ARB** | - | 30 (88) | 26 (87) | |
| **Beta-Blocker** | - | 24 (71) | 27 (90) | |
| **Aldosterone antagonist** | - | 18 (53) | 12 (40) | |
| **Diuretic** | - | 16 (47) | 13 (43) | |
| **Aspirin** | - | 6 (18) | 26 (87) | |
| **Statin** | - | 4 (12) | 26 (87) | |
| **Warfarin** | - | 7 (21) | 10 (33) | |

Values are mean ± standard deviations or percentages. DCM indicates dilated cardiomyopathy; IHD, ischaemic heart disease; yrs, years; BP, blood pressure; bpm, beats per minute; LBBB, left bundle branch block; BNP, brain natriuretic peptide; ACE-I, angiotensin-converting enzyme inhibitors; ARB, angiotensin receptor blockers; MHFQ, Minnesota heart failure questionnaire. * P <0.05 but >0.0001, IHD versus DCM. ł P <0.05 but >0.0001, IHD versus Controls; § P<0.05 but >0.0001, DCM versus Controls; ¶ P<0.001, IHD versus Controls; ‖ P<0.001, DCM versus Controls.

As expected, IHD and DCM patients had significantly higher BNP levels compared to controls (P <0.0001). The mean distance walked on the 6MWT was 20% less in DCM patients and 25% less in IHD patients compared to controls (P <0.0001). Heart failure symptoms, as assessed by the MHFQ score, were similar between the IHD and DCM patients.

## Myocardial structure and systolic function

CMR results for LV volumes and function are summarised in **Table 5.2**. As expected the 2 patient groups had significantly increased LV volumes (P <0.0001) and decreased systolic function (DCM LVEF 36 ± 11%, IHD LVEF 39 ± 12%) compared to controls (LVEF 67 ± 4%). There were no significant differences in cardiac volumes or function between the 2 patient groups. Both patient groups had a more spherical ventricle with impaired mid-ventricular circumferential and longitudinal systolic strain compared to controls (P <0.0001).

**Table 5.2: CMR results in controls, IHD patients and DCM patients.**

| Variable | Controls (n=36) | DCM patients (n=34) | IHD patients (n=30) | P value |
|---|---|---|---|---|
| **LV end diastolic volume, ml** | 159 ± 31 | 273 ± 118 * | 231 ± 68 ł | <0.0001 |
| **LV EDV indexed BSA, ml/m$^2$** | 82 ± 14 | 135 ± 52 * | 116 ± 33 ł | <0.0001 |
| **LV end systolic volume, ml** | 53 ± 13 | 182 ± 108 * | 146 ± 65 ł | <0.0001 |
| **LV stroke volume, ml** | 106 ± 20 | 90 ± 25 ¶ | 85 ± 22 § | 0.0006 |
| **LV ejection fraction, %** | 67 ± 4 | 36 ± 11 * | 39 ± 12 ł | <0.0001 |
| **Cardiac output, L/min** | 6.7 | 5.6 ¶ | 5.2 ł | <0.0001 |
| **LV mass, g** | 113 ± 35 | 137 ± 46 ¶ | 137 ± 30 § | 0.0044 |
| **LV mass index, g/m2** | 58 ± 15 | 69 ± 20 ¶ | 68 ± 13 § | 0.0029 |
| **Infarcted myocardium, %** | - | - | 40 ± 8 | |
| **LV sphericity index** | 1.7 ± 0.2 | 1.4 ± 0.2 * | 1.4 ± 0.2 ł | <0.0001 |
| **Left atrial ejection fraction, %** | 56 ± 6 | 39 ± 12 * | 38 ± 14 ł | <0.0001 |
| **LV mid-ventricular circumferential systolic strain, % (negative)** | 19 ± 3 | 10 ± 4 * | 12 ± 4 ł | <0.0001 |
| **LV mid-ventricular diastolic strain rate, s$^{-1}$** | 83 ± 19 | 48 ± 21 * | 53 ± 18 ł | <0.0001 |
| **LV global longitudinal strain, % (negative)** | 15 ± 2 | 10 ± 3 * | 8 ± 4 ł | <0.0001 |

Values are mean ± standard deviations or percentages. DCM indicates dilated cardiomyopathy; IHD, ischaemic heart disease; LV, left ventricle; EDV, end diastolic volume; BSA, body surface area. * P <0.0001, DCM versus Controls; ł P<0.0001, IHD versus Controls; § P<0.05 but >0.0001, IHD versus Controls; ¶ P<0.05 but >0.0001, DCM versus Controls

## Changes in left ventricular 4D flow components volume

Left ventricular flow visualisation examples are shown in **Figure 5.1**. The distribution of the residual volume varied in IHD patients according to the location of any regional wall motion abnormalities. However, in DCM patients the residual volume was evenly distributed at the periphery of the LV cavity. Despite the different spatial locations of the flow components the changes in proportion of the flow components, compared to controls, were similar between the DCM and IHD groups, as shown in **Figure 5.2**.

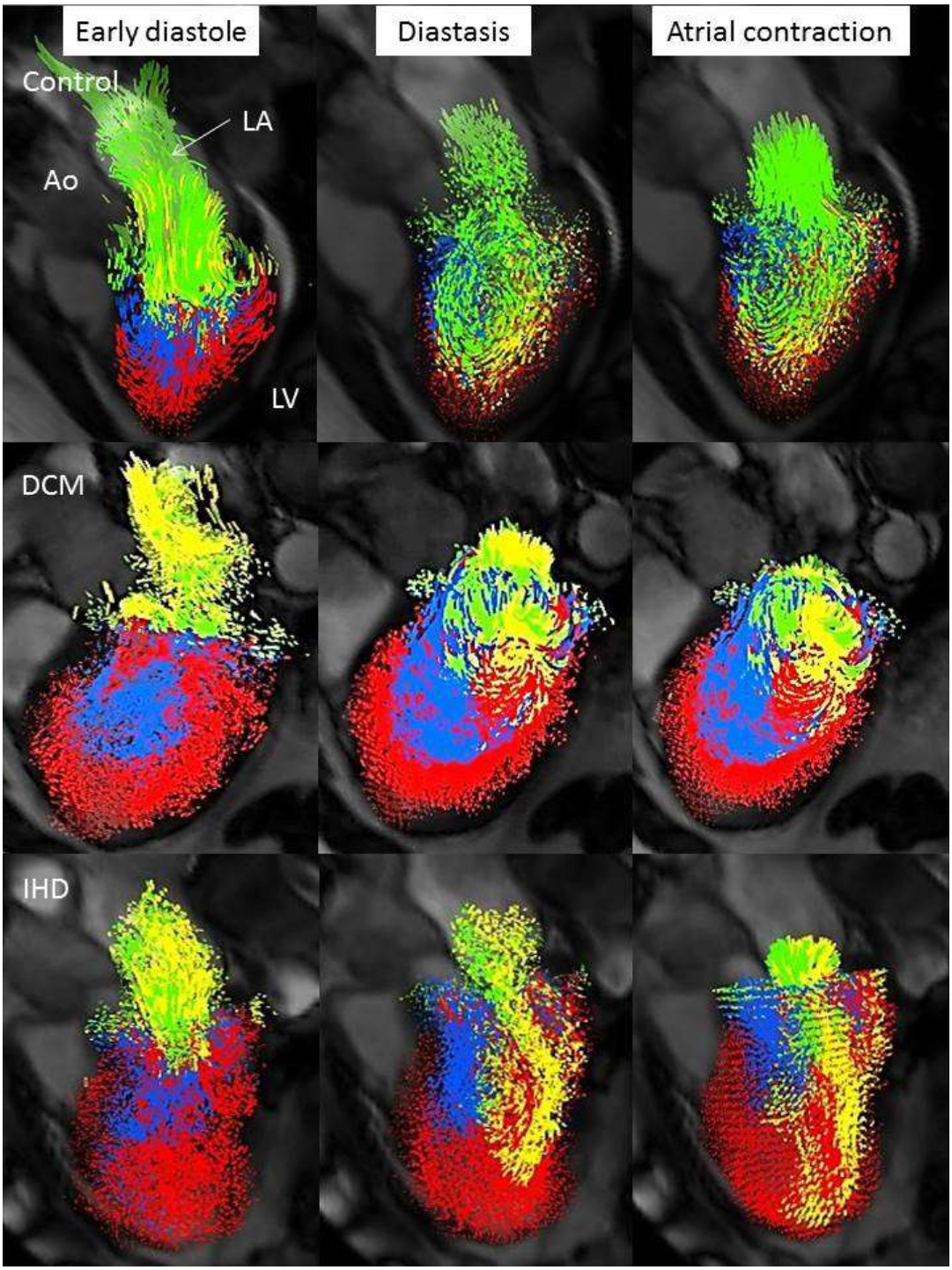


***Figure 5.1:*** *Representative diastolic LV visualisations in a healthy control (direct flow 35%, residual volume 29%), DCM (direct flow 10%, residual volume 55%) and IHD patient with an antero-apical LAD infarct (direct flow 8%, residual volume 56%). Note despite similar proportions of residual volume between the IHD & DCM patient the distribution of this component differs; with a global distribution in the DCM patient and a more localised distribution in the IHD patient, corresponding to the area of infarction and regional wall motion abnormality. Direct flow, green; retained inflow, yellow; delayed ejection flow, blue and residual volume,red.*

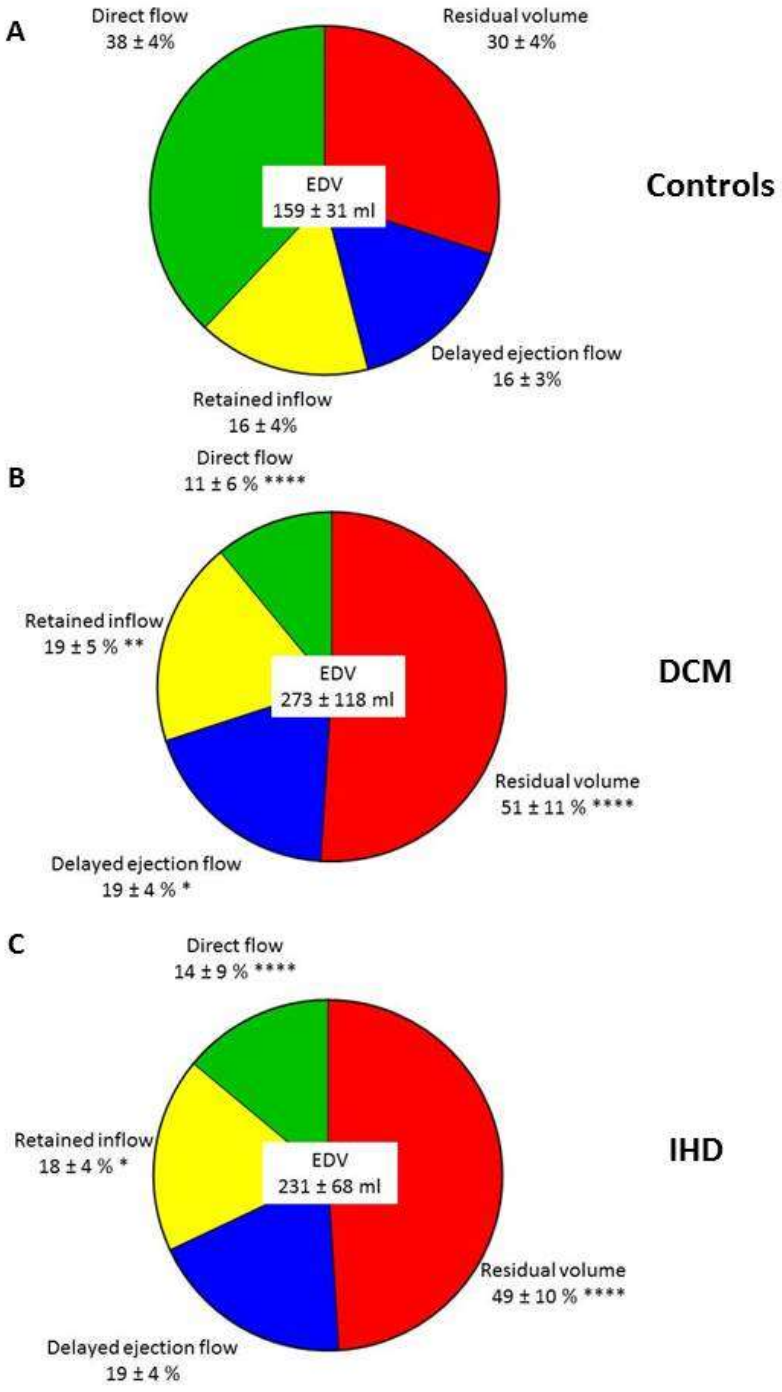


***Figure 5.2:*** *Flow components by percentage of the end-diastolic volume for controls, DCM and IHD patients. Data are mean ± standard deviation. ****P<0.0001, *** P <0.001, **P< 0.01, *P<0.05 compared to corresponding component in controls.*

DCM was associated with a 71% decrease and IHD a 63% decrease in the direct flow component volume ratio compared to controls (P <0.0001). This decrease in direct flow corresponded to a similar increase in the residual volume component volume ratio in both DCM (63% increase) and IHD patients (70% increase) compared to controls (P <0.0001). The retained inflow component volume ratio increased by 19% and 13% respectively for the DCM and IHD groups compared to controls (P = 0.003 for DCM, P = 0.02 for IHD). There was no significant difference in the delayed ejection flow component volume ratio between the IHD and control group whilst the DCM group had a 19% increase in the delayed ejection flow component volume ratio compared to controls (P = 0.04).

## Changes in left ventricular kinetic energy profiles

The kinetic energy values for all 4 flow components differed significantly for the DCM and IHD patients compared to controls, but not between the 2 patient groups, as shown in **Figure 5.3**. In controls the efficient direct flow component possessed the greatest kinetic energy, in DCM and IHD patients this was decreased (average kinetic power 59% decrease in IHD and DCM compared to controls, P <0.0001) and the kinetic energy of the other 3 flow components increased compared to controls. The decrease in KE direct flow and the increase in the KE of the other 3 flow components for patients relative to controls was seen in both the KE at ED and the average kinetic power across the cardiac cycle. However, the magnitude of this change differed depending upon which measure of KE was assessed.

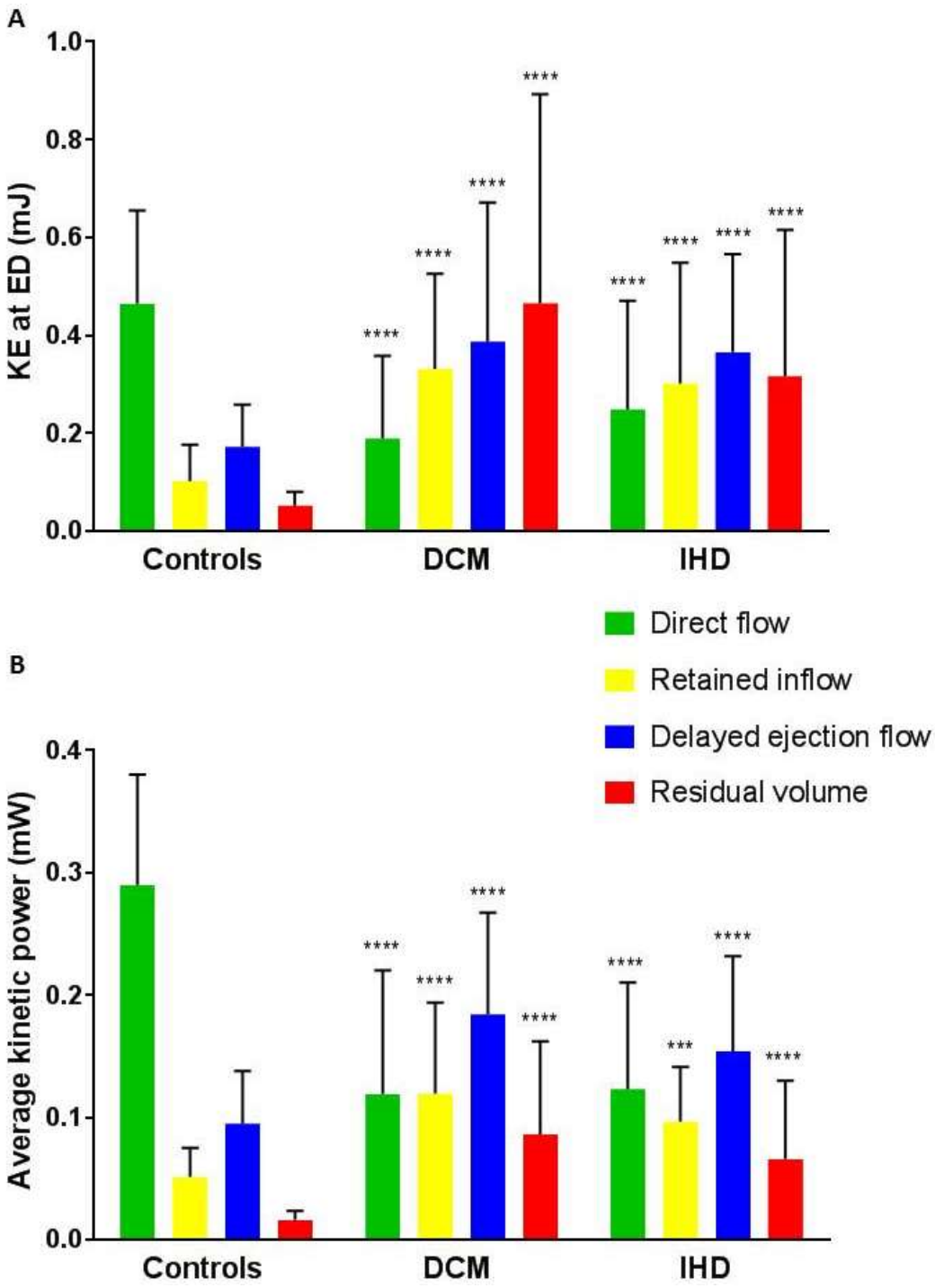


***Figure 5.3:*** *Kinetic energy profiles for controls, DCM and IHD patients.* ***(A)*** *Kinetic energy at end diastole for the 4 flow components;* ***(B)*** *Average kinetic power throughout the cardiac cycle for the 4 flow components. Bars show mean value and error bars indicate standard deviation. ****P<0.0001, *** P <0.001 compared to corresponding component value in controls.*

The derangement in the volume ratio and the kinetic energy values of the flow components progressed as the LV ejection fraction decreased, as illustrated in **Figure 5.4**, where the results are grouped according to LVEF (LVEF>55%, n=4; EF 45-54% n = 11; EF 36-44% n = 21; EF $\leq$ 35%, n=28).

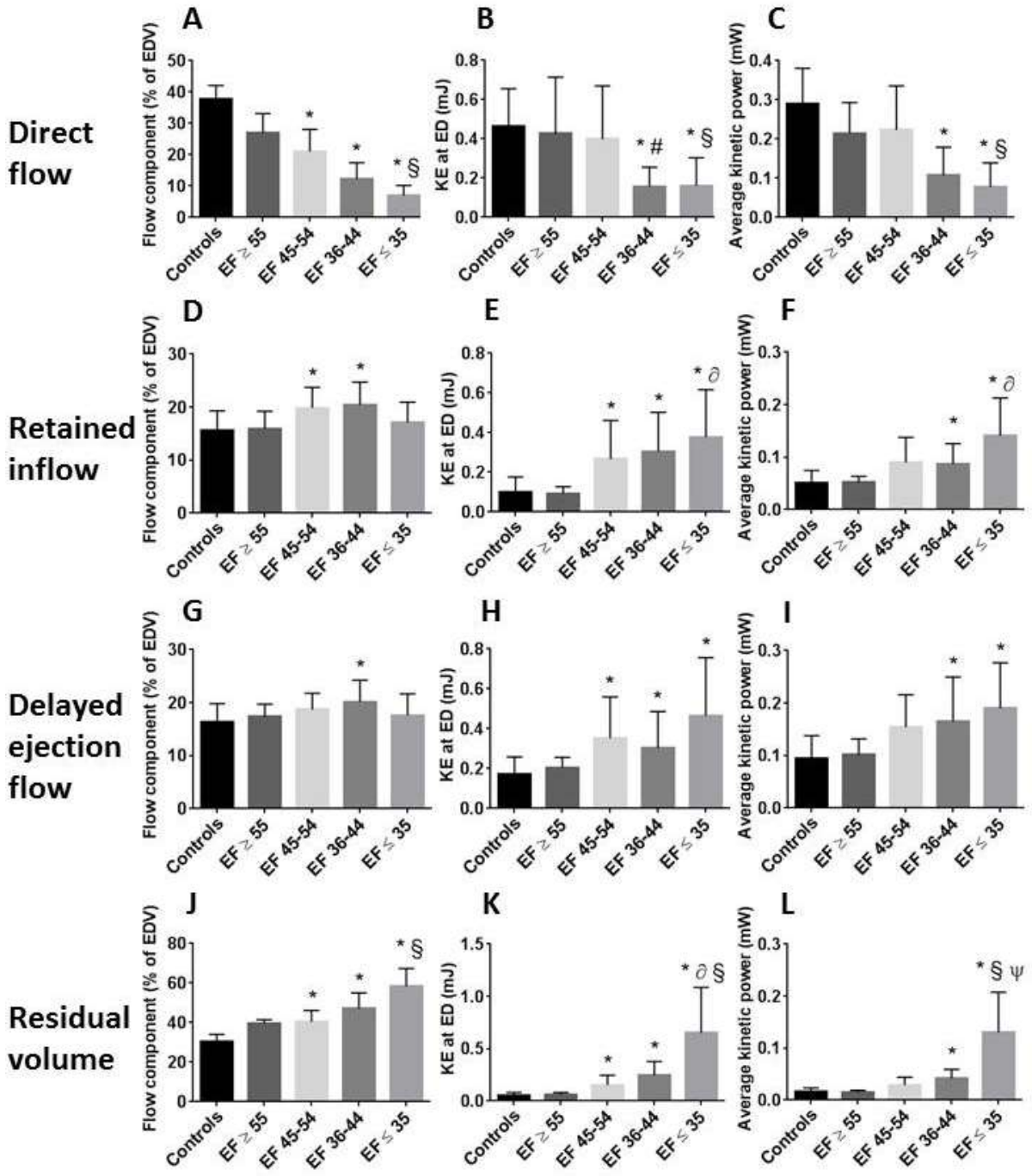


***Figure 5.4:*** *Differences in flow component percentage, kinetic energy at end diastole and average kinetic power for the 4 flow components according to left ventricular ejection fraction (LVEF). Bars show mean value and error bars indicate standard deviation. *P <0.05 compared to controls, § P <0.05 LVEF ≤ 35% compared to LVEF 45-54%, Ψ P <0.05 LVEF ≤ 35% compared to LVEF 36-44% , ∂ P < 0.05 LVEF ≤ 35% compared to LVEF ≥ 55%, # LVEF P <0.05 LVEF 36-44% compared to LVEF 45-54%.*

In 4 patients ventricular function had recovered to normal levels and this was accompanied by normalisation or near normalisation of flow parameters. The volume ratio of the direct flow component decreases in line with the reduction in ejection fraction. However, the change in the KE begins to drop only with the development of more advanced heart failure, with an EF <45%. The volume ratio of retained inflow initially increases as EF decreases, but then once the LV EF is <35% returns to a similar level seen in controls. A similar pattern is seen in the delayed ejection flow. The kinetic energy possessed by the retained inflow and delayed ejection flow increases as LV EF decreases. The proportion of the residual volume component and its associated kinetic energy increases steadily as left ventricular impairment worsens. However, when the LVEF changed from 36-44% to <35% there was a further more pronounced increase in the kinetic energy (threefold increase in average kinetic power, P <0.05 compared to EF 36-44%).

## Correlations amongst classical remodelling markers, novel 4D flow parameters and prognostic data

The correlations for the direct flow and residual volume kinetic energy across all study participants are shown in **Table 5.3**. The direct flow kinetic energy correlated negatively with the conventional remodelling parameters of the LV EDV, LV ESV and positively with the LV EF (P <0.0001). The residual volume kinetic energy correlated negatively with the LV EF and positively with the LV EDV and LV ESV (P <0.0001). Both the direct flow and residual volume kinetic energy correlated, but in opposite directions, with the patients symptoms as

represented by MHFQ, their functional capacity as assessed by the 6MWT and biochemical evidence of cardiac remodelling in the form of BNP.

**Table 5.3: Correlations between ventricular remodelling parameters, prognostic markers, kinetic energy at both end-diastole and average kinetic power for direct flow and residual volume.**

| Variable | Direct flow kinetic energy at ED | | Direct flow average kinetic power | | Residual volume kinetic energy at ED | | Residual volume average kinetic power | |
|---|---|---|---|---|---|---|---|---|
| | r | P value | r | P value | r | P value | r | P value |
| **LV EDV** | -0.35 | <0.0001 | -0.45 | <0.0001 | 0.79 | <0.0001 | 0.82 | <0.0001 |
| **LV ESV** | -0.55 | <0.0001 | -0.67 | <0.0001 | 0.89 | <0.0001 | 0.90 | <0.0001 |
| **LV EF** | 0.66 | <0.0001 | 0.78 | <0.0001 | -0.88 | <0.0001 | -0.87 | <0.0001 |
| **MHFQ** | -0.56 | <0.0001 | -0.63 | <0.0001 | 0.60 | <0.0001 | 0.59 | <0.0001 |
| **6MWT** | 0.46 | <0.0001 | 0.63 | <0.0001 | -0.51 | <0.0001 | -0.43 | <0.0001 |
| **LV circumferential systolic strain** | -0.56 | <0.0001 | -0.71 | <0.0001 | 0.78 | <0.0001 | 0.79 | <0.0001 |
| **BNP** | -0.45 | <0.0001 | -0.59 | <0.0001 | 0.53 | <0.0001 | 0.52 | <0.0001 |

Correlations are performed with Pearson or Spearman's correlation as appropriate. LV indicates, left ventricular; EDV, end diastolic volume; ESV, end systolic volume; EF, ejection fraction; MHFQ, Minnesota heart failure questionnaire; 6MWT, 6 minute walk test; BNP, Brain-type natriuretic peptide; Ed, end diastole.

In order to assess whether remodelling parameters were predictive of the functional capacity of the patients, as represented by the 6MWT, a multiple linear regression model was created. The independent variables entered into the model were age, height, LV EF, BNP, average direct flow kinetic power and mid LV peak systolic strain. The independent predictors of the 6MWT were found to be age ($\beta$ = -0.305, P = 0.024) and the direct flow

average kinetic power ($\beta$ = 0.279, P =0.039, overall $R^2$ of the model = 0.464, P = 0.003). In order to avoid co-linearity of predictors the other prognostic cardiac remodelling parameters of ESV and EDV and were substituted into the model above instead of LV EF, but in both of these subsequent models age and direct flow average kinetic power remained the only independent predictors.

## 5.5 Discussion

The relationships between ventricular morphology, prognostic markers, blood flow components volume ratio and kinetic energy during cardiac remodelling due to dilated and ischaemic cardiomyopathy were assessed using 4D flow CMR. I confirmed the previous finding of derangement of blood flow components volume and kinetic energy values within DCM patients; namely a reduction in the efficient direct flow component and an increase in the residual volume [74]. I now also demonstrate that these changes in flow components and KE are similar in ischaemic cardiomyopathy, despite a different aetiology of the initiating myocardial insult. The kinetic energy at ED and the average kinetic power of the direct flow and residual volume components have been shown here to correlate with conventional remodelling parameters and prognostic markers, suggesting a role as a novel imaging biomarker of cardiac remodelling. Importantly, I show, in our model that the average kinetic power of the direct flow component is predictive of the patient's functional capacity (as represented by the distance achieved during the 6MWT), whereas the LV EF, LV EDV and LV ESV were not found to be independent predictors. The average kinetic power of the direct flow component includes both the diastolic and systolic phase of the cardiac cycle

and hence provides information about more aspects of ventricular function than LV EF, EDV or ESV do. In diastole this includes a component related to diastolic function, in that efficient diastolic relaxation, as seen in health, increases the overall mitral inflow velocities during diastole. Additional information is provided about the ejection fraction - in that the direct flow component is reduced proportionately to the residual volume in both patient groups. In systole the direct flow average kinetic power provides information upon left ventricular systolic function in terms of the velocity of flow in the outflow tract which is determined by the dP/dt of the LV. As the average kinetic power of the direct flow encompasses these different aspects of cardiac function it may provide a sensitive marker for early cardiac dysfunction before an overt change in ejection fraction or diastolic function is seen. Comparison of the sensitivity for detection of early pathological changes by the average kinetic power of the direct flow with echo and CMR markers of myocardial strain would be an area for future research.

In health the average kinetic power of the direct flow component will be dominated by the systolic LV function as the maximum LVOT velocity is 20-30% higher than the maximal mitral valve inflow velocity due to the shorter systolic ejection period compared to diastolic filling time and smaller LVOT cross sectional area compared to the MV inflow area; a factor increased by the KE function being the product of the square of the velocity. The systolic component becomes less as the LVOT velocities fall in DCM, whereas if diastolic dysfunction accompanies LV systolic function the mitral inflow velocities increase.

## Consequences of alterations in left ventricular flow components and kinetic energy

Blood flow within the normal LV is complex, with interactions of dynamically arranged regions of straight and turning flow and vortices that develop and diminish with the phases of the cardiac cycle [118]. In health, most of the left atrial blood inflow volume and hence kinetic energy is due to direct flow, which preserves its kinetic energy as it transits the left ventricle within the same cardiac cycle [48].

I identified that in DCM and IHD patients the majority of the inflowing volume and KE is due to the retained inflow component. Hence, instead of immediate ejection as part of the direct flow component volume, the kinetic energy possessed by the retained inflow volume resides within the LV for at least one cardiac cycle prior to ejection. The KE of this inflowing blood from the left atrium has several possible fates in the receiving ventricle; 1) it may be transferred as kinetic energy to the blood already residing in the LV (delayed ejection flow and residual volume), 2) converted into potential energy that is either a)stored within the elastic recoil of the myocardium or b) causes an elevation in ventricular pressure or 3) dissipated in the form of friction/heat [74]. With any of these fates, energy is inefficiently dissipated within the ventricle, and as has been shown is increased in the residing LV components compared to the situation in health (when the inflow KE directly transits the LV).

The residual volume of the LV determines how much intra-cardiac volume is available for the exchanging components of the LV volume. The precise role of the residual volume has

not been elucidated, however, even in health, it accounts for approximately a third of the intra-cardiac volume [3], so it would be reasonable to assume it confers a physiological advantage. Many processes that occur as a consequence of cardiac remodelling have initial advantageous effects that over time become deleterious; it may be that initially the increasing residual volume in ventricular dysfunction confers an advantage such as acting as a buffer to redistribute the KE so as to reduce transfer of kinetic energy to potential energy. However, once the EF falls below 35% our results suggest that a failure of any compensatory mechanism has occurred as the average kinetic power of the residual volume increases rapidly. Another potential explanation is that as the KE residing within the LV increases, a compensatory mechanism to disperse excessive movement of the blood occurs; namely conversion of KE to potential energy either within the elastic recoil of the LV wall or as an increase in ventricular pressure. However, when either the myocardium remodels and becomes less compliant or the LV pressure exceeds a certain level, the conversion of KE to potential energy will stop and may explain why I see the sharp rise in the average kinetic power possessed by the residual volume once end-stage remodelling has been reached. The kinetic energy of the residual volume may also have a role in prevention of blood stasis and thrombus formation as suggested by a study that found lower apical blood velocities in DCM patients with LV thrombus compared to those without [124]. However, a causal effect was not established and it may be that the presence of thrombus causes the lower velocities rather than vice versa. To further clarify these potential mechanistic ideas longitudinal studies and potentially invasive pressure measurements would be required.

Our results demonstrate that the decrease in direct flow and increase in residual volume proportions and kinetic energy occur in line with the reduction in LV EF. The presence of additional compensatory mechanisms is suggested by an initial increase in proportion of the exchanging LV components (retained inflow and delayed ejection flow), as the ejection fraction became moderately impaired. This was previously found in a study assessing dilated cardiomyopathy with a mean EF of 42% [74]. However, I found this increase in exchanging components to be a temporary change; as ejection fraction fell to <35%, the proportion of these components returned to baseline. This initial increase in exchanging components may act as a compensatory mechanism in the early phases of HF. However, this increase appears to be unsustainable and may contribute to a further reduction in ejection fraction in more advanced heart failure.

## Candidate pathophysiological mechanisms for transduction of flow abnormalities to cardiac remodelling

Blood flow within the left ventricle is subject to the laws of fluid mechanics including that of Laplace; ventricular wall stress is proportional to both ventricular pressure and cavity radius and inversely proportional to wall thickness [14]. KE conversion resulting in increased LV pressure, especially diastolic pressure, would result in increased ventricular wall stress/stretch, which may be important in the activation of cardiac remodelling pathways [119]. Translating stretch-stimuli to downstream signalling requires numerous complicated pathways; the mechanosensing apparatus in health is controlled by transient receptor potential channels, integrins and various sarcomere associated proteins as well as the

sarcomere spanning protein titin. In pathological remodelling G-proteins and strain-sensitive cellular elements play an additional role [125]. Once cardiac myocytes have sensed mechanical stretch they convert this into intracellular growth signals and changes in gene expression [126].

An ultimate goal of cardiac remodelling is successful adaptation to and reduction of increased wall tension, as well as facilitating preservation or even augmentation of cardiac pump function [125]. Hence, a common early feature of cardiac remodelling is an increase in wall thickness in order to reduce wall stress and decrease oxygen demand, however when the wall stress is sustained the myocardium slowly transitions to a state of decompensation and subsequent HF. Part of the cardiac myocyte response to mechanical stress is to reactivate a pattern of gene expression that is similar to that required during fetal growth which includes BNP [14]. Re-expression of fetal genes in cardiac remodelling provides further evidence for the potential influence of cardiac blood flow upon morphological changes; in fetal cardiac development mechanical signals from blood flow, promote ventricular cell enlargement and contractility, via induction of gene expression [127]. Cardiac apoptosis may also play a role in the response of cardiac myocytes to biomechanical stress; mice lacking the gp 130 cell survival pathway have normal baseline cardiac phenotype but display rapid onset dilated cardiomyopathy with massive myocyte apoptosis in response to biomechanical stress [128]. High end-diastolic wall stress may also result in episodic hypoperfusion of the subendocardium, worsening contractile function and increasing

oxidative stress leading to activation of genes that are sensitive to free radical generation such as tumour necrosis factor (TNF) [129].

In addition to the changes seen within cardiac myocytes in response to mechanical stretch multiple second messenger systems, including autocrine and paracrine growth factors, such as angiotensin II, are activated in animal models [126].

Most of our understanding of cardiac remodelling comes from post-myocardial infarction studies where the underlying mechanisms of cardiac remodelling derive both directly from the infarction itself, including cell death and loss of contractile activity, as well as secondary ventricular dilatation and remodelling in infarct-remote zones as a consequence of enhanced haemodynamic burden. Over time, infarct expansion occurs where unremitting mechanical forces stretch the abnormally stressed tissue resulting in a dilated, more spherical left ventricle with abnormal levels of wall stress and distorted and ineffective contractile dysfunction [14]. The end consequences of cardiac remodelling explain why our results are similar between the two disease groups; even though IHD is initially a localised abnormality, the effects leading to heart failure result in a global myocardial disease process that appears similar to DCM.

Additional evidence for the importance of the effect of mechanical function, and hence blood flow within the heart upon myocardial cellular processes, is provided by tissue samples obtained before and after implantation of a left ventricular assist device in HF patients which demonstrate reverse remodelling changes including regression of cell thickening and elongation [130], reversion of gene expression controlling calcium cycling [131]

and subsequent downregulation of matrix metalloproteinases with reduced collagen damage[132], as well as restoration of the integrity of the dystrophin cytoskeleton, which may be disrupted in myocytes from failing hearts [133].

## 5.6 Limitations

The 4D flow data in this study were acquired at rest and, although associations are found with the patients' functional capacity as assessed by 6MWT, these relationships and understanding of flow changes in heart failure may be better elucidated by assessing the intra-ventricular blood flow during pharmacological or exercise stress. The analysis tool for quantification of the LV flow components is currently unreliable in the presence of significant regurgitant valvular pathology as the regurgitant pathlines would be excluded from the analysis. Given the use of mitral regurgitation as a classical model of volume overload further information about cardiac remodelling may be gained if it is possible to overcome this analysis obstacle.

This study has highlighted some interesting relationships between classical remodelling parameters and novel 4D flow markers, but in line with its proof of principle concept and observational nature is unable to comment upon the causality of these relationships with any certainty. However, much of the process of cardiac remodelling on an organ, cellular and biochemical level has not been fully elucidated and it may be that the use of novel 4D flow imaging biomarkers in interventional studies of therapeutics may provide additional insight into the pathophysiology of the cardiac remodelling process.

## 5.7 Clinical implications

The extent of cardiac remodelling as assessed by conventional imaging markers such as end-diastolic volume, end-systolic volume and ejection fraction are known to relate to cardiac mortality [134-136]. The value of ejection fraction to guide ongoing therapy in heart failure has been a source of debate, as it represents a surrogate marker to the extent of cardiac remodelling [16] and for any given ejection fraction range, left ventricular volumetric measurements appear to provide incremental prognostic value [135]. A meta-analysis evaluated the degree to which therapy induced changes in the remodelling parameters of LVEF, LV EDV and LV ESV were associated with therapeutic effect on mortality outcomes in phase 3 trials of patients with HF. It found a significant correlation and a salient predictability signal between short term therapeutic effects upon LV remodelling and longer term effects upon mortality [137]. Therefore the ability to assess the effect of a therapeutic intervention upon the remodelling process itself is central to the assessment of effectiveness.

Therapies for heart failure, including ACE inhibitors and β-blockers, have become established and resulted in significant reduction in patient morbidity and mortality [138]. However, the incidence of HF and burden of disease continue to increase and the need for new heart failure therapies remains [14]. Despite numerous early preliminary phase I-II studies describing potential novel therapies, very few of these compounds have been successful in phase III clinical trials. The reason for this failure of development of novel heart failure therapies is multifactorial including; the difficulty of achieving adequate study

power to demonstrate a mortality benefit now annual mortality rates have reduced and inability to identify effective therapies in phase II trials, which may be compounded by the use of surrogate endpoints that are a consequence of cardiac remodelling rather than an active part of the process [137]. Therefore the identification in this study of novel 4D flow imaging biomarkers that may be mechanistic in the cardiac remodelling process, rather than a surrogate marker, warrants further investigation with longitudinal therapeutic intervention studies.

## 5.8 Conclusion

The proportion and kinetic energy of left ventricular 4D flow components are altered in dilated and ischaemic cardiomyopathy compared to health. Derangements in the kinetic energy of the direct flow and residual volume components are related to conventional remodelling parameters and prognostic markers. LV 4D components represent novel imaging biomarkers that might provide additional insights into cardiac remodelling.

# Chapter 6

# At 7 tesla accuracy of phosphorus magnetic resonance spectroscopy increases in patients with dilated cardiomyopathy

# 6.1 Abstract

**Introduction**

In patients with dilated cardiomyopathy (DCM), cardiac energy metabolism is known to be impaired. Phosphorus magnetic resonance spectroscopy ($^{31}$P-MRS) offers unique insight into cardiac energetics but has a low intrinsic signal-to-noise ratio (SNR) in humans. This study assessed whether SNR increased, as predicted by theory, at 7T field strength (compared to 3T) and whether more precise metabolite quantification was achieved in DCM patients at 7T (compared to 3T). The associations between LV 4D flow parameters and cardiac energetics were additionally assessed in this study cohort.

**Methods**

Matched data acquisition was performed on 25 dilated cardiomyopathy patients at 3T and 7T. 10 healthy controls underwent $^{31}$P-MRS at 7T. All participants underwent 4D flow imaging at 3T.

**Results**

In DCM patients, phosphocreatine (PCr) SNR increased 2.5x at 7T relative to 3T. The phosphocreatinine to adenosine triphosphate concentration ratio (PCr/ATP) was, as expected, similar at both field strengths (1.48 at 3T vs 1.54 at 7T, P = 0.49) with a reduction in the standard deviation of PCr/ATP from 0.44 at 3T to 0.39 at 7T. The Cramer-Ráo uncertainty (CRLB) in PCr concentration also decreased by 47% from 3T to 7T, reflecting the

higher quality of 7T $^{31}$P spectra. DCM patients had a significantly lower PCr/ATP ratio than controls at 7T (1.54 ± 0.39 vs 1.95 ± 0.25, P=0.005). PCr/ATP correlated with the average kinetic power of the retained inflow, delayed ejection flow and residual volume flow components.

**Conclusions**

7T Cardiac $^{31}$P-MRS is feasible in DCM patients, it has higher SNR, and this allows more accurate quantification of the PCr/ATP ratio than at 3T. PCr/ATP was significantly lower in DCM patients than controls at 7T, consistent with previous findings at lower field strengths. The PCr/ATP ratio correlated to novel 4D flow markers, suggesting a relationship between the derangement of intra-cardiac blood flow parameters and myocardial energetics.

## 6.2 Introduction

Heart failure is a global health problem associated with significant morbidity and mortality [139]. Dilated cardiomyopathy (DCM) is a cause of heart failure characterised by increased ventricular volumes and global impairment of systolic function [140] . Phosphorus magnetic resonance spectroscopy ($^{31}$P-MRS) provides unique insight into cardiac energetics *in vivo*, but it is a technique with an intrinsically low signal to noise ratio (SNR). This is because of low metabolite concentrations [141], a low gyromagnetic ratio $\gamma_{31P}$, and relatively long T1 relaxation times; hence, $^{31}$P-MRS has ~$10^{-5}$x lower $SNR/\sqrt{t}$ than $^{1}$H magnetic resonance imaging [142]. Previous studies using $^{31}$P-MRS have demonstrated the energetic derangement in DCM patients, characterised by an impairment in the phosphocreatine (PCr) to adenosine triphosphate (ATP) concentration ratio ("PCr/ATP"). Importantly, PCr/ATP is a superior predictor of mortality than the New York heart association (NYHA) functional class or left ventricular ejection fraction (LV EF) [51, 143]. However, investigation of a relationship between altered myocardial energetics and derangements in LV blood flow markers has not been performed previously.

Previous advances in $^{31}$P-MRS have been facilitated by the 2.1x increase in SNR achieved on changing field strength from 1.5T to 3T [141], however the technique has remained limited by SNR. As whole-body human ultra-high magnetic field (UHF) MRI scanners become more widely available this limitation will lessen and greater advances within the field of $^{31}$P-MRS should be feasible. With state-of-the-art 3T protocols, there is currently a marked variability in PCr/ATP ratios even within a healthy cohort [144, 145], making individual assessments of

cardiac energetics unreliable. A further significant increase in SNR, from a higher magnetic field strength, should allow detection of smaller changes in metabolite concentrations or measurement of changes in smaller patient groups, which will further the understanding of cardiac energetics. Most significantly, with modest further improvements in SNR, theory predicts that $^{31}$P-MRS will yield metabolite measurements that are accurate enough to track individuals' response to treatment. Previous work by our group has demonstrated $^{31}$P-MRS to be feasible in healthy volunteers at 7T [142].

This study aims to investigate whether $^{31}$P-MRS at 7T is feasible in patients and if the theoretically predicted 2.3 times increase in SNR at 7T compared to 3T [142] applies to a patient cohort and allows improved precision in metabolite quantification. In this patient study I compared the best-in-class 3T methods against our new 7T hardware and methods in order to quantify the real-world improvement with the increase in field strength. Additionally, relationships between cardiac energetics and 4D flow parameters were investigated.

## 6.3 Methods

### Study population

25 patients with dilated cardiomyopathy were prospectively recruited from cardiology clinics, clinical cardiac magnetic resonance imaging lists and heart failure services. Patients were included if they had a diagnosis of DCM with a left ventricular ejection fraction (LVEF) of <50%. Patients who were not in sinus rhythm were excluded, as were patients with a

contra-indication to MRI scanning, which at 7T excluded any participant with metal implants (see **Appendix 2**). 10 age-matched healthy controls with no history of cardiac disease were additionally recruited to undergo $^{31}$P-MRS at 7T only.

## Study protocol

All participants underwent imaging at 3T for retrospectively gated 4D flow data acquisition and cine images for LV volumes, mass and function in addition to the $^{31}$P MRS acquisitions described below. Study participants also undertook a 6 minute walk test, had venous blood drawn for BNP analysis and patient participants completed a Minnesota Heart Failure Questionnaire.

## $^{31}$P-MRS acquisition protocol

Each patient underwent two $^{31}$P-MRS scans: one at 3 tesla (Trio, Siemens, Germany) with a Siemens "Heart-Liver" coil (Siemens, Germany) manufactured for use at 1.5T but re-tuned for 3T, described previously [145].

And one at 7 tesla (Magnetom, Siemens, Germany) using a 16-channel receive array (this is half of a commercial 3T 1H cardiac coil retuned for use at 7T) (Rapid Biomedical GmbH, Rimpar, Germany). These coils were chosen because they were the best-performing on phantom calibration scans at 3T and at 7T. Participants were scanned prone at 3T (required for the coil) and supine at 7T (for improved comfort). Both scans were performed sequentially on the same day to minimise any physiological variation. Localiser images were acquired with pulse oximeter gating. Spectroscopy sequences were acquired without gating

to avoid the possibility of bias due to potentially increased mis-triggering at 7T [146]. Controls underwent $^{31}$P-MRS as described at 7T only.

Localisation at 3T was performed with balanced steady-state free precession (bSSFP) cine images acquired using the body coil for transmit and a $^{1}$H loop in the "Heart-Liver" coil for receive. Localisation at 7T was performed as previously described by Rodgers *et al* [142], using fast low angle shot (FLASH) cine images acquired with a 10cm $^{1}$H Tx/Rx loop coil (Rapid Biomedical GmbH, Rimpar, Germany) which was then replaced with the $^{31}$P coil, with the participant in the same position, for the spectroscopy acquisition. Spectra were recorded using a 3D phase-encoded ultra-short echo time chemical shift imaging (UTE-CSI) pulse sequence with a 16x16x8 matrix, 15x15x25 mm$^3$ (i.e. 5.6 mL) nominal voxel size, acquisition weighting with 10 averages at k=0 and $T_R$=1s as previously described by our group [142]. At 7T, excitation was at a fixed power supported by the coil (400 V) giving a flip angle of ~30° in the inter-ventricular septum. At 3T, flip angles were matched approximately to those at 7T using the subject-specific $B_1^+$ maps. Excitation was centred at -250Hz relative to PCr at 3T to ensure a uniform flip angle from 2,3-DPG (at ~6ppm) to β-ATP (at ~16ppm) [147]. The same excitation pulse was used at 7T, placed at +266Hz relative to PCr and covering metabolites from 2,3-DPG (at ~6ppm) to α-ATP (at ~-7.5ppm). A 25mm-thick saturation band was placed to suppress signal from skeletal muscle in the anterior chest wall. At 3T, the standard Siemens "RSat" saturation slab sequence building block was used. At 7T, the BISTRO [148] saturation scheme successfully employed in previous work, comprising 5x HS8 Tp=8ms R=11 pulses [149, 150] whose amplitude ramped linearly up to a final pulse at ~70 V

was used. The exact voltage was set to the maximum permissible given the specific absorption rate (SAR) RF heating limits for each participant.

Data analysis was performed using custom Matlab software (version 2014a, the Mathworks Inc, Natick, MA). A voxel overlying the mid-ventricular septum was extracted for analysis. The spectrum was fitted using our Matlab implementation of the "advanced method for accurate, robust and efficient spectral fitting" (AMARES) [151] together with prior knowledge specifying 11 Lorentzian peaks (α,β,γ-ATP, PCr, PDE and 2x 2,3-DPG) and fixed amplitude ratios and scalar couplings for the multiplets. The fitted amplitudes were then corrected for blood contamination by subtracting 30% of the average of the two 2,3-DPG signals from each of the ATP amplitudes [152]. The remaining PCr and ATP signals were corrected for the effects of partial saturation [153] using the flip angle at the centre of the voxel, assuming no motion effects and with $T_1$ values from the literature for 3T [145] and 7T [142]. The final PCr/ATP ratio is taken as the ratio of the blood and saturation-corrected values of PCr / γ-ATP, discounting the α-ATP peak because it has contributions from $NADPH^+$ and the β-ATP peak because it had a phase artefact in some subjects. Finally, the spectral SNR was determined by applying a matched filter and then measuring the SNR as the peak height / baseline SD [154]. The final uncertainty in metabolite concentrations was expressed using the Cramer-Ráo lower bounds (CRLB) [155].

## 6.4 Results

### Study population

25 idiopathic DCM patients (mean age 54 ± 12 years, 68% male) and 10 age-matched controls (mean age 52 ± 12 years, 80% male) were recruited; demographic and clinical data are shown in **Table 6.1**. Despite 72% of patients being on beta-blockers and 92% on angiotensin converting enzyme (ACE) inhibitors or angiotensin II receptor blockers, there was no significant difference in heart rate or blood pressure compared to controls. CMR results for LV volumes and function are shown in **Table 6.2**. As expected the mean LV EF was significantly lower in DCM patients than in controls (35 ± 10% vs 65 ± 3%, P <0.0001) and DCM patients had significantly increased end-diastolic volumes (EDV) compared to controls (295 ± 123ml vs 164 ± 31ml, P < 0.0001). The peak circumferential systolic strain in patients was significantly impaired compared to controls (-10 ± 4% vs -19 ± 2%, P < 0.0001) as was the peak diastolic strain rate (45 ± 22 $s^{-1}$ in DCM, 90 ± 7 $s^{-1}$ in controls, P < 0.0001). DCM patients had higher blood BNP levels and achieved significantly shorter distances on the 6 minute walk test compared to controls. Hence the DCM patients recruited to this study had signs of significant left ventricular dysfunction but remained clinically compensated at rest, as indicated by a normal resting cardiac output (5.8 ± 1.4 L/min).

**Table 6.1: Demographic and clinical characteristics of study participants.**

| | Healthy controls (n=10) | Dilated cardiomyopathy (n=25) | P value |
|---|---|---|---|
| **Age, yrs** | 52 ± 12 | 54 ± 12 | 0.646 |
| **Male, %** | 80 | 68 | 0.686 |
| **BMI, kg/m$^2$** | 23 ± 2 | 28 ± 5 | 0.002 |
| **Systolic blood pressure, mmHg** | 124 ± 13 | 130 ± 20 | 0.429 |
| **Diastolic blood pressure, mmHg** | 77 ± 9 | 72 ± 13 | 0.296 |
| **Heart rate, beats per minute** | 64 ± 12 | 62 ± 13 | 0.660 |
| **Minnesota Heart Failure Questionnaire** | - | 19 ± 17 | |
| **6 minute walk test, m** | 634 ± 89 | 509 ± 80 | <0.0001 |
| **BNP, (pmol/L)** | 5.3 ± 2.4 | 33.5 ± 43.8 | 0.006 |
| | **Medications, n (%)** | | |
| **Beta-Blockers** | - | 18 (72) | |
| **ACE Inhibitors/ARB** | - | 23 (92) | |
| **Diuretics** | - | 12 (48) | |
| **Aldosterone antagonist** | - | 14 (56) | |

Values are mean ± standard deviations or percentages. BMI indicates body mass index; BNP, Brain-type natriuretic peptide; ACE, angiotensin-converting enzyme; ARB, angiotensin II receptor blockers

**Table 6.2: Left ventricular geometry and function.**

| | Healthy controls (n=10) | Dilated cardiomyopathy (n=25) | P value |
|---|---|---|---|
| **LV ejection fraction, %** | 65 ± 3 | 35 ± 10 | <0.0001 |
| **LV end diastolic volume , ml** | 164 ± 31 | 295 ± 123 | <0.0001 |
| **LV EDV indexed BSA, ml/m$^2$** | 87 ± 15 | 145 ± 55 | <0.0001 |
| **LV end-systolic volume, ml** | 56 ± 11 | 200 ± 117 | <0.0001 |
| **LV stroke volume, ml** | 107 ± 21 | 95 ± 22 | 0.152 |
| **Cardiac output, L/min** | 6.7 ± 1.4 | 5.8 ± 1.4 | 0.124 |
| **LV mass, g** | 114 ± 26 | 156 ± 65 | 0.056 |
| **LV mass indexed BSA g/m$^2$** | 60 ± 10 | 77 ± 28 | 0.071 |
| **LV wall thickness** | 8.8 ± 1.9 | 8.7 ± 1.5 | 0.842 |
| **Peak circumferential systolic strain, %** | -19 ± 2 | -10 ± 4 | <0.0001 |
| **Peak circumferential diastolic strain rate, s$^{-1}$** | 90 ± 7 | 45 ± 22 | <0.0001 |

Values are mean ± standard deviations or percentages. Abbreviations used: LV, left ventricular; EDV, end diastolic volume; BSA, body surface area.

## $^{31}$P-MRS results

**Table 6.3** summarises the quantitative $^{31}$P-MRS results. As expected, there was no significant difference in the PCr/ATP ratio measured at 7T compared to 3T (1.54 vs 1.48, P=0.4945) for DCM patients, as shown in **Figure 6.1A**, and the 7T PCr/ATP ratio for the controls (1.95 ± 0.25) was within the accepted range. As demonstrated in previous lower

field strengths studies [51, 143, 156] the PCr/ATP ratio was significantly reduced by 21% in the DCM patients compared to controls (1.54 ± 0.39 vs 1.95 ± 0.25, P = 0.005) at 7T.

**Table 6.3: Comparison of cardiac $^{31}$P spectra recorded in 25 DCM patients and 10 healthy controls at 3T and 7T.**

| | Dilated cardiomyopathy (n=25) | | | | Controls (n=10) |
|---|---|---|---|---|---|
| | **3T** | **7T** | **Ratio 7T/3T** | **P value** | **7T** |
| **PCr SNR** | 6.5 ± 2.4 | 16.4 ± 7.6 | 2.52 | <0.0001 | 20.2 ± 6.6 |
| **PCr Amplitude CV, %** | 24.8 ± 9.3 | 10.1 ± 5.2 | 0.41 | <0.0001 | 7.5 ± 2.9 |
| **Linewidth, Hz** | 10 ± 3 | 36 ± 17 | 3.60 | <0.0001 | 46 ± 21 |
| **Linewidth, ppm** | 0.19 ± 0.06 | 0.30 ± 0.14 | 1.58 | 0.0039 | 0.38 ± 0.17 |
| **Flip angle, °** | 31 ± 3 | 30 ± 4 | 0.97 | 0.4565 | 30 ± 4 |
| **PCr SNR (90° FA, TR »T1)** | 18.8 ± 6.9 | 43.8 ± 19.2 | 2.33 | <0.0001 | 55.6 ± 19.3 |
| **Blood- and saturation-corrected PCr/ATP** | 1.48 ± 0.44 | 1.54 ± 0.39 | 1.04 | 0.4945 | 1.96 ±0.25 |
| **Mean CRLB on PCr/ATP** | 46.4 ± 16.3 | 24.8 ± 10.5 | 0.53 | <0.00001 | 21.5 ± 7.8 |

Values are mean ± standard deviation. PCr indicates phosphocreatine; SNR, signal-to-noise ratio; CV, coefficient of variation; Hz, Hertz; ppm, parts per million; FA, flip angle; TR, repetition time; T1, longitudinal (spin-lattice) relaxation time; ATP, adenosine triphosphate; CRLB, Cramér Rao lower bound (an estimator of the precision of fitted parameters)

Importantly, the PCr/ATP ratio has a smaller inter-subject standard deviation (SD) at 7T (0.39 at 7T vs 0.44 at 3T). Typical spectra for a DCM patient at the two field strengths are shown in **Figure 6.2**. These spectra have had a matched filter applied and have been

normalised to the baseline noise SD, so the PCr peak height is by definition the PCr SNR; this clearly visually demonstrates the increased SNR at 7T compared to 3T. The SNR for PCR increased by 2.5x between 3T and 7T field strengths. Importantly there is a 47% decrease in the Cramér-Rao lower bounds (CRLB) between 3T and 7T, showing that the higher quality spectra obtained at 7T enable more accurate metabolite quantification (**Figure 6.1B**). Note, however, that the mean PCr linewidth increased from 10 Hz at 3T to 36 Hz at 7T. Since, I saw a 2.5x SNR increase in spite of this increase in linewidth, this suggests using optimised per-subject $B_0$ shim settings may further improve the quality of cardiac $^{31}$P-MRS at 7T (**Figure 6.1C**).

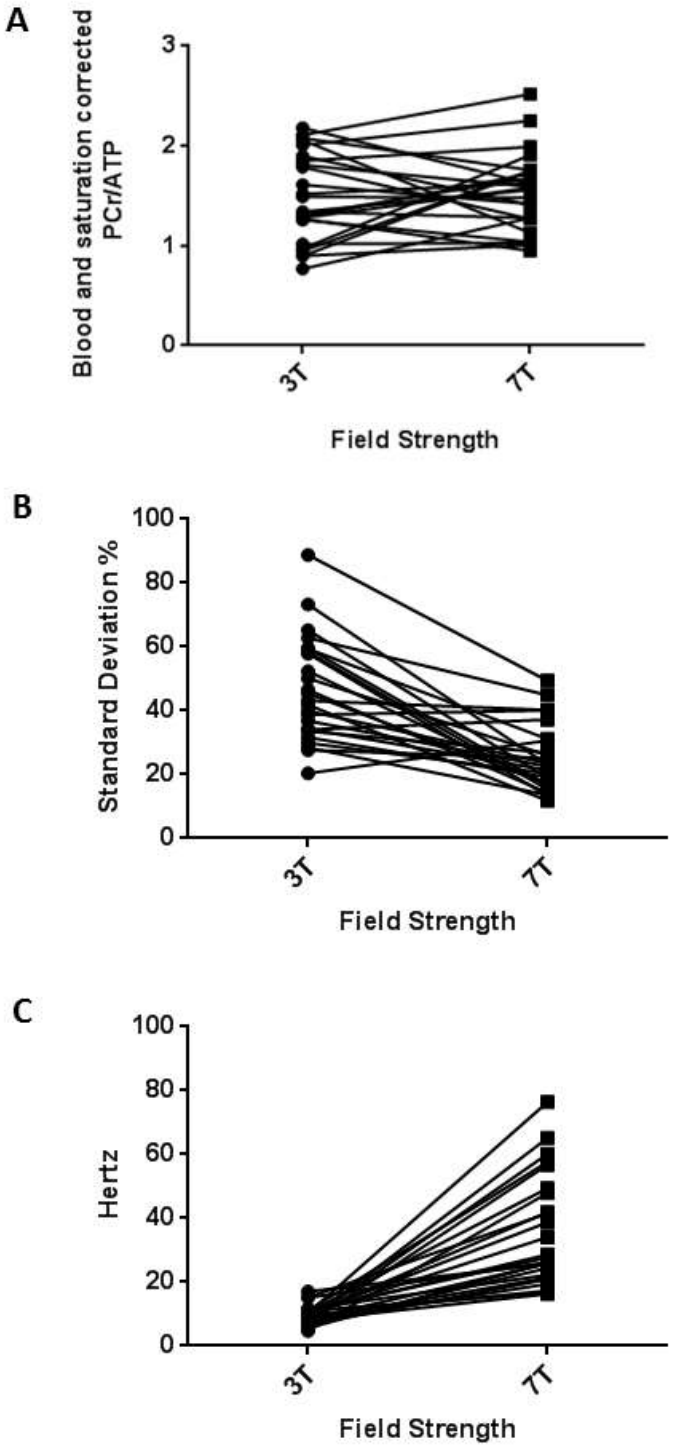


***Figure 6.1: (A)*** *PCR/ATP ratio for each DCM patient at 3T compared to 7T.* ***(B)*** *CRLB for each DCM patient at 3T compared to 7T.* ***(C)*** *Line width for PCr in Hertz at 3T compared to 7T for each patient.*

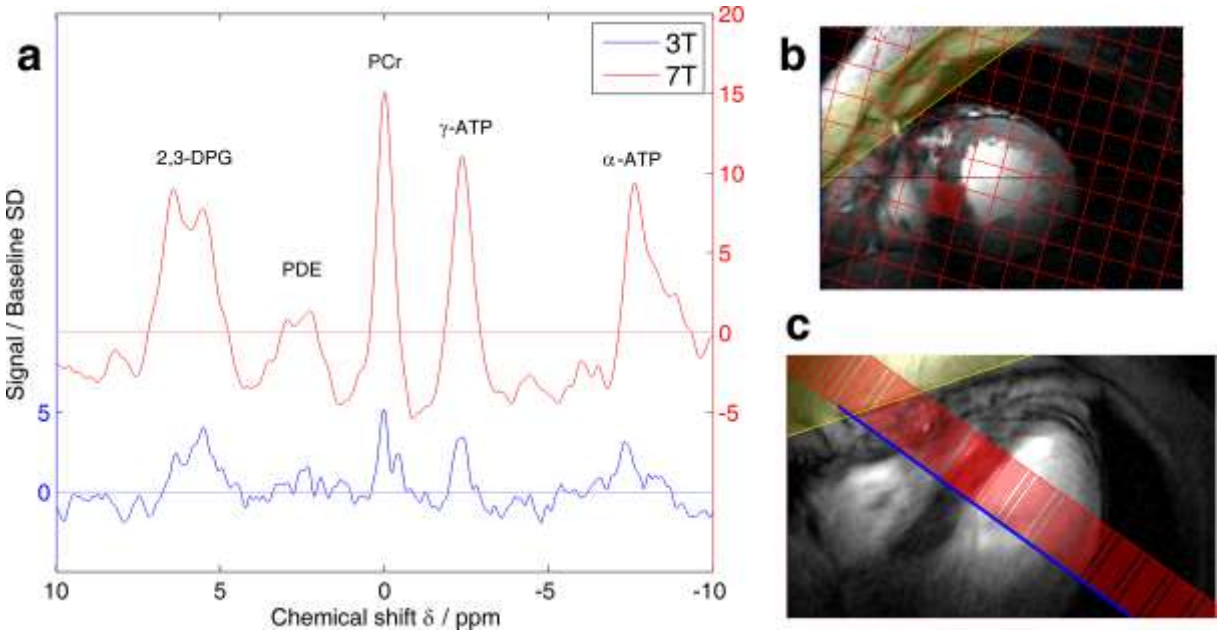


***Figure 6.2: Comparison of spectra in a typical patient at 3T and 7T.***

## Changes in 4D flow parameters

As found in chapter 5, the DCM patients in this sub-study cohort had reduced direct flow and increased residual volume compared to controls (**Figure 6.3**). The average kinetic power of each flow component was significantly different between DCM patients and controls, with a decrease in the kinetic power of the direct flow component and an increase in the average kinetic power of the other 3 components **(Figure 6.4)**.

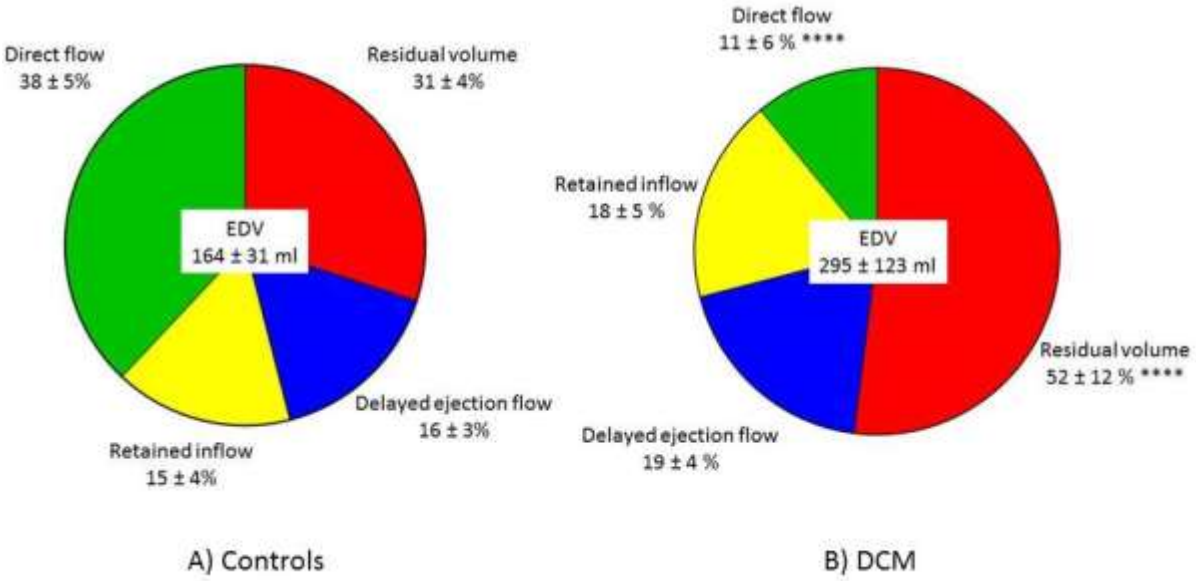


***Figure 6.3:*** *Flow components by percentage of the end-diastolic volume for controls and DCM patients. Data are mean ± standard deviation. ****P<0.0001 compared to corresponding component in controls.*

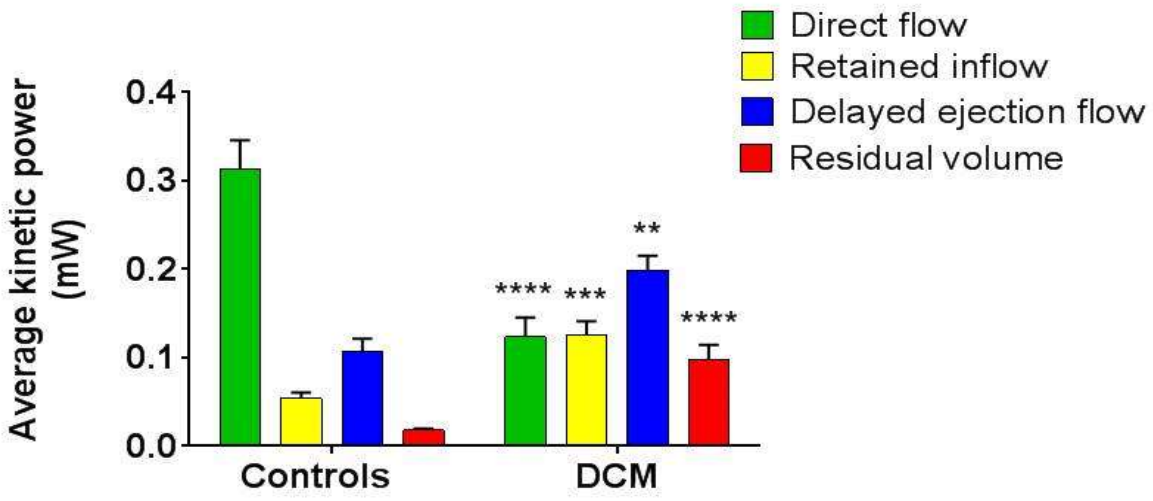


***Figure 6.4:*** *Average kinetic power throughout the cardiac cycle for the 4 flow components for controls and DCM patients. Bars show mean value and error bars indicate standard deviation. ****P<0.0001, *** P <0.001, ** P <0.01 compared to corresponding component value in controls.*

## Associations between myocardial energetics and 4D flow parameters

The PCr/ATP ratio correlated with the classical LV remodelling parameters of LVEF (r = 0.507, P = 0.02), LV EDV (r = - 0.587, P = 0.0002) and LV ESV (r = -0.473, P = 0.004) as well as the contractile function of the heart, as represented by the mid ventricular peak systolic circumferential strain (r = 0.507, P = 0.003). Additionally the PCr/ATP ratio correlated with some of the novel 4D flow remodelling parameters including the proportion of direct flow (r = 0.415, P = 0.013) and the average kinetic power of the residual volume, retained inflow and delayed ejection flow as shown in **Figure 6.5B-D**. There was no correlation with the average kinetic power of the direct flow component (r = 0.213, P = 0.219).

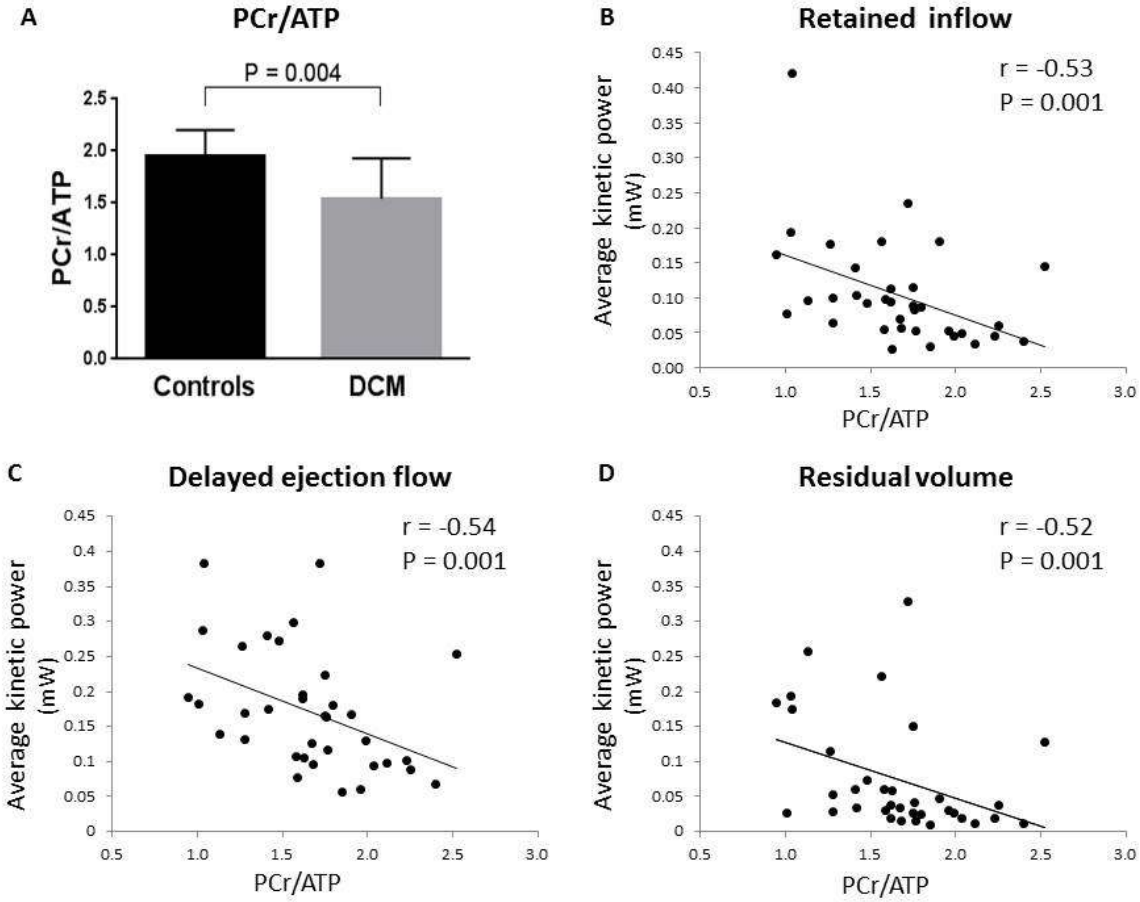


***Figure 6.5.*** *Myocardial energetics results and correlations in DCM patients.* ***(A)*** *PCr/ATP ratio in controls compared to DCM patients. Correlations between PCr/ATP ratio and* ***(B)*** *retained inflow average kinetic power;* ***(C)*** *delayed ejection flow average kinetic power and* ***(D)*** *residual volume average kinetic power.*

## 6.5 Discussion

To our knowledge, this study is the first to perform cardiac MR on patients at 7T. It demonstrates that cardiac 7T MR is well tolerated by subjects and that comparable data quality is obtained relative to normal volunteers. All participants scanned at 3T also successfully completed the 7T scan. I demonstrated the superiority of cardiac $^{31}$P spectra at 7T relative to 3T, with a 2.5x increased SNR. As shown by our group previously in healthy volunteers [142] the PCr/ATP ratio was similar in DCM patients at both field strengths suggesting that cardiac $^{31}$P-MRS suffers no new bias at 7T. The coefficient of variation in the measurement of PCr/ATP based on the CRLBs, which represents a 95% confidence interval (Student's t-test) for the measurement of PCr/ATP from the acquired spectra, shows an approximately twofold improvement at 7T over 3T. The inter-subject SD of the PCr/ATP ratio was reduced at 7T compared to 3T, suggesting an increased precision in measurement of the true physiological spread of PCr/ATP ratio. .

Compared to the 2.8x SNR increase from 3T to 7T previously reported in normal volunteers with matched 10cm loop RF coils[142], I observed a 2.5x increase in this population of patients with our best available RF coils at both field strengths. The increase in SNR can either be used to (1) obtain higher SNR spectra; (2) or to increase spatial resolution, thus reducing spectral contamination from the blood pool and skeletal muscle, as well as providing the opportunity to investigate regional metabolite concentrations; or (3) to decrease the acquisition time for cardiac $^{31}$P-MRS. A decrease in acquisition time is important, because it allows dynamic changes in metabolite concentrations to be probed with increased

temporal resolution or under more acute stress conditions than could be tolerated for the full 28-min protocol.

As found in previous studies at lower field strengths, at 7T the PCr/ATP ratio of DCM patients was significantly lower than that of controls [51, 143, 156]. Although I did not acquire control data at 3T for this study, previous work by our group has shown average PCr/ATP ratios in healthy controls to be 2.07 ± 0.38 using similar protocols [145], which would be significantly higher than the 3T PCr/ATP ratio of 1.48 ± 0.44 in our DCM patients. Our 7T results are also consistent with the findings from lower-field $^{31}$P-MRS studies [143] that the PCr/ATP ratio correlates with the LV EF. I further observed that the correlations with the PCr/ATP ratio extended also to other markers of LV remodelling such as LVEDV and LVESV, and more subtle earlier markers of LV dysfunction such as impaired peak systolic strain and impaired diastolic strain rates. These findings suggest that the reduced variability within the measurement of PCr/ATP afforded by the use of 7T might improve the ability of the PCr/ATP ratio to correlate with other important cardiac parameters in future studies.

## Myocardial energetics and intra-ventricular blood flow

I demonstrated an interesting association between the impairment of myocardial energetics seen in dilated cardiomyopathy and the alterations in intra-cardiac blood flow kinetic energy. ATP is fundamental to the majority of energy consuming reactions in the heart, including contraction of cardiac myofilaments. In health, myocardial ATP levels are tightly regulated in order to maintain a constant level. In disease states with inefficient energy production or energy utilisation, the ATP levels initially remain constant at the

expense of PCr; hence measurement of the PCr/ATP ratio is a sensitive indicator of the underlying myocardial energetic state [157]. However, absolute levels of ATP do drop in advancing heart failure and thus the PCr/ATP ratio may underestimate the true energetic deficient in this setting. As in previous lower field strength studies [156] I confirmed, using ultra-high field $^{31}$P-MRS, a reduction in PCr/ATP in DCM patients compared to controls.

Interestingly the associations between PCr/ATP are with the average kinetic power of the flow components that remain within the cardiac chamber for at least one cycle, rather than with the KE of the direct flow. One possible explanation for the association is the larger LV blood volume requires more energy input from ventricular contraction to achieve a similar stroke volume. An alternative explanation may relate to altered cardiac substrate metabolism as a consequence of reactivation of the fetal gene program by mechanical LV stretch (which is mostly caused by the components that remain within the cardiac chamber for at least one cycle), as mentioned previously. Hence, it may be that the activation of this gene program shifts myocardial metabolism from dominant fat metabolism to dominant glucose metabolism [158]. Although, more efficient in terms of oxygen consumption per unit of ATP generated, glucose has significantly lower potential energy than fat per mole, which might impair ATP generation in advanced HF [13]. In support of this mechanical unloading of failing hearts with left ventricular assist devices is associated with at least partial normalisation of cardiac metabolism [159] . Future studies combining 4D flow and myocardial metabolic studies using PET or hyperpolarised [1-$^{13}$C]pyruvate may help to address this.

There was a lack of association of myocardial energetics to the KE of the direct flow component, two potential explanations are; 1) The KE value is very small compared to the potential energy that the contractile function of the myocardium must input for successful ejection of the outgoing blood volume during systole [49, 50] and 2) the increase in cardiac afterload created by LV dilatation and increased LV wall stress in combination with LV wall thinning, which is often seen in DCM, causes a functional 'afterload mismatch' which may contribute to reduced cardiac output and hence decrease direct flow independently of myocardial energetics [156].

The kinetic energy values calculated from the LV flow components however are very small compared to the power that the heart has to generate to provide a cardiac output of 6L/min. The power the heart generates is determined by the flow: 100$cm^3$/second multiplied by the average systolic pressure: 133,000 dynes/$cm^2$, i.e. 13,300,000 ergs/sec = 1.33 watts. This means that the maximal kinetic energies measured of ~0.3mW only represent about 0.02% of that required to maintain circulatory flow in a high pressure circuit. Pressure is the dominant factor in the power and energy equation, which explains why hypertensive cardiomyopathy patients often improve when their hypertension is treated; as the reduction in systolic BP reduces the systolic energy requirements dramatically. Considering this in Joules; the average energy output from the heart is 115,000 Joules/day which with a heart rate of 60 beats per minute is 1.3J/beat. This is calculated from the prior knowledge that ATP utilisation in the normal heart is

3.2 umol/g/sec and in a failing heart is 1.6 umol/g/sec, with each ATP releasing 25-50 kJ/mole.

The KE energy values I found were in the order of 0.5 mJ which is in keeping with that found previously by *Eriksson et al* [50]. However, whilst they point out that the KE is a 1000$^{th}$ compared to the work of the heart they did not mention that the heart functions at only 10% efficient in terms of energy conversion to work. Thus in terms of energy consumption this ratio falls to 1/10,000.

## 6.6 Limitations

Although the mean PCr SNR increased by 2.5x at 7T vs 3T, it is worth noting that the individual-subject ratio ranged between 0.68 and 6.56. This likely reflects differences in the coil-to-septum distance and in the loading of the two coils at 3T and 7T, depending on the specific body shape and cardiac anatomy of each subject. Other groups have made similar observations regarding the positioning of $^{31}$P-MRS surface coils [141] [160]. It is possible that a more reliable increase in SNR would have been observed by also scanning prone at 7T, but this makes it difficult to swap between the $^{1}$H RF coil for localisation and the $^{31}$P coil for spectroscopy without moving the subject. And in early attempts to do this, it was found that prone cardiac 7T scans more frequently produced feelings of nausea than supine scans. This has been explained in terms of differences in induced currents in the vestibular system [161]. Nevertheless, the overall gain is clear at 7T.

The increased linewidth at 7T relative to 3T is likely due to the increased effect of different tissue magnetic susceptibilities at the higher field strengths; optimised per-participant $B_0$ shimming should be able to mitigate this effect in future.

As the technology for ultra-high-field MR becomes more advanced, and as ultra-high field magnets become more widely available, the restrictive patient screening requirements will remain a hurdle to be overcome before 7T MR can be used in larger studies. At present, very few patient implants have been tested at 7T. The recruitment for this study was substantially reduced by the safety requirements of the 7T (~40% of screened potential participants had a safety contraindication). In order for 7T magnets to be utilised clinically widespread testing of common metal implants at this field strength will need to occur.

## 6.6 Conclusion

In this the first cardiac 7T MR study on patients, I have shown that 7T $^{31}$ P-MRS is feasible in DCM patients, and that it gives similar increases in SNR and metabolite quantification precision as were observed in a pilot study on normal volunteers. Interestingly, derangements in novel 4D flow parameters were associated with impairment of myocardial energetics. The availability of cardiac 7T $^{31}$P-MRS methods provides a powerful tool that will enable us to better understand myocardial energetics, and to perform studies in smaller populations than has been possible until now.

# Chapter 7

# General conclusions

This work was conducted to investigate the interactions between intra-cardiac blood flow patterns and cardiovascular disease processes. This thesis is the first to report on the association between atypical right atrial flow patterns and the risk of embolism via a PFO. Identification of atypical right atrial flow patterns may help better identify which patients are at risk of recurrent paradoxical embolism via their PFO and allow appropriate targeting of management strategies, including PFO closure.

By far the greatest part of the work described in this thesis focused upon the use of 4D flow to assess blood flow within the left ventricle. Before application to a patient cohort I carefully validated this novel MRI sequence in a cohort of healthy controls and demonstrated LV 4D flow parameters to be a repeatable and stable imaging parameter within this normal population. In DCM and IHD patients, it was demonstrated that left ventricular blood flow is less efficient with increasing amounts of kinetic energy remaining within the flow components that reside within the LV. To my knowledge this is the first report of associations between conventional remodelling parameters, prognostic data and 4D flow parameters. I found, in a model created to predict the patient's functional capacity (as represented by the distance achieved during the 6MWT) that the average kinetic power of the direct flow component was independently predictive of the 6MWT result, whereas the LV EF, LV EDV and LV ESV were not found to be independent predictors.

4D flow imaging parameters represent a novel imaging biomarker in heart failure. The derangements in kinetic energy may allow further insight into the cardiac remodelling

process, as instead of being surrogate markers of the disease process, the changes seen could potentially be causative in the mechanism of cardiac remodelling.

Overall, however, as these studies are observational, it is not possible to determine causality and future longitudinal work, preferably after a therapeutic intervention would be needed to assess this further.

$^{31}$P-MRS allows unique insight into cardiac energetics *in vivo* but it is a technique that has not yet seen widespread use, partly as a consequence of the method's low intrinsic signal-to-noise ratio. Higher field strength application of the technique may overcome this limitation. This work compared cardiac $^{31}$P-MRS at 7 tesla field strength to 3 tesla, in dilated cardiomyopathy patients, and demonstrated that 7T provides improved precision in metabolite quantitation with significant increases in signal to noise relative to $^{31}$P-MRS at 3T. A relationship between the myocardial energetics and derangement in flow parameters was demonstrated in DCM patients for the first time.

The study of intra-cardiac blood flow as the primary parameter of interest has provided interesting insights into the pathophysiology of heart failure. Identification and use of novel imaging biomarkers may assist in the successful development of therapeutics for heart failure patients.

The answers provided by this body of work stimulate further questions. Longitudinal patient studies are required to explore changes in LV flow parameters over time and with disease progression in the same patient. The relationship between cardiac energetics and

4D flow parameters could be further explored by combined studies involving 4D flow and myocardial metabolic studies using PET or hyperpolarised [1-$^{13}$C]pyruvate. The 4D flow data acquisitions within this thesis were conducted at rest, further insights into intra-cardiac blood flow are likely to be gained by acquisition of 4D flow imaging during physiological or pharmacological stress.

# Bibliography


1. Harvey W, Walaeus J. *Guilielmi garveji ... De motiu cordis et sanguinis in animalibus*. Patavii,: apud Sebastianum Sardum. Sumptibus Dominici Ricciardi; 1643.
2. Richter Y, Edelman ER. Cardiology is flow. *Circulation*. 2006;113:2679-2682
3. Eriksson J, Carlhall CJ, Dyverfeldt P, Engvall J, Bolger AF, Ebbers T. Semi-automatic quantification of 4d left ventricular blood flow. *Journal of Cardiovascular Magnetic Resonance*. 2010;12:9
4. Furst B. The heart: Pressure-propulsion pump or organ of impedance? *Journal of cardiothoracic and vascular anesthesia*. 2015
5. Vincent JL. Understanding cardiac output. *Crit Care*. 2008;12:174
6. Hill JA, Olson EN. Cardiac plasticity. *The New England journal of medicine*. 2008;358:1370-1380
7. Manner J. On rotation, torsion, lateralization, and handedness of the embryonic heart loop: New insights from a simulation model for the heart loop of chick embryos. *The anatomical record. Part A, Discoveries in molecular, cellular, and evolutionary biology*. 2004;278:481-492
8. Kilner PJ, Yang GZ, Wilkes AJ, Mohiaddin RH, Firmin DN, Yacoub MH. Asymmetric redirection of flow through the heart. *Nature*. 2000;404:759-761
9. Watanabe H, Sugiura S, Hisada T. The looped heart does not save energy by maintaining the momentum of blood flowing in the ventricle. *American journal of physiology. Heart and circulatory physiology*. 2008;294:H2191-2196
10. Kilner PJ. Letter to the editor: "Postulated functional advantages of a looped as opposed to a linearly arranged heart". *American journal of physiology. Heart and circulatory physiology*. 2010;298:H726; author reply H727
11. Warburton DE, Gledhill N, Jamnik VK. Reproducibility of the acetylene rebreathe technique for determining cardiac output. *Med Sci Sports Exerc*. 1998;30:952-957
12. Kilner PJ, Henein MY, Gibson DG. Our tortuous heart in dynamic mode--an echocardiographic study of mitral flow and movement in exercising subjects. *Heart Vessels*. 1997;12:103-110
13. Neubauer S. The failing heart--an engine out of fuel. *The New England journal of medicine*. 2007;356:1140-1151
14. Burchfield JS, Xie M, Hill JA. Pathological ventricular remodeling: Mechanisms: Part 1 of 2. *Circulation*. 2013;128:388-400
15. Andersen JB, Rourke BC, Caiozzo VJ, Bennett AF, Hicks JW. Physiology: Postprandial cardiac hypertrophy in pythons. *Nature*. 2005;434:37-38
16. Cohn JN, Ferrari R, Sharpe N. Cardiac remodeling--concepts and clinical implications: A consensus paper from an international forum on cardiac remodeling. Behalf of an international forum on cardiac remodeling. *Journal of the American College of Cardiology*. 2000;35:569-582
17. McMurray JJ, Pfeffer MA. Heart failure. *Lancet*. 2005;365:1877-1889
18. National heart failure audit. 2012-2013

19. Beltrami CA, Finato N, Rocco M, Feruglio GA, Puricelli C, Cigola E, Quaini F, Sonnenblick EH, Olivetti G, Anversa P. Structural basis of end-stage failure in ischemic cardiomyopathy in humans. *Circulation*. 1994;89:151-163
20. Anversa P, Sonnenblick EH. Ischemic cardiomyopathy: Pathophysiologic mechanisms. *Progress in cardiovascular diseases*. 1990;33:49-70
21. Ginzton LE, Conant R, Rodrigues DM, Laks MM. Functional significance of hypertrophy of the noninfarcted myocardium after myocardial infarction in humans. *Circulation*. 1989;80:816-822
22. Grossman W, Jones D, McLaurin LP. Wall stress and patterns of hypertrophy in the human left ventricle. *The Journal of clinical investigation*. 1975;56:56-64
23. McKay RG, Pfeffer MA, Pasternak RC, Markis JE, Come PC, Nakao S, Alderman JD, Ferguson JJ, Safian RD, Grossman W. Left ventricular remodeling after myocardial infarction: A corollary to infarct expansion. *Circulation*. 1986;74:693-702
24. Pfeffer MA, Lamas GA, Vaughan DE, Parisi AF, Braunwald E. Effect of captopril on progressive ventricular dilatation after anterior myocardial infarction. *The New England journal of medicine*. 1988;319:80-86
25. Jefferies JL, Towbin JA. Dilated cardiomyopathy. *Lancet*. 2010;375:752-762
26. Watkins H, Ashrafian H, Redwood C. Inherited cardiomyopathies. *N Engl J Med*. 2011;364:1643-1656
27. Towbin JA, Bowles NE. The failing heart. *Nature*. 2002;415:227-233
28. Ho CY, Seidman CE. A contemporary approach to hypertrophic cardiomyopathy. *Circulation*. 2006;113:e858-862
29. Assomull RG, Prasad SK, Lyne J, Smith G, Burman ED, Khan M, Sheppard MN, Poole-Wilson PA, Pennell DJ. Cardiovascular magnetic resonance, fibrosis, and prognosis in dilated cardiomyopathy. *Journal of the American College of Cardiology*. 2006;48:1977-1985
30. Pelc NJ, Bernstein MA, Shimakawa A, Glover GH. Encoding strategies for three-direction phase-contrast mr imaging of flow. *Journal of magnetic resonance imaging : JMRI*. 1991;1:405-413
31. Pelc NJ, Herfkens RJ, Shimakawa A, Enzmann DR. Phase contrast cine magnetic resonance imaging. *Magnetic resonance quarterly*. 1991;7:229-254
32. Pelc NJ, Sommer FG, Li KC, Brosnan TJ, Herfkens RJ, Enzmann DR. Quantitative magnetic resonance flow imaging. *Magnetic resonance quarterly*. 1994;10:125-147
33. Firmin DN, Gatehouse PD, Konrad JP, Yang GZ, Kilner PJ, Longmore DB. Rapid 7-dimensional imaging of pulsatile flow. *Comput Cardiol*. 1993:353-356
34. Wigstrom L, Sjoqvist L, Wranne B. Temporally resolved 3d phase-contrast imaging. *Magnet Reson Med*. 1996;36:800-803
35. Buonocore MH. Visualizing blood flow patterns using streamlines, arrows, and particle paths. *Magnet Reson Med*. 1998;40:210-226
36. Napel S, Lee DH, Frayne R, Rutt BK. Visualizing 3-dimensional flow with simulated streamlines and 3-dimensional phase-contrast mr imaging. *Jmri-J Magn Reson Im*. 1992;2:143-153
37. Wigstrom L, Ebbers T, Fyrenius A, Karlsson M, Engvall J, Wranne B, Bolger AF. Particle trace visualization of intracardiac flow using time-resolved 3d phase contrast mri. *Magnet Reson Med*. 1999;41:793-799
38. Kvitting JP, Ebbers T, Wigstrom L, Engvall J, Olin CL, Bolger AF. Flow patterns in the aortic root and the aorta studied with time-resolved, 3-dimensional, phase-contrast magnetic

resonance imaging: Implications for aortic valve-sparing surgery. *The Journal of thoracic and cardiovascular surgery*. 2004;127:1602-1607

39. Markl M, Draney MT, Hope MD, Levin JM, Chan FP, Alley MT, Pelc NJ, Herfkens RJ. Time-resolved 3-dimensional velocity mapping in the thoracic aorta: Visualization of 3-directional blood flow patterns in healthy volunteers and patients. *Journal of computer assisted tomography*. 2004;28:459-468
40. Hope TA, Markl M, Wigstrom L, Alley MT, Miller DC, Herfkens RJ. Comparison of flow patterns in ascending aortic aneurysms and volunteers using four-dimensional magnetic resonance velocity mapping. *Journal of magnetic resonance imaging : JMRI*. 2007;26:1471-1479
41. Harloff A, Simon J, Brendecke S, Assefa D, Helbing T, Frydrychowicz A, Weber J, Olschewski M, Strecker C, Hennig J, Weiller C, Markl M. Complex plaques in the proximal descending aorta: An underestimated embolic source of stroke. *Stroke; a journal of cerebral circulation*. 2010;41:1145-1150
42. Bammer R, Hope TA, Aksoy M, Alley MT. Time-resolved 3d quantitative flow mri of the major intracranial vessels: Initial experience and comparative evaluation at 1.5t and 3.0t in combination with parallel imaging. *Magnetic resonance in medicine : official journal of the Society of Magnetic Resonance in Medicine / Society of Magnetic Resonance in Medicine*. 2007;57:127-140
43. Hara H, Virmani R, Ladich E, Mackey-Bojack S, Titus J, Reisman M, Gray W, Nakamura M, Mooney M, Poulose A, Schwartz RS. Patent foramen ovale: Current pathology, pathophysiology, and clinical status. *Journal of the American College of Cardiology*. 2005;46:1768-1776
44. Homma S, Sacco RL. Patent foramen ovale and stroke. *Circulation*. 2005;112:1063-1072
45. Meier B, Lock JE. Contemporary management of patent foramen ovale. *Circulation*. 2003;107:5-9
46. Nellessen U, Daniel WG, Matheis G, Oelert H, Depping K, Lichtlen PR. Impending paradoxical embolism from atrial thrombus: Correct diagnosis by transesophageal echocardiography and prevention by surgery. *Journal of the American College of Cardiology*. 1985;5:1002-1004
47. Lechat P, Mas JL, Lascault G, Loron P, Theard M, Klimczac M, Drobinski G, Thomas D, Grosgogeat Y. Prevalence of patent foramen ovale in patients with stroke. *New Engl J Med*. 1988;318:1148-1152
48. Carlhall CJ, Bolger A. Passing strange: Flow in the failing ventricle. *Circulation. Heart failure*. 2010;3:326-331
49. Carlsson M, Heiberg E, Toger J, Arheden H. Quantification of left and right ventricular kinetic energy using four-dimensional intracardiac magnetic resonance imaging flow measurements. *American journal of physiology. Heart and circulatory physiology*. 2012;302:H893-900
50. Eriksson J, Dyverfeldt P, Engvall J, Bolger AF, Ebbers T, Carlhall CJ. Quantification of presystolic blood flow organization and energetics in the human left ventricle. *Am J Physiol-Heart C*. 2011;300:H2135-H2141
51. Neubauer S, Krahe T, Schindler R, Horn M, Hillenbrand H, Entzeroth C, Mader H, Kromer EP, Riegger GA, Lackner K, et al. 31p magnetic resonance spectroscopy in dilated cardiomyopathy and coronary artery disease. Altered cardiac high-energy phosphate metabolism in heart failure. *Circulation*. 1992;86:1810-1818

52. Neubauer S, Horn M, Godde M, Harre K, Pabst T, Newell JB, Peters W, Hahn D, Ertl G, Kochsiek K. The myocardial creatine-phosphate atp ratio, measured by 31p-mr spectroscopy, as a predictor of mortality in patients with dilated cardiomyopathy. *Circulation*. 1995;92:2131-2131
53. Neubauer S, Horn M, Pabst T, Harre K, Stromer H, Bertsch G, Sandstede J, Ertl G, Hahn D, Kochsiek K. Cardiac high-energy phosphate metabolism in patients with aortic valve disease assessed by 31p-magnetic resonance spectroscopy. *J Investig Med*. 1997;45:453-462
54. Sardanelli F, Zandrino F, Molinari G, Cordone S, Delfino L, Levrero F. Magnetic resonance spectroscopy of ischemic heart disease. *Rays*. 1999;24:149-164
55. Jung WI, Hoess T, Bunse M, Widmaier S, Sieverding L, Breuer J, Apitz J, Schmidt O, van Erckelens F, Dietze GJ, Lutz O. Differences in cardiac energetics between patients with familial and nonfamilial hypertrophic cardiomyopathy. *Circulation*. 2000;101:E121
56. Shivu GN, Abozguia K, Phan TT, Ahmed I, Henning A, Frenneaux M. (31)p magnetic resonance spectroscopy to measure in vivo cardiac energetics in normal myocardium and hypertrophic cardiomyopathy: Experiences at 3t. *Eur J Radiol*. 2008:255-9
57. Okada M, K. M, Inubushi T, Kinoshita M. Influence of aging or left ventricular hypertrophy on the human heart: Contents of phosphorus metabolites measured by 31p mrs. *MRM*. 1998;39:772-782
58. Beer M, Sandstede J, Landschütz W, Seyfarth T, Lipke C, Köstler H, Pabst T, Kenn W, Meininger M, von Kienlin M, Horn M, Harre K, Hahn D, Neubauer S. Absolute concentrations of myocardial high-energy phosphate metabolites in normal, hypertrophied and failing human myocardium, measured non-invasively with 31p-sloop-magnetic resonance spectroscopy. *J Am Coll Cardiol*. 2002;40:1267-1274
59. Scheuermann-Freestone M, Madsen PL, Manners D, Blamire AM, Buckingham RE, Styles P, Radda GK, Neubauer S, Clarke K. Abnormal cardiac and skeletal muscle energy metabolism in patients with type 2 diabetes. *Circulation*. 2003;107:3040-3046
60. Shivu GN, Phan TT, Abozguia K, Ahmed I, Wagenmakers A, Henning A, Narendran P, Stevens M, Frenneaux M. Relationship between coronary microvascular dysfunction and cardiac energetics impairment in type 1 diabetes mellitus. *Circulation*. 2010;121:1209-1215
61. Conway MA, Allis J, Ouwerkerk R, Niioka T, Rajagopalan B, Radda GK. Detection of low phosphocreatine to atp ratio in failing hypertrophied human myocardium by 31p magnetic resonance spectroscopy. *Lancet*. 1991;338:973-976
62. Ide T, Tsutsui H, Hayashidani S, Kang D, Suematsu N, Nakamura K, Utsumi H, Hamasaki N, Takeshita A. Mitochondrial DNA damage and dysfunction associated with oxidative stress in failing hearts after myocardial infarction. *Circ Res*. 2001;88:529-535
63. Liao R, Nascimben L, Friedrich J, Gwathmey JK, Ingwall JS. Decreased energy reserve in an animal model of dilated cardiomyopathy. Relationship to contractile performance. *Circ Res*. 1996;78:893-902
64. Grove TH, Ackerman JJ, Radda GK, Bore PJ. Analysis of rat heart in vivo by phosphorus nuclear magnetic resonance. *Proc Natl Acad Sci U S A*. 1980;77:299-302
65. Bottomley PA. Noninvasive study of high-energy phosphate metabolism in human heart by depth-resolved 31p nmr spectroscopy. *Science*. 1985;229:769-772
66. Rector TS, Cohn JN. Assessment of patient outcome with the minnesota living with heart failure questionnaire: Reliability and validity during a randomized, double-blind, placebo-controlled trial of pimobendan. Pimobendan multicenter research group. *Am Heart J*. 1992;124:1017-1025

67. Ats statement: Guidelines for the six-minute walk test. *American journal of respiratory and critical care medicine*. 2002;166:111-117
68. Barker AJ, Markl M, Burk J, Lorenz R, Bock J, Bauer S, Schulz-Menger J, von Knobelsdorff-Brenkenhoff F. Bicuspid aortic valve is associated with altered wall shear stress in the ascending aorta. *Circulation. Cardiovascular imaging*. 2012;5:457-466
69. Markl M, Harloff A, Bley TA, Zaitsev M, Jung B, Weigang E, Langer M, Hennig J, Frydrychowicz A. Time-resolved 3d mr velocity mapping at 3t: Improved navigator-gated assessment of vascular anatomy and blood flow. *Journal of magnetic resonance imaging : JMRI*. 2007;25:824-831
70. Frydrychowicz A, Harloff A, Jung B, Zaitsev M, Weigang E, Bley TA, Langer M, Hennig J, Markl M. Time-resolved, 3-dimensional magnetic resonance flow analysis at 3 t: Visualization of normal and pathological aortic vascular hemodynamics. *Journal of computer assisted tomography*. 2007;31:9-15
71. Stalder AF, Russe MF, Frydrychowicz A, Bock J, Hennig J, Markl M. Quantitative 2d and 3d phase contrast mri: Optimized analysis of blood flow and vessel wall parameters. *Magnetic resonance in medicine : official journal of the Society of Magnetic Resonance in Medicine / Society of Magnetic Resonance in Medicine*. 2008;60:1218-1231
72. Bolger AF, Heiberg E, Karlsson M, Wigstrom L, Engvall J, Sigfridsson A, Ebbers T, Kvitting JPE, Carlhall CJ, Wranne B. Transit of blood flow through the human left ventricle mapped by cardiovascular magnetic resonance. *Journal of Cardiovascular Magnetic Resonance*. 2007;9:741-747
73. Heiberg E, Sjogren J, Ugander M, Carlsson M, Engblom H, Arheden H. Design and validation of segment--freely available software for cardiovascular image analysis. *BMC medical imaging*. 2010;10:1
74. Eriksson J, Bolger AF, Ebbers T, Carlhall CJ. Four-dimensional blood flow-specific markers of lv dysfunction in dilated cardiomyopathy. *Eur Heart J-Card Img*. 2013;14:417-424
75. Pennell DJ, Sechtem UP, Higgins CB, Manning WJ, Pohost GM, Rademakers FE, van Rossum AC, Shaw LJ, Yucel EK. Clinical indications for cardiovascular magnetic resonance (cmr): Consensus panel report. *Journal of cardiovascular magnetic resonance : official journal of the Society for Cardiovascular Magnetic Resonance*. 2004;6:727-765
76. Götte MJW, Germans T, Rüssel IK, Zwanenburg JJM, Marcus JT, van Rossum AC, van Veldhuisen DJ. Myocardial strain and torsion quantified by cardiovascular magnetic resonance tissue tagging: Studies in normal and impaired left ventricular function. *Journal of the American College of Cardiology*. 2006;48:2002-2011
77. Shehata ML, Cheng S, Osman NF, Bluemke DA, Lima JA. Myocardial tissue tagging with cardiovascular magnetic resonance. *J Cardiovasc Magn Reson*. 2009;11:55
78. Axel L, Dougherty L. Mr imaging of motion with spatial modulation of magnetization. *Radiology*. 1989;171:841-845
79. Petersen SE, Jerosch-Herold M, Hudsmith LE, Robson MD, Francis JM, Doll HA, Selvanayagam JB, Neubauer S, Watkins H. Evidence for microvascular dysfunction in hypertrophic cardiomyopathy: New insights from multiparametric magnetic resonance imaging. *Circulation*. 2007;115:2418-2425
80. Flett AS, Hasleton J, Cook C, Hausenloy D, Quarta G, Ariti C, Muthurangu V, Moon JC. Evaluation of techniques for the quantification of myocardial scar of differing etiology using cardiac magnetic resonance. *JACC. Cardiovascular imaging*. 2011;4:150-156
81. Mozaffarian D, Benjamin EJ, Go AS, Arnett DK, Blaha MJ, Cushman M, de Ferranti S, Despres JP, Fullerton HJ, Howard VJ, Huffman MD, Judd SE, Kissela BM, Lackland DT, Lichtman JH,

Lisabeth LD, Liu SM, Mackey RH, Matchar DB, McGuire DK, Mohler ER, Moy CS, Muntner P, Mussolino ME, Nasir K, Neumar RW, Nichol G, Palaniappan L, Pandey DK, Reeves MJ, Rodriguez CJ, Sorlie PD, Stein J, Towfighi A, Turan TN, Virani SS, Willey JZ, Woo D, Yeh RW, Turner MB, Comm AHAS, Subcomm SS. Heart disease and stroke statistics-2015 update a report from the american heart association. *Circulation*. 2015;131:E29-E322

82. Sacco RL, Ellenberg JH, Mohr JP, Tatemichi TK, Hier DB, Price TR, Wolf PA. Infarcts of undetermined cause - the nincd stroke data-bank. *Annals of neurology*. 1989;25:382-390
83. Meier B, Frank B, Wahl A, Diener HC. Secondary stroke prevention: Patent foramen ovale, aortic plaque, and carotid stenosis. *Eur Heart J*. 2012;33:705-U713
84. Webster MWI, Smith HJ, Sharpe DN, Chancellor AM, Swift DL, Bass NM, Glasgow GL. Patent foramen ovale in young stroke patients. *Lancet*. 1988;2:11-12
85. Cabanes L, Mas JL, Cohen A, Amarenco P, Cabanes PA, Oubary P, Chedru F, Guerin F, Bousser MG, Derecondo J. Atrial septal aneurysm and patent foramen ovale as risk-factors for cryptogenic stroke in patients less-than 55 years of age - a study using transesophageal echocardiography. *Stroke; a journal of cerebral circulation*. 1993;24:1865-1873
86. Debelder MA, Tourikis L, Leech G, Camm AJ. Risk of patent foramen ovale for thromboembolic events in all age-groups. *Am J Cardiol*. 1992;69:1316-1320
87. Ditullio M, Sacco RL, Gopal A, Mohr JP, Homma S. Patent foramen ovale as a risk factor for cryptogenic stroke. *Ann Intern Med*. 1992;117:461-465
88. Hausmann D, Mugge A, Becht I, Daniel WG. Diagnosis of patent foramen ovale by transesophageal echocardiography and association with cerebral and peripheral embolic events. *Am J Cardiol*. 1992;70:668-672
89. Handke M, Harloff A, Olschewski M, Hetzel A, Geibel A. Patent foramen ovale and cryptogenic stroke in older patients. *New Engl J Med*. 2007;357:2262-2268
90. Hust MH, Staiger M, Braun B. Migration of paradoxic embolus through a patent foramen ovale diagnosed by echocardiography - successful thrombolysis. *Am Heart J*. 1995;129:620-622
91. Furlan AJ, Investigators CI. The closure i trial. Recurrent neurological events in patients with patent foramen ovale treated with percutaneous closure versus best medical therapy. *Stroke; a journal of cerebral circulation*. 2011;42:E82-E82
92. Meier B, Kalesan B, Mattle HP, Khattab AA, Hildick-Smith D, Dudek D, Andersen G, Ibrahim R, Schuler G, Walton AS, Wahl A, Windecker S, Juni P. Percutaneous closure of patent foramen ovale in cryptogenic embolism. *The New England journal of medicine*. 2013;368:1083-1091
93. Carroll JD, Saver JL, Thaler DE, Smalling RW, Berry S, MacDonald LA, Marks DS, Tirschwell DL, Investigators R. Closure of patent foramen ovale versus medical therapy after cryptogenic stroke. *New Engl J Med*. 2013;368:1092-1100
94. Furlan AJ. Brief history of patent foramen ovale and stroke. *Stroke; a journal of cerebral circulation*. 2015;46:E35-E37
95. Kent DM, Ruthazer R, Weimar C, Mas JL, Serena J, Homma S, Di Angelantonio E, Di Tullio MR, Lutz JS, Elkind MSV, Griffith J, Jaigobin C, Mattle HP, Michel P, Mono ML, Nedeltchev K, Papetti F, Thaler DE. An index to identify stroke-related vs incidental patent foramen ovale in cryptogenic stroke. *Neurology*. 2013;81:619-625
96. Homma S, Sacco RL, Di Tullio MR, Sciacca RR, Mohr JP, PICSS PCSS. Effect of medical treatment in stroke patients with patent foramen ovale - patent foramen ovale in cryptogenic stroke study. *Circulation*. 2002;105:2625-2631

97. Schuchlenz HW, Saurer G, Weihs W, Rehak P. Persisting eustachian valve in adults: Relation to patent foramen ovale and cerebrovascular events. *J Am Soc Echocardiog*. 2004;17:231-233
98. Kizer JR, Devereux RB. Clinical practice - patent foramen ovale in young adults with unexplained stroke. *New Engl J Med*. 2005;353:2361-2372
99. Bissell MM, Hess AT, Biasiolli L, Glaze SJ, Loudon M, Pitcher A, Davis A, Prendergast B, Markl M, Barker AJ, Neubauer S, Myerson SG. Aortic dilation in bicuspid aortic valve disease flow pattern is a major contributor and differs with valve fusion type. *Circ-Cardiovasc Imag*. 2013;6:499-507
100. Kheradvar A, Pedrizzetti G. *Vortex formation in the cardiovascular system*. London ; New York: Springer; 2012.
101. Hope MD, Hope TA, Meadows AK, Ordovas KG, Urbania TH, Alley MT, Higgins CB. Bicuspid aortic valve: Four-dimensional mr evaluation of ascending aortic systolic flow patterns. *Radiology*. 2010;255:53-61
102. Jarvis K, Schnell S, Gabbour M, Barker AJ, Lorenz R, Carr J, Robinson JD, Popescu AR, de Freitas RA, Rigsby C, Markl M. In vivo quantification of blood mixing in single ventricle patients with fontan circulation using 4d flow mri *Journal of Cardiovascular Magnetic Resonance*. 2013;15:E88
103. Rana BS, Thomas MR, Calvert PA, Monaghan MJ, Hildick-Smith D. Echocardiographic evaluation of patent foramen ovale prior to device closure. *JACC. Cardiovascular imaging*. 2010;3:749-760
104. Van H, Poommipanit P, Shalaby M, Gevorgyan R, Tseng CH, Tobis J. Sensitivity of transcranial doppler versus intracardiac echocardiography in the detection of right-to-left shunt. *JACC. Cardiovascular imaging*. 2010;3:343-348
105. Mas JL, Zuber M. Recurrent cerebrovascular events in patients with patent foramen ovale, atrial septal aneurysm, or both and cryptogenic stroke or transient ischemic attack. *Am Heart J*. 1995;130:1083-1088
106. Kent DM, Thaler DE, Investigators RS. The risk of paradoxical embolism (rope) study: Developing risk models for application to ongoing randomized trials of percutaneous patent foramen ovale closure for cryptogenic stroke. *Trials*. 2011;12
107. Fox ER, Picard MH, Chow CM, Levine RA, Schwamm L, Kerr AJ. Interatrial septal mobility predicts larger shunts across patent foramen ovales: An analysis with transmitral doppler scanning. *Am Heart J*. 2003;145:730-736
108. Goel SS, Tuzcu EM, Shishehbor MH, de Oliveira EF, Borek PP, Krasuski RA, Rodriguez LL, Kapadia SR. Morphology of the patent foramen ovale in asymptomatic versus symptomatic (stroke or transient ischemic attack) patients. *Am J Cardiol*. 2009;103:124-129
109. Hagen PT, Scholz DG, Edwards WD. Incidence and size of patent foramen ovale during the 1st 10 decades of life - an autopsy study of 965 normal hearts. *Mayo Clin Proc*. 1984;59:17-20
110. Pasipoularides A. Diastolic filling vortex forces and cardiac adaptations: Probing the epigenetic nexus. *Hell J Cardiol*. 2012;53:458-469
111. Markl M, Geiger J, Arnold R, Stroh A, Damjanovic D, Foll D, Beyersdorf F. Comprehensive 4-dimensional magnetic resonance flow analysis after successful heart transplantation resolves controversial intraoperative findings and reveals complex hemodynamic alterations. *Circulation*. 2011;123:E381-E383

112. Markl M, Bonk C, Klausmann D, Stalder AF, Frydrychowicz A, Hennig J, Beyersdorf F. Three-dimensional magnetic resonance flow analysis in a ventricular assist device. *J Thorac Cardiov Sur*. 2007;134:1471-1476
113. Bland JM, Altman DG. Statistical methods for assessing agreement between two methods of clinical measurement. *Lancet*. 1986;1:307-310
114. Bogaert JG, Bosmans HT, Rademakers FE, Bellon EP, Herregods MC, Verschakelen JA, Van de Werf F, Marchal GJ. Left ventricular quantification with breath-hold mr imaging: Comparison with echocardiography. *MAGMA*. 1995;3:5-12
115. Hudsmith LE, Petersen SE, Francis JM, Robson MD, Neubauer S. Normal human left and right ventricular and left atrial dimensions using steady state free precession magnetic resonance imaging. *Journal of cardiovascular magnetic resonance : official journal of the Society for Cardiovascular Magnetic Resonance*. 2005;7:775-782
116. Boudoulas H, Rittgers SE, Lewis RP, Leier CV, Weissler AM. Changes in diastolic time with various pharmacologic agents - implications for myocardial perfusion. *Circulation*. 1978;58:247-247
117. Nichols M, Townsend N, Scarborough P, Rayner M. Cardiovascular disease in europe 2014: Epidemiological update. *Eur Heart J*. 2014;35:2950-2959
118. Yang GZ, Merrifield R, Masood S, Kilner PJ. Flow and myocardial interaction: An imaging perspective. *Philos T R Soc B*. 2007;362:1329-1341
119. Tsutamoto T, Wada A, Maeda K, Hisanaga T, Maeda Y, Fukai D, Ohnishi M, Sugimoto Y, Kinoshita M. Attenuation of compensation of endogenous cardiac natriuretic peptide system in chronic heart failure - prognostic role of plasma brain natriuretic peptide concentration in patients with chronic symptomatic left ventricular dysfunction. *Circulation*. 1997;96:509-516
120. Koglin J, Pehlivanli S, Schwaiblmair M, Vogeser M, Cremer P, von Scheidt W. Role of brain natriuretic peptide in risk stratification of patients with congestive heart failure. *Journal of the American College of Cardiology*. 2001;38:1934-1941
121. Berger R, Huelsman M, Strecker K, Bojic A, Moser P, Stanek B, Pacher R. B-type natriuretic peptide predicts sudden death in patients with chronic heart failure. *Circulation*. 2002;105:2392-2397
122. V B, Weiner DH, Yusuf S, Rogers WJ, Mcintyre KM, Bangdiwala SI, Kronenberg MW, Kostis JB, Kohn RM, Guillotte M, Greenberg B, Woods PA, Bourassa MG. Prediction of mortality and morbidity with a 6-minute walk test in patients with left-ventricular dysfunction. *Jama-J Am Med Assoc*. 1993;270:1702-1707
123. Alla F, Briancon S, Guillemin F, Juilliere Y, Mertes PM, Villemot JP, Zannad F. Self-rating of quality of life provides additional prognostic information in heart failure. Insights into the epical study. *Eur J Heart Fail*. 2002;4:337-343
124. Maze SS, Kotler MN, Parry WR. Flow characteristics in the dilated left-ventricle with thrombus - qualitative and quantitative doppler analysis. *Journal of the American College of Cardiology*. 1989;13:873-881
125. Spaich S, Katus HA, Backs J. Ongoing controversies surrounding cardiac remodeling: Is it black and white-or rather fifty shades of gray? *Frontiers in physiology*. 2015;6:202
126. Sadoshima J, Izumo S. The cellular and molecular response of cardiac myocytes to mechanical stress. *Annu Rev Physiol*. 1997;59:551-571
127. Lindsey SE, Butcher JT, Yalcin HC. Mechanical regulation of cardiac development. *Frontiers in physiology*. 2014;5

128. Hirota H, Chen J, Betz UA, Rajewsky K, Gu Y, Ross J, Jr., Muller W, Chien KR. Loss of a gp130 cardiac muscle cell survival pathway is a critical event in the onset of heart failure during biomechanical stress. *Cell*. 1999;97:189-198
129. Mann, Bristow. Mechanisms and models in heart failure: The biomechanical model and beyond (vol 111,pg 2837, 2005). *Circulation*. 2005;112:E75-E75
130. Terracciano CMN, Hardy J, Birks EJ, Khaghani A, Banner NR, Yacoub MH. Clinical recovery from end-stage heart failure using left-ventricular assist device and pharmacological therapy correlates with increased sarcoplasmic reticulum calcium content but not with regression of cellular hypertrophy. *Circulation*. 2004;109:2263-2265
131. Heerdt PM, Holmes JW, Cai B, Barbone A, Madigan JD, Reiken S, Lee DL, Oz MC, Marks AR, Burkhoff D. Chronic unloading by left ventricular assist device reverses contractile dysfunction and alters gene expression in end-stage heart failure. *Circulation*. 2000;102:2713-2719
132. Li YY, Feng Y, McTiernan CF, Pei W, Moravec CS, Wang P, Rosenblum W, Kormos RL, Feldman AM. Downregulation of matrix metalloproteinases and reduction in collagen damage in the failing human heart after support with left ventricular assist devices. *Circulation*. 2001;104:1147-1152
133. Vatta M, Stetson SJ, Perez-Verdia A, Entman ML, Noon GP, Torre-Amione G, Bowles NE, Towbin JA. Molecular remodelling of dystrophin in patients with end-stage cardiomyopathies and reversal in patients on assistance-device therapy. *Lancet*. 2002;359:936-941
134. Migrino RQ, Young JB, Ellis SG, White HD, Lundergan CF, Miller DP, Granger CB, Ross AM, Califf RM, Topol EJ. End-systolic volume index at 90 to 180 minutes into reperfusion therapy for acute myocardial infarction is a strong predictor of early and late mortality. The global utilization of streptokinase and t-pa for occluded coronary arteries (gusto)-i angiographic investigators. *Circulation*. 1997;96:116-121
135. White HD, Norris RM, Brown MA, Brandt PW, Whitlock RM, Wild CJ. Left ventricular end-systolic volume as the major determinant of survival after recovery from myocardial infarction. *Circulation*. 1987;76:44-51
136. Lee TH, Hamilton MA, Stevenson LW, Moriguchi JD, Fonarow GC, Child JS, Laks H, Walden JA. Impact of left ventricular cavity size on survival in advanced heart failure. *Am J Cardiol*. 1993;72:672-676
137. Kramer DG, Trikalinos TA, Kent DM, Antonopoulos GV, Konstam MA, Udelson JE. Quantitative evaluation of drug or device effects on ventricular remodeling as predictors of therapeutic effects on mortality in patients with heart failure and reduced ejection fraction a meta-analytic approach. *Journal of the American College of Cardiology*. 2010;56:392-406
138. Xie M, Burchfield JS, Hill JA. Pathological ventricular remodeling: Therapies: Part 2 of 2. *Circulation*. 2013;128:1021-1030
139. Roger VL. Epidemiology of heart failure. *Circ Res*. 2013;113:646-659
140. Francone M. Role of cardiac magnetic resonance in the evaluation of dilated cardiomyopathy: Diagnostic contribution and prognostic significance. *ISRN radiology*. 2014;2014:365404
141. Tyler DJ, Hudsmith LE, Clarke K, Neubauer S, Robson MD. A comparison of cardiac p-31 mrs at 1.5 and 3 t. *Nmr Biomed*. 2008;21:793-798
142. Rodgers CT, Clarke WT, Snyder C, Vaughan JT, Neubauer S, Robson MD. Human cardiac 31p magnetic resonance spectroscopy at 7 tesla. *Magnetic resonance in medicine : official*

*journal of the Society of Magnetic Resonance in Medicine / Society of Magnetic Resonance in Medicine*. 2014;72:304-315

143. Neubauer S, Horn M, Pabst T, Godde M, Lubke D, Jilling B, Hahn D, Ertl G. Contributions of 31p-magnetic resonance spectroscopy to the understanding of dilated heart muscle disease. *Eur Heart J*. 1995;16 Suppl O:115-118
144. Hudsmith LE, Tyler DJ, Emmanuel Y, Petersen SE, Francis JM, Watkins H, Clarke K, Robson MD, Neubauer S. P-31 cardiac magnetic resonance spectroscopy during leg exercise at 3 tesla. *Int J Cardiovas Imag*. 2009;25:819-826
145. Tyler DJ, Emmanuel Y, Cochlin LE, Hudsmith LE, Holloway CJ, Neubauer S, Clarke K, Robson MD. Reproducibility of p-31 cardiac magnetic resonance spectroscopy at 3 t. *Nmr Biomed*. 2009;22:405-413
146. Frauenrath T, Hezel F, Renz W, d'Orth TD, Dieringer M, von Knobelsdorff-Brenkenhoff F, Prothmann M, Schulz-Menger J, Niendorf T. Acoustic cardiac triggering: A practical solution for synchronization and gating of cardiovascular magnetic resonance at 7 tesla. *Journal of Cardiovascular Magnetic Resonance*. 2010;12:67
147. De Graaf RA. *In vivo nmr spectroscopy: Principles and techniques*. Chichester: John Wiley & Sons; 2007.
148. Luo Y, de Graaf RA, DelaBarre L, Tannus A, Garwood M. Bistro: An outer-volume suppression method that tolerates rf field inhomogeneity. *Magn. Reson. Med.* 2001;45:1095-1102
149. Tannus A, Garwood M. Adiabatic pulses. *NMR Biomed.* 1997;10:423-434
150. Schaller B, Clarke WT, Neubauer S, Robson MD, Rodgers CT. Suppression of skeletal muscle signal using a crusher coil: A human cardiac p-mr spectroscopy study at 7 tesla. *Magnetic resonance in medicine : official journal of the Society of Magnetic Resonance in Medicine / Society of Magnetic Resonance in Medicine*. 2015
151. Vanhamme L, van den Boogaart A, Van Huffel S. Improved method for accurate and efficient quantification of mrs data with use of prior knowledge. *J. Magn. Reson.* 1997;129:35-43
152. Horn M, Kadgien M, Schnackerz K, Neubauer S. P-31-nuclear magnetic resonance spectroscopy of blood: A species comparison. *J Cardiov Magn Reson*. 2000;2:143-149
153. Ernst RR, Anderson WA. Application of fourier transform spectroscopy to magnetic resonance. *Rev. Sci. Instrum.* 1966;37:93-102
154. Ernst RR, Bodenhausen G, Wokaun A. *Principles of nuclear magnetic resonance in one and two dimensions*. Oxford: Clarendon Press; 1987.
155. Cavassila S, Deval S, Huegen C, van Ormondt D, Graveron-Demilly D. Cramér-rao bounds: An evaluation tool for quantitation. *NMR Biomed.* 2001;14:278-283
156. Neubauer S, Horn M, Cramer M, Harre K, Newell JB, Peters W, Pabst T, Ertl G, Hahn D, Ingwall JS, Kochsiek K. Myocardial phosphocreatine-to-atp ratio is a predictor of mortality in patients with dilated cardiomyopathy. *Circulation*. 1997;96:2190-2196
157. Dass S, Cochlin LE, Suttie JJ, Holloway CJ, Rider OJ, Carden L, Tyler DJ, Karamitsos TD, Clarke K, Neubauer S, Watkins H. Exacerbation of cardiac energetic impairment during exercise in hypertrophic cardiomyopathy: A potential mechanism for diastolic dysfunction. *Eur Heart J*. 2015;36:1547-1554
158. Taegtmeyer H, Sen S, Vela D. Return to the fetal gene program: A suggested metabolic link to gene expression in the heart. *Annals of the New York Academy of Sciences*. 2010;1188:191-198

159. Chokshi A, Drosatos K, Cheema FH, Ji R, Khawaja T, Yu S, Kato T, Khan R, Takayama H, Knoll R, Milting H, Chung CS, Jorde U, Naka Y, Mancini DM, Goldberg IJ, Schulze PC. Ventricular assist device implantation corrects myocardial lipotoxicity, reverses insulin resistance, and normalizes cardiac metabolism in patients with advanced heart failure. *Circulation*. 2012;125:2844-2853
160. Hardy CJ, Bottomley PA, Rohling KW, Roemer PB. An nmr phased array for human cardiac 31p spectroscopy. *Magnetic resonance in medicine : official journal of the Society of Magnetic Resonance in Medicine / Society of Magnetic Resonance in Medicine*. 1992;28:54-64
161. Klix S, Els A, Paul K, Graessl A, Oezerdem C, Weinberger O, Winter L, Thalhammer C, Huelnhagen T, Rieger J, Mehling H, Schulz-Menger J, Niendorf T. On the subjective acceptance during cardiovascular magnetic resonance imaging at 7.0 tesla. *Plos One*. 2015;10

# Appendix 1: Minnesota Questionnaire

MINNESOTA LIVING WITH HEART FAILURE® QUESTIONNAIRE

The following questions ask how much your heart failure (heart condition) affected your life during the past month (4 weeks). After each question, circle the 0, 1, 2, 3, 4 or 5 to show how much your life was affected. If a question does not apply to you, circle the 0 after that question.

| **Did your heart failure prevent you from living as you wanted during the past month (4 weeks) by -** | **No** | | | **Very Little** | | **Very Much** |
|---|---|---|---|---|---|---|
| 1. causing swelling in your ankles or legs? | 0 | 1 | 2 | 3 | 4 | 5 |
| 2. making you sit or lie down to rest during the day? | 0 | 1 | 2 | 3 | 4 | 5 |
| 3. making your walking about or climbing stairs difficult? | 0 | 1 | 2 | 3 | 4 | 5 |
| 4. making your working around the house or yard difficult? | 0 | 1 | 2 | 3 | 4 | 5 |
| 5. making your going places away from home difficult? | 0 | 1 | 2 | 3 | 4 | 5 |
| 6. making your sleeping well at night difficult? | 0 | 1 | 2 | 3 | 4 | 5 |
| 7. making your relating to or doing things with your friends or family difficult? | 0 | 1 | 2 | 3 | 4 | 5 |
| 8. making your working to earn a living difficult? | 0 | 1 | 2 | 3 | 4 | 5 |
| 9. making your recreational pastimes, sports or hobbies difficult? | 0 | 1 | 2 | 3 | 4 | 5 |
| 10. making your sexual activities difficult? | 0 | 1 | 2 | 3 | 4 | 5 |
| 11. making you eat less of the foods you like? | 0 | 1 | 2 | 3 | 4 | 5 |
| 12. making you short of breath? | 0 | 1 | 2 | 3 | 4 | 5 |
| 13. making you tired, fatigued, or low on energy? | 0 | 1 | 2 | 3 | 4 | 5 |
| 14. making you stay in a hospital? | 0 | 1 | 2 | 3 | 4 | 5 |
| 15. costing you money for medical care? | 0 | 1 | 2 | 3 | 4 | 5 |
| 16. giving you side effects from treatments? | 0 | 1 | 2 | 3 | 4 | 5 |
| 17. making you feel you are a burden to your family or friends? | 0 | 1 | 2 | 3 | 4 | 5 |
| 18. making you feel a loss of self-control in your life? | 0 | 1 | 2 | 3 | 4 | 5 |
| 19. making you worry? | 0 | 1 | 2 | 3 | 4 | 5 |
| 20. making it difficult for you to concentrate or remember things? | 0 | 1 | 2 | 3 | 4 | 5 |
| 21. making you feel depressed? | 0 | 1 | 2 | 3 | 4 | 5 |

# *Appendix 2: 7T Safety Regulations*

**Important Information**

- Under no circumstances should this list be given to volunteers.
- This safety information in this list is only applicable for the FMRIB Magnetom 7T.
- Without the risk versus benefit analysis that exists for clinical MRI, we must be much more cautious in a research environment.
- Therefore a volunteer is excluded from having an MRI at FMRIB will, in many cases, be able to undergo a clinical MRI examination at a lesser field strength.

**Screening**

- It is a requirement that you go through the 7T Volunteer Screening Form at the initial recruitment stage.
- Any 'yes' responses that are not covered by the scanner specific Surgery and Implant Safe List must be checked with the radiographers via MRIsafety@fmrib.ox.ac.uk
- Implants & surgeries that fall under FIR are likely to be excluded for 7T. The overriding concern, even with apparently trivial surgery, is the use of surgical clips, which while safe at 3T, pose a safety hazard at 7T.

**Using The List**

- Anything NOT on this list must be treated as Further Information Required.
- With very few exceptions, 6 weeks must have passed between surgery and scanning.

**Using MRIsafety@fmrib.ox.ac.uk**

- If you have an MRI safety query that is not covered in the list, classified as Further Information Required or as Likely Exclusion, you should email MRIsafety@fmrib.ox.ac.uk
  - The subject line of your email should contain FMRIB study number, the volunteer's date of birth (DD/MM/YYYY) and their gender eg "2013_50 – 01/01/1980 – M".
  - The body of the email should contain your query along with
    - A description of the procedure
    - The manufacturer, model name or number of any implants used

- The date of the procedure, hospital and country of surgery if not the UK

- Please send a separate email for each volunteer.
- This is a ticked system and on submission you will receive a reply with a reference number for your query. Please reply to this acknowledgment email if you wish to add further information to your query.
- The radiographers will then investigate the MRI compatibility of the surgery or implant.
- Please note that manufacturers can take several weeks to provide compatibility information.
- <u>If scanning is approved you should bring a copy of this email to the scanning session.</u>

**<u>High Value Subjects</u>**

- In exceptional cases it may still be possible to scan a high value subject that has an implant.
- Examples include where manufacturer safety information either doesn't exist or contraindicates scanning, or implant information cannot be obtained.
- Applications to scan such subjects need to demonstrate that their exclusion will have a significant detrimental effect on the study.
- If an application is accepted an implant risk assessment will be carried out along with an examination of any ethical and legal considerations.

**<u>Head and Brain Surgery/Implants</u>**

Safe

- Cysts removed from scalp (as long as no bone was cut), stitches/staples for lacerations (as long as removed and no bone was cut), removal of nasal polyps, tonsillectomies and adenoidectomies

Further information required

- In general any participant with a history of brain surgery, including burr holes or biopsies, will be excluded from scanning (the risk comes from clips that may have been used during the surgery and not recorded)

- Other aspects that need to be considered include the presence of any implants including, but not limited to, cranial fixation devices, shunts (fixed or programmable), clips on sensitive structures, stents, coils.

Likely Exclusion

- Participants with aneurysm clips, neurostimulators

**Eye Surgery/Implants**

Safe

- Squint surgery, minor cosmetic surgery, laser eye surgery for vision correction, cataract surgery done post 2000

Further information required

- All other eye operations including, but not limited to, surgery for a detached retina, lens implants not associated with cataract surgery, cataract surgery done prior to 2000
- All eye implants eg eye prostheses, metal weights in eyelids, eye lid springs

Likely Exclusion

- Any subjects with a history of a metallic penetrating eye injury where there is no radiological evidence of it being removed (even if removed medically)

**Ear Surgery/Implants**

Safe

- Grommets are safe to scan regardless of when they were implanted or whether they are still present, cosmetic ear procedures (eg pinoplasy)

Further information required

- All other ear surgeries eg stapedectomies, stapedotomies, surgery for a ruptured ear drum Likely Exclusion
- Participants with cochlear implants

**Spine Surgery/Implants**

Safe

- Any surgeries that have not introduced any metallic implants or clips eg discectomies, micro-discectomies, decompressions, laminectomies

Further information required

- Spinal fusions, Anterior Cervical Discectomies and Fusions (ACDFs)

Likely Exclusion

- Harrington rods, spinal cord stimulators

**Thoracic Surgery/Implants**

Safe

- Nil

Further information required

- Lumpectomies, mastectomies, lobectomies, breast implants, tissue expanders

**Heart Surgery/Implants**

Safe

- Diagnostic angiography of coronary vessels

Further information required

- Coronary bypasses (including sternal wiring), coronary stents, PFO closure devices, artificial heart valves, if there is any history of a pacemaker or defibrillator that has now been removed (pacing wires aren't always removed)

Likely Exclusion

- Pacemakers, defibrillators

**Abdominal Surgery/Implants**

Safe

- Haemorrhoidectomies, endoscopies (after 6 weeks)

Further information required

- All other IUDs, contraceptive coils and diaphragms
- Appendectomies, cholecystectomies, sterilisations, vasectomies, C-sections, gynaecological procedures, hysterectomies
- Hernia repairs involving mesh, filters, stents, implanted drug delivery devices, colostomies, cystoscopies, diaphragms, pessaries, insulin or infusion pumps, implanted drug infusion devices, urinary catheters, penile implants

Likely Exclusion

- Capsule endoscopy devices eg pill cam (until they have passed)

**Contraceptive Implants**

Safe

- The Mirena IUS is safe provided it is outside of the transmit volume of the coil eg studies that are only using the 32 channel TxRx coil
- Nexplanon and Implanon contraceptive implants

Further Information Required

- All other IUDs, contraceptive coils and diaphragms

**Orthopaedic Surgery/Implants**

Safe

- Arthroscopies, any surgery not involving implanted devices or clips

Further information required

- Open Reduction Internal Fixations (ORIFs) followed by removal of metallic implants (often removal can be incomplete)
- All joint replacements, ORIFS, bone/joint pins, screws, nails, wires, plates, etc

**Vessel Surgery/Implants**

Safe

- Nil

Further information required

- Varicose veins (clips can be used), vessel grafts, stents, filters, vascular access ports and/or catheters

**Dental Surgery/Implants**

Safe

- Fillings, crowns, dental posts (entirely within the tooth) associated with root canal treatment

Further information required

- Retainers, bridges, braces
- Dental implants (are screwed into the jaw)
- Jaw surgery – need to identify precisely what they've had done before a decision can be made re safety and artefact

**Metallic Foreign Bodies - Orbits**

- Any participants with a history of an orbital metallic FB should firstly have the risks associated with scanning, including blindness, explained to them
- In cases of penetrative injuries, scanning must not proceed unless there is a written radiological opinion confirming the absence of any metallic fragments
- In cases of non-penetrative intraocular metallic foreign body scanning cannot proceed unless the participant can state categorically that all metal fragments have been removed medically

- It is not ethical for a research participant to be subjected to x-rays in order to clear them for a research MRI scan. However if a written radiological opinion can be obtained on existing imaging that rules out a metallic foreign body the participant can be scanned.

**Metallic Foreign Bodies - Non-Orbits**

- Unless the participant can state categorically that all of the metal fragments have been removed by a doctor, they should be excluded from scanning.
- It is not appropriate for a research participant to be subjected to x-rays in order to clear them for a research MRI scan. However if a written radiological opinion can be obtained on existing imaging that rules out a metallic foreign body being present, then the participant can be scanned.

**Miscellaneous**

- Artificial limbs, prosthetics eg false eyes, callipers, braces or corsets
  - Must be removed prior to entering the MR CONTROLLED AREA (scanner side of 7T console room)
  - We have MR SAFE walking sticks or an MR SAFE wheelchair if required

- Medicated patches
  - All medicated patches must be removed prior to scanning eg nicotine, contraceptive, pain relief, nitro
  - If the patch is for a prescription medicine the participant must check with their GP that it can be removed safely for the duration of the scan
  - It is recommended that the participant brings a replacement patch as it is not always possible to reapply a patch after it has been removed

- Mascara and Eyeliner
  - Mascara and eyeliner needs to be removed prior to the scan
  - While fMRIB has makeup removing solution it is recommended that participants are warned so they can bring their own remover and makeup to reapply afterwards

- Tattoos and Permanent Makeup
  - Participants with tattoos that will be **within** the area of the transmit coil will be excluded from scanning, eg lip or eyebrow tattoos for head imaging
  - Participants with tattoos outside of the transmit coil should be warned of the rare complication of heating and to inform the radiographer or scanop immediately if they feel any uncomfortable heating
  - Furthermore participants with new tattoos will not be scanned until 48 hours after to avoid the risk of smearing or blurring

- Body piercing jewellery
  - All metallic body piercing jewellery must be removed for scanning
  - Jewellery that is entirely plastic can remain in place
  - It is recommended that participants change metal piercings to plastic piercings prior to attending for their scan (some piercings may have to be swapped by the original piercer)

- Transdermal anchors
  - Participants with transdermal anchors should be excluded from imaging unless there is manufacturer information regarding MR compatibility

- Rings
  - All rings should be removed if possible
  - If not then the participant should be warned re heating and to alert the scanop if this happens.

# *Appendix 3: Conference Abstracts*

## Oral presentations

**1) Accepted for Early Career Award Basic Translational Oral Abstract Presentation, Society for Cardiovascular Magnetic Resonance Scientific Sessions, 2016**

Victoria M Stoll, Aaron Hess, Jonatan Eriksson, Petter Dyverfeldt, Tino Ebbers, Saul G Myerson, Carl- Johan Carlhäll, Stefan Neubauer. **"In both ischaemic and dilated cardiomyopathy left ventricular 4D flow components and kinetic energy profiles correlate with established markers of prognosis and represent novel imaging biomarkers.**"

## Moderated poster presentations

**1) 2015 SCMR/EuroCMR Joint Scientific Sessions**

**Victoria M Stoll**, Aaron Hess, Malenka M Bissell, Jonatan Eriksson, Petter Dyverfeldt, Tino Ebbers, Saul G Myerson, Carl- Johan Carlhäll, Stefan Neubauer. "**Reproducibilty and variability of left ventricular 4D flow in healthy volunteers."**

**2) 2015 SCMR/EuroCMR Joint Scientific Sessions**

**Victoria M Stoll**, William T Clarke, Saul Myerson, Matthew D Robson, Stefan Neubauer, Christopher T Rodgers **"7T versus 3T phosphorous magnetic resonance spectroscopy in patients with dilated cardiomyopathy."**

**3) BHF Symposium, University of Oxford, 2015**

**Victoria M Stoll**, Aaron Hess, Eylem Levelt, Jonatan Eriksson, Petter Dyverfeldt, Tino Ebbers, Saul G Myerson, Carl- Johan Carlhäll, Stefan Neubauer **"Deranged intra-cardiac blood flow components and kinetic energy in dilated cardiomyopathy- correlation with established markers of prognosis."**

**4) American Heart Association Scientific Sessions 2015, Orlando**

**Victoria M Stoll**, Aaron Hess, Eylem Levelt , Jonatan Eriksson, Petter Dyverfeldt, Tino Ebbers, Saul G Myerson, Carl- Johan Carlhäll, Stefan Neubauer. **"Deranged intra-cardiac blood flow components and kinetic energy in dilated cardiomyopathy are an additional marker of disease severity and correlate with established markers of prognosis."**

**5) American Heart Association Scientific Sessions 2015, Orlando**

**Victoria M Stoll**, William T Clarke, Saul Myerson, Matthew D Robson, Christopher T Rodgers, Stefan Neubauer. **"Phosphorus magnetic resonance spectroscopy is more precise at 7 tesla field strength than 3 tesla in patients with dilated cardiomyopathy."**

**6) Accepted for the Society for Cardiovascular Magnetic Resonance Scientific Sessions 2016, Los Angeles**

**Victoria Stoll,** Aaron Hess, Oliver Rider, Hayley Harvey, Alex Pitcher, Margaret Loudon, Malenka Bissell, Saul Myerson, Oliver Ormerod, Stefan Neubauer. **"In the presence of a**

**patent foramen ovale paradoxical embolism risk increases with non-vortical right atrial blood flow."**